

Dissertation
submitted to the
Combined Faculty of Natural Sciences and Mathematics
of the Ruperto Carola University Heidelberg, Germany
for the degree of
Doctor of Natural Sciences

Presented by
Ardin Marius Ouayoue Noutong, M.Sc in Biochemistry
born in Yaounde, Cameroon
Oral examination on 14.10.2021

Elucidating the function of exported proteins important for the survival of the malaria parasite *Plasmodium falciparum* during its intra-erythrocytic development.

Referees: Prof. Dr. Michael Lanzer
PD Dr. Jude Przyborski

"Printed and/or published with the support of the German Academic Exchange Service"

Dedication

I dedicate this thesis to HEAVENLY PARENT and TRUE PARENT, whose guidance, teachings, wisdom and love helped me to withstand all the difficult moments I underwent during this degree.

Acknowledgements

I sincerely thank Prof. Dr Jude Przyborski for giving me the opportunity under his direct supervision to do my PhD thesis in his laboratory. I am really thankful to him for believing in me and giving me a chance to learn and grow during these years. I thank him for the initial constant and support for my DAAD scholarship application. I am grateful to him for his insightful scientific discussions and rapid feedbacks after reading my thesis.

I highly thank the DAAD for funding my German language course and my PhD studies over the past 4,5 years.

I am grateful to my TAC members, Prof. Dr Michael Lanzer and Dr Marius Lemberg. I sincerely appreciate their insightful contributions that helped my project to progress and consequently its successful completion. A big thanks to Prof. Dr Lanzer for accepting to be my supervisor and for the Cell culture space as well as the facilities in his lab. Thanks to Profs. Drs Jacomina Locker and Oliver Fackler for accepting to examine this research work.

I also want to thank the parasitology department secretaries, Miriam Griesheimer and Sandra Niebel at Heidelberg University, for their support in the administrative and organisation of work-related procedures. A big thanks to Kerstin Kaletsch, our secretary in Gießen, for always being available for any question and taking good care of all my administrative procedures.

Thank you to the AG Przyborski group members at the Heidelberg University and the AG Przyborski/Becker of Giessen University. Special thanks to all my colleagues at Heidelberg University ranging from AG Osier, AG Portugal, AG Lanzer, AG Guizetti, AG Ganter and AG Frischknecht. I highly thank Dr Fauzia Musasia for her guidance, support and great advice. In addition, I gracefully thank Dr Nikolaos Tsopoulidis for his infinite mentorship in molecular cloning, insightful scientific discussions and unwavering support over these years.

I am deeply grateful to my entire family, especially the big family Modjo and all his members. I am forever grateful to my mom Kamneng Ivette and my wife, Sanja Bako, for their constant support, consideration and love.

Thanks to all my friends for their support during all this time.

Abstract

Plasmodium falciparum is the causative agent of the most devastating human malaria worldwide. The disease is transmitted when a female *Anopheles* mosquito injects sporozoites into human skin, which migrate and infect the liver. Upon completion of the liver stage, the parasite enters the bloodstream and infects circulating red blood cells (RBCs), thereby starting the intra-erythrocytic cycle. The environment within RBCs represents a challenging milieu for the parasite to develop and propagate normally. Therefore, to ensure its survival, *P. falciparum* exports over 400 proteins to the host cell involved in several host cell modifications. These parasite-induced host cell renovations are responsible for much of the pathology associated with malaria. Despite the intensive and continuous research work over the years, some fundamental questions remain unanswered, especially the role of many exported proteins. Elucidating their function is of utmost importance as a better understanding of parasite biology is needed to prioritize targets. Functional analysis of such proteins has been hampered in the past due to the lack of adequate genetic systems in this model organism. However, the recent advent of genetic tools such as the selection linked integration targeted gene disruption (SLI-TGD) strategy now allows rapid gene disruption in the *P. falciparum* system. Additionally, the glucosamine-6-phosphate activated ribozyme (*glmS*) system was developed to conditionally knockdown the expression of essential proteins, thereby enabling their functional characterization. In this project, we aimed to identify and characterize exported proteins essential for the survival and propagation of the parasite during the intra-erythrocytic development. For this purpose, we used a bioinformatics pipeline approach to prioritize our targets and select 15 genes encoding for exported proteins. Subsequently, these genes were subjected to a screening using the SLI-TGD approach. Furthermore, the *glmS* ribozyme system was used to analyze and characterize essential genes that could not be disrupted in the SLI-TGD screening. Of the 15 gene candidates screened in this project, 14 genes could not be disrupted, but only the *pfj23* gene could be knocked out. Analyses of parasites depleted of Pfj23 revealed aberrant SBP1 distribution and segmented Maurer's clefts architecture. Also, infected erythrocytes with disrupted Pfj23 displayed deformed and worm-like elongated knobs morphologies. Moreover, the binding of infected RBCs to chondroitin sulfate A was significantly reduced upon Pfj23 inactivation. Among the 14 genes that could not be disrupted, the *PF3D7_0301800* gene was selected to generate a regulatable copy of its protein using the *glmS* ribozyme system. Characterization of PF3D7_0301800 revealed aberrant KAHRP distribution upon its downregulation. Additionally, knockdown of PF3D7_0301800 displayed iRBCs with smooth surface without knobs referred to as the "knobless" phenotype. Further

analyses could reveal the role of PF3D7_0301800 in KAHRP trafficking and knobs formation. Hence, understanding the function of PF3D7_0301800 and Pfj23 could provide essential insights into the parasite's biology.

Zusammenfassung

Plasmodium falciparum ist der Erreger der weltweit verheerendsten menschlichen Malaria. Die Krankheit wird übertragen, wenn eine weibliche Anopheles-Mücke Sporozoiten in die menschliche Haut injiziert, die daraufhin wandern und die Leber infizieren. Nach Abschluss des Leberstadiums gelangt der Parasit in den Blutkreislauf und infiziert zirkulierende rote Blutkörperchen (RBKs), wodurch der intra-erythrozytäre Zyklus beginnt. Das Milieu innerhalb der Erythrozyten stellt für den Parasiten eine Herausforderung dar, um sich normal zu entwickeln und zu vermehren. Um sein Überleben zu sichern, exportiert *P. falciparum* daher über 400 Proteine in die Wirtszelle, die an verschiedenen Modifikationen der Wirtszelle beteiligt sind. Diese durch den Parasiten induzierten Veränderungen der Wirtszelle sind für einen Großteil der mit Malaria verbundenen Pathologie verantwortlich. Trotz intensiver und kontinuierlicher Forschungsarbeit bleiben einige grundlegende Fragen unbeantwortet, insbesondere die Rolle vieler exportierter Proteine. Die Aufklärung ihrer Funktion ist von größter Bedeutung, da ein besseres Verständnis der Parasitenbiologie erforderlich ist, um Angriffspunkte zu definieren. Die Funktionsanalyse solcher Proteine wurde in der Vergangenheit durch das Fehlen geeigneter genetischer Systeme in diesem Modellorganismus erschwert. Das jüngste Aufkommen von genetischen Werkzeugen, wie z.B. die "Selection Linked Integration Targeted Gene Disruption (SLI-TGD)"-Strategie, ermöglicht nun jedoch eine schnelle Gen-Disruption im *P. falciparum*-System. Zusätzlich wurde das Glucosamin-6-Phosphat-aktivierte Ribozym-System (*glmS*) entwickelt, um die Expression von essentiellen Proteinen gezielt zu verringern und so deren funktionelle Charakterisierung zu ermöglichen. Unser Ziel in diesem Projekt war es, exportierte Proteine zu identifizieren und zu charakterisieren, die für das Überleben und die Vermehrung des Parasiten während der intra-erythrozytären Entwicklung essentiell sind. Zu diesem Zweck verwendeten wir einen bioinformatischen Pipeline-Ansatz, um unter Einbezug verschiedener Kriterien 15 Gene auszuwählen, die für exportierte Proteine kodieren. Anschließend wurden diese Gene einem Screening mit dem SLI-TGD-Ansatz unterzogen. Darüber hinaus wurde das *glmS*-Ribozym-System verwendet, um essentielle Gene zu analysieren und zu charakterisieren, die im SLI-TGD-Screening nicht verändert werden konnten. Von den 15 Genkandidaten, die in diesem Projekt gescreent wurden, konnten 14 Gene nicht verändert werden, lediglich das Pfj23-Gen konnte ausgeschaltet werden. Analysen von Parasiten, bei denen Pfj23 ausgeschaltet wurde, zeigten eine abweichende SBP1-Verteilung und eine segmentierte Architektur der Maurer's Spalten. Außerdem zeigten infizierte Erythrozyten mit deletiertem Pfj23 deformierte und wurmartig verlängerte Knob- Morphologien. Darüber hinaus war die Bindung von infizierten Erythrozyten an

Chondroitinsulfat A bei Inaktivierung von Pfj23 deutlich reduziert. Unter den 14 Genen, die nicht verändert werden konnten, wurde das Gen *PF3D7_0301800* ausgewählt, um eine regulierbare Kopie seines Proteins mit Hilfe des *glmS*-Ribozym-Systems zu erzeugen. Die Charakterisierung von *PF3D7_0301800* zeigte nach dessen Herunterregulierung eine aberrante KAHRP-Verteilung. Zusätzlich zeigte der Knockdown von *PF3D7_0301800* iRBKs mit glatter Oberfläche ohne Knobs, die als "knobless" Phänotyp bezeichnet werden. Weitere Analysen könnten die Rolle von *PF3D7_0301800* während des KAHRP-Trafficking und der Knobbildung aufdecken. Daher könnte das Verständnis der Funktion von *PF3D7_0301800* und Pfj23 wichtige Einblicke in die Biologie des Parasiten liefern.

Table of content

1 Introduction and Background	2
1.1 Malaria: definition, origin, and epidemiology.	2
1.2 Symptoms and treatment of malaria.	3
1.3 Pathology of malaria: <i>Plasmodium</i> life cycle.	4
1.4 The protein export pathway in <i>Plasmodium falciparum</i> -infected erythrocytes.	6
1.4.1 The gateway to the host cell: directing parasite protein cargo for export.	7
1.4.2 Crossing the PVM and requirement of a translocon complex.	8
1.4.3 Transport of proteins in the host cell cytoplasm.	9
1.5 <i>Plasmodium falciparum</i> -induced host cell modifications and role of exported proteins in these renovations.	11
1.5.1 Host cell modifications during the invasion and ring stages.	12
1.5.2 Host cell remodelling during the transition from ring to trophozoite stage.	14
1.5.3 Host cell remodelling during the trophozoite and schizont stages.	23
1.6 Genetic systems to study <i>Plasmodium falciparum</i> genes.	23
1.6.1 Direct genes' inactivation systems.	24
1.6.2 Conditional gene expression systems.	26
1.7 Rational and aim of the study.	29
2 Results.....	32
2.1 Knockout screening of <i>P. falciparum</i> 's genes encoding for exported proteins using the selection integration targeted gene disruption (SLI-TGD).	32
2.1.1 Selection of the gene candidates.	32
2.1.2 Generation of parasite mutants with disrupted genes of interest.	33
2.1.3 Gene candidates classification after the SLI-TGD screening.	36
2.2 Phenotypic characterisation of Pfj23.....	36
2.2.1 Pfj23 is nonessential for parasite survival during the blood-stage development.	36
2.2.2 Investigation of the effect of Pfj23 truncation on the distribution of various exported protein markers within the infected red blood cells (iRBCs).....	39
2.2.3 Truncation of Pfj23 displays altered Maurer's clefts ultrastructure.	41
2.2.4 Δ Pfj23 parasite-infected RBCs display deformed and elongated worm-like knobs morphologies.	42
2.2.5 Δ Pfj23 parasite-infected RBCs result in reduced binding to Chondroitin Sulfate A (CSA) under static binding conditions.	43
2.3 Analysis of gene candidates using the <i>glmS</i> ribozyme system.	45
2.3.1 Generation of the SLI- <i>glmS</i> transfectants.....	46

2.4 Phenotypic characterisation of PF3D7_0301800.	47
2.4.1 Generation of parasite-infected erythrocytes with a <i>glmS</i> regulatable copy of the PF3D7_0301800 protein.	47
2.4.2 Downregulation of PF3D7_0301800 does not impair the growth of the parasite.	49
2.4.3 Downregulation of PF3D7_0301800 does not impair the distributions of SBP1, REX1 and EMP3.	50
2.4.4 Downregulation of PF3D7_0301800 impairs the distribution of KAHRP.	51
2.4.5 PF3D7_0301800 does not colocalise with KAHRP.	51
2.4.6 Downregulation of PF3D7_0301800 leads to a knobless phenotype.	52
3 Discussion	56
3.1 Selection linked integration targeted gene disruption (SLI-TGD) screening.	56
3.2 Truncation of Pfj23 and its phenotypic characterization.	59
3.3 Selection linked integration <i>glmS</i> (SLI- <i>glmS</i>) approach.	63
3.4 Generation of the SLI- <i>glmS</i> regulatable copy of the PF3D7_0301800 protein and phenotypic characterization.	63
4 Material and Methods.....	68
4.1 Methods	68
4.1.1 Molecular and biochemical based methods.....	68
4.1.2 Cell culture methods.	75
4.1.3 Microscopy based methods.....	81
4.2 Materials.....	83
4.2.1 <i>Plasmodium falciparum</i> strains and Cell lines used in this project.	83
4.2.2 <i>E. coli</i> strains used in this project.	85
4.2.3 Plasmids	85
4.2.4 Oligonucleotides.....	86
4.2.5 Antibodies and Enzymes.....	88
4.2.6 Chemicals.	89
4.2.7 Kits.....	90
4.2.8 Equipments.....	91
4.2.9 Plastic Ware.....	92
References	93
Appendices	104

List of Figures

Figure 1: Map of the distribution of malaria worldwide (WHO 2020).....	3
Figure 2: Life cycle of <i>Plasmodium falciparum</i> in humans and mosquitoes.	6
Figure 3: Schematic of the protein trafficking	10
Figure 4: Development of <i>Plasmodium falciparum</i> in human erythrocytes.....	11
Figure 5: Biogenesis of the parasitophorous vacuole	13
Figure 6: Structure of a Maurer's cleft and its protein contains.	15
Figure 7: New Permeability Pathways (NPP) in the infected erythrocyte.....	16
Figure 8: Various host cell modifications.	19
Figure 9: Structure of knobs in the infected erythrocyte.....	20
Figure 10: Cytosdhesion of infected erythrocytes on various receptors.....	22
Figure 11: CRISPR/Cas9 editing system. A) The Cas9 nuclease protein	25
Figure 12: Schematic of genetic systems for conditional gene	28
Figure 13: Genetic strategy of the SLI-TGD system for gene disruption.....	34
Figure 14: Experimental design and workflow for the disruption o.....	35
Figure 15: P _{fj23} is nonessential for the parasite blood-stage growth.....	38
Figure 16: Indirect immunofluorescence assay (IFA) analysis.....	40
Figure 17: Transmission electron microscopy (TEM) of CS2 and Δ P _{fj23}	41
DFigure 18: P _{fj23} truncation leads to aberrant knobs morphologies.....	42
Figure 19: P _{fj23} truncation leads to aberrant knobs morphologies.	43
Figure 20: P _{fj23} truncation reduces binding to Chondroitin sulfate.....	44
Figure 21: Selection linked integration (SLI) glucosamine-6-phosphate	45
Figure 22: Experimental design and workflow strategy.....	47
Figure 23: Generation of a <i>glmS</i> regulatable copy of the PF3D7_0301800 protein.	48
Figure 24: Knockdown of PF3D7_0301800 does not affect parasite's growth	50
Figure 25: Immunofluorescence assays on KAHRP upon the knockdown.....	52
Figure 26: A) Scanning and transmission electron microscopy (SEM and TEM)	54
Figure 27: Comparison of our study with other aberrant Maurer's clefts.....	61
Figure 28: Three steps of the PCR reaction. Denaturation, annealing.....	68
Figure 29: 1kb+ DNA size standard (ThermoFisher Scientific).	71
Figure 30 SDS-PAGE band profile of the PageRuler Prestained Protein Ladder.....	74

List of Tables

Table 1: List of gene candidates.	33
Table 2: Essentiality classification of the gene candidates.	37
Table 3: List of the generated transfectants using the SLI- <i>glmS</i> approach.	46
Table 4: Comparison of SLI-TGD screening with other studies.	58
Table 5: Pipetting scheme for one polyacrylamide gel.....	74

List of appendix

Appendix 1: Scanning electron microscopy (SEM) of CS2 and Δ Pfj23-parasites.....	104
Appendix 2: Transmission electron microscopy (SEM) of CS2 and Δ Pfj23-parasites	105
Appendix 3: Scanning electron microscopy (SEM).....	106
Appendix 4: Transmission electron microscopy (TEM).....	108
Appendix 5: Transmission electron microscopy (TEM).....	108
Appendix 6: Full Western blot data showing the expression.....	109
Appendix 7: Vector maps	113

Abbreviations

ATP	Adenosine triphosphate
ATS	Acidic terminal segment
Bp	Base pairs
BTS	Basic terminal segment
BSA	Bovine serum albumin
BSD	Blasticidin-S-deaminase
CAS9	CRISPR associated 9
CO ₂	Carbon dioxide
CRISPR	Clustered regularly interspaced short palindromic repeats
CSA	Chondroitin sulphate A
C-terminus	Carboxy terminus
D	Aspartic acid
DD	Destabilization domain
ddH ₂ O	Double distilled H ₂ O
DiCre	Dimerizable cyclization recombinase
DNA	Deoxyribonucleic acid
E	Glutamic acid
EPIC	Exported protein-interacting complex
ER	Endoplasmic reticulum
EXP1	Exported protein 1
EXP2	Exported protein 2
FKBP	FK506-binding protein
FRB	FKBP rapamycin-binding
g	Gravitational force
gDNA	Genomic DNA
GFP	Green fluorescent protein
GlcN	Glucosamine
glmS	Glucosamine-6-phosphate ribozyme
GOI	Gene of interest
GPI	Glycosylphosphatidylinositol
H	Histidine
h	Hour
hpi	Hours post invasion
HRP	Horse reddish peroxidase
HSP	Heat shock protein
HSP101	Heat shock protein 101
IFA	Immunofluorescence assay
iRBC	Infected red blood cell
KAHRP	Knob associated histidine rich protein
kDa	Kilo Dalton
KS	Knock side away
L	Leucine
MAHRP1	Maurer's clefts histidine-rich protein 1
MAHRP2	Maurer's clefts histidine-rich protein 2
mg	Milli grams
min	Minutes
mM	Milli Molar
MSP1	Merozoite protein 1

ng	Nano grams
nl	Nano litres
nm	Nano meters
N-terminus	Amino terminus
O ₂	Oxygene
PAM	Protospacer-adjacent motif
PBS	Phosphate buffered saline
PCR	Polymerase chain reaction
PEXEL	<i>Plasmodium</i> export element
PfEMP1	<i>P. falciparum</i> erythrocyte membrane protein 1
PfEMP3	<i>P. falciparum</i> erythrocyte membrane protein 3
PfHSP70x	<i>P. falciparum</i> heat shock protein 70-x
PHIST	<i>Plasmodium</i> helical interspersed subtelomeric
PIESP1	Parasite-infected erythrocyte surface protein 1
PIESP2	Parasite-infected erythrocyte surface protein 2
PM5	Plasmepsin 5
PNEP	PEXEL negative exported proteins
POI	Protein of interest
PTEX	<i>Plasmodium</i> transporter of exported proteins
PTEX150	<i>Plasmodium</i> transporter of exported proteins 150
PTEX 88	<i>Plasmodium</i> transporter of exported proteins 88
PTP1	PfEMP1 trafficking protein 1
PTP5	PfEMP1 trafficking protein 5
PV	Parasitophorus vacuole
PVM	Parasitophours vacuole mebrane
R	Arginine
RBC	Red blood cell
RESA	Ring-infected erythrocyte surface antigen
REX1	Ring exported protein 1
REX2	Ring exported protein 2
RIFIN	Repetitive interspersed family
RNA	Ribonucleic acid
RON3	Rhoptry neck protein 3
SARS-CoV2	Severe acute respiratory syndrome coronavirus 2
SBP1	Skeleton binding protein 1
SEM	Scanning electron microscopy
Sec61	Sec translocon 61
SLI	Selection- linked integration
SLI-TGD	Selection linked integration targeted gene deletion
SLI-glmS	Selection linked integration glucosamine-6-activated ribozyme system
spp	specie
SP	Signal Peptide
SPC25	Signal peptidase complex
STEVOR	Subtelomeric variant open reading frame
TEM	Transmission electron microscopy
TRX2	Thioredoxin 2
TM	Transmembrane domain
TRAD	Tet repressor and activating domain sequence
TRAD	Tet repressor and activating domain sequence
U	Units
UTR	Untranslated region

V
WHO
μg
μl
μm
°C

Volts
World health organization
Micro grams
Micro liters
Micro meters
Degree Celsius

INTRODUCTION

1 Introduction and Background

1.1 Malaria: definition, origin, and epidemiology.

Malaria is an infectious disease caused by the protozoan parasite belonging to the genus of *Plasmodium* spp.. The name of the disease came from the Italian "mala'aria" which means spoiled air because its origin was first believed to be from marshlands or swamps. In 1880, the French scientist Alphonse Laveran discovered the disease and the stages of the parasite's development during its blood growth. Followed this discovery, many scientific works were intensified to unravel the cause of the illness. It was only between 1898 and 1900 that Giovanni Battista Grassi, Amico Bignami, Giuseppe Bastianelli, Angelo Celli, Camillo Golgi, and Ettore Marchiafava established a direct relation of mosquitoes as vectors of human malaria (CDC 2015; Cox 2010). Many *Plasmodium* species are found in birds, reptiles, and mammals, but only five parasite species are known to transmit human malaria. These include *P. falciparum*, *P. vivax*, *P. malariae*, *P. ovale* and *P. knowlesi*. The *P. falciparum* parasite is mainly found in sub-Saharan Africa and is responsible for most deaths, particularly in children under five years (Snow et al. 2017; WHO 2020). *P. vivax*, which occurs mainly in South America, was primarily assumed not to be present in Africa because of the Duffy negative blood phenotype in most African populations. However, recent studies reported many cases of this malaria specie in various African countries. Hence, making *P. vivax* the most widespread human malaria and representing the second largest contributor to clinical malaria globally (Battle et al. 2019; Twohig et al. 2019). *P. ovale* and *P. malariae* species are mainly found in Africa. Additionally, the ovale malaria is also found in Oceania and Asia but not in South America. These two species appear to cause the disease rarely and are less virulent than *P. falciparum* or *P. vivax* but are generally found in multispecies infections (Mueller, Zimmerman, and Reeder 2007; Sutherland 2016; Sutherland et al. 2010). The recent *P. knowlesi* parasite was discovered in macaques monkeys. It causes the disease mainly in Southeast Asia and represents the most common cause of human malaria in Malasia (White 2008; Zaw and Lin 2019).

The global distribution of the disease, as depicted in Figure 1, showed that all five human malaria are estimated to be ~229 million cases occurring in endemic countries and responsible for over 387000 deaths (WHO 2020). The advent of the COVID-19 pandemic caused by the severe acute respiratory syndrome coronavirus 2 (SARS-CoV2) had spread worldwide, including all malaria-endemic countries. It resulted in November 2020 of about 22 million cases and 600 000 deaths in malaria countries (WHO 2020). The COVID-19 pandemic represents a vital challenge of the

WHO malaria elimination programme. Therefore, malaria remains a serious public health problem in endemic countries, and understanding the parasite's biology will contribute to its elimination.

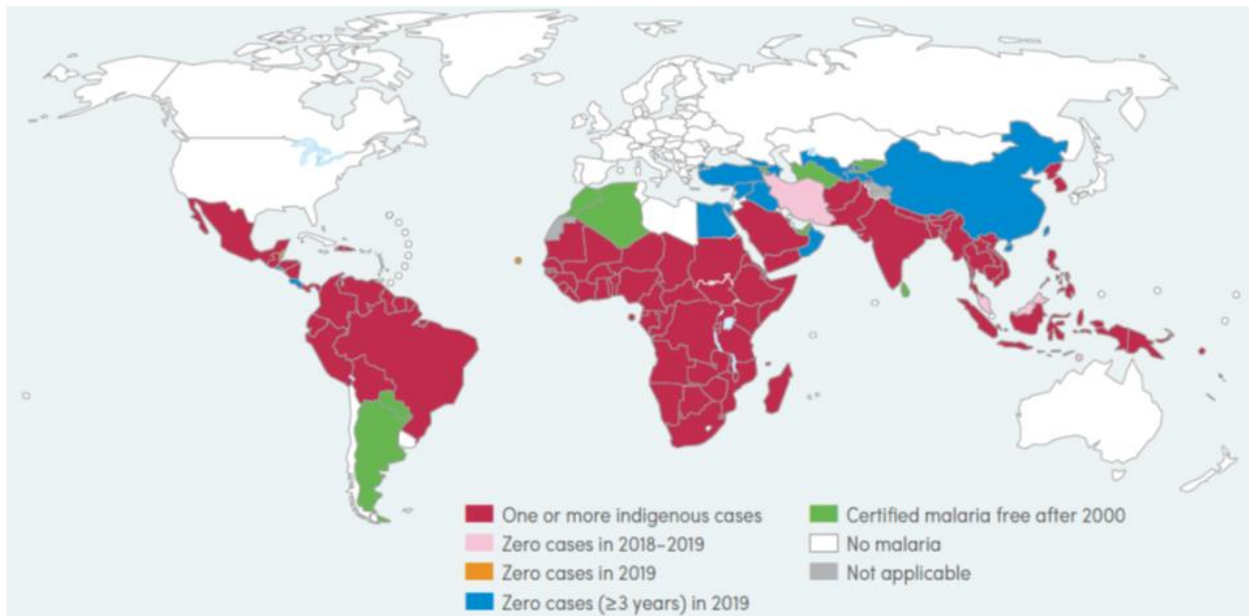


Figure 1: Map of the distribution of malaria worldwide (WHO 2020).

1.2 Symptoms and treatment of malaria.

Malaria is a complex illness with different symptoms manifested into uncomplicated and severe disease appearances: Uncomplicated malaria is characterized by the presence of symptoms without laboratory or clinical signs to indicate organ malfunction (Milner 2018). These symptoms generally include headache, myalgia, fever, cough, anorexia, and chills making clinical diagnosis unreliable (Ashley, Pyae Phyo, and Woodrow 2018). Also, patients with uncomplicated malaria can present physical symptoms such as irregular and intermittent fever and occasionally accompanied by confusion or agitation (Breman 2009). In general, only 1% to 2% of *P. falciparum* infections lead to severe or ultimately fatal malaria (Wassmer et al. 2015). A patient is declared with severe malaria when the parasite has already been detected via the microscopy of a blood smear, PCR, or rapid diagnostic test, but with no other confirmed case of another disease. Also, the patient should have at least one of the following clinical features: prostration and reduced consciousness. Additional clinical indicators of severe malaria include many convulsions, jaundice, shock, pulmonary oedema, acute kidney injury, abnormal bleeding, and coma (Zekar and Sharman 2021).

The first line of curing for uncomplicated malaria patients is the artemisinin-based combination therapies (ACT). The treatment with ACTs lasts three days and is highly effective due to its immediate and broader range effect on the parasite's development (Lalloo et al. 2016). Other treatment options such as quinine sulfate plus doxycycline, tetracycline, clindamycin, atovaquone-proguanil, and mefloquine are available, but they showed lower efficacy than ACTs. Patients showing severe malaria should be cured with intravenous antimalarial therapy for at least 24 hours until the oral medicine is accepted. This therapy involves the intravenous or intramuscular injection of artesunate or artemether in combination with acetaminophen for fever control and glucose to maintain the euglycemia of the patient (Plewes et al. 2019; Zekar and Sharman 2021).

1.3 Pathology of malaria: *Plasmodium* life cycle.

Plasmodium spp. have an extremely complex life cycle alternating between vertebrate hosts and the female *Anopheles* mosquitoes. The transmission begins when an infected *Anopheles* mosquito takes a blood meal from a vertebrate host and injects sporozoites into the skin (Figure 2A). These sporozoites' fate is not well understood, but they can take 1–3 hr to exit from the bite site (Cowman et al. 2016). Gliding motility enables sporozoites to enter the bloodstream, thereby escaping host immunity or clearance through the lymphatic system. In the bloodstream, sporozoites reach and traverse the liver sinusoidal barriers comprising endothelial and Kupffer cells (macrophage-like cells) to infect hepatocytes (Tavares et al. 2013; Venugopal et al. 2020). The invasion of the liver cells involves multiple proteins. The main protein essential in the process is the circumsporozoite protein (CSP), which allows sporozoites to bind to endothelial cells. Following binding, the apical organelles release adhesins proteins such as the thrombospondin-related anonymous protein (TRAP) and apical membrane antigen-1 (AMA-1), thereby enabling their entry (Herrera et al. 2015). Upon entry, sporozoites establish and develop within the parasitophorous vacuole (PV) and differentiate through asexual replication to form schizonts. Over 2–10 days of development (depending on the species), thousands of merozoites per hepatocyte packed in parasite-filled vesicles called merozoites are released into the bloodstream (Figure 2B) (Mota et al. 2001; Sturm et al. 2006). Some parasite species, such as *P. ovale* and *P. vivax*, can enter a latency period by forming hypnozoites (a non-replicating form of the parasite) instead of a schizont. Hypnozoites enable long-term survival of the parasite and can later lead to the reoccurrence of the disease (Venugopal et al. 2020).

In the blood circulation, merozoites invade erythrocytes, in which they develop within a compartment known as parasitophorous vacuole membrane (PVM) (Figure 2C). In comparison to regular human cells, red blood cells (RBC) have restricted biosynthetic capacity. Therefore, to have access to nutrients and avoid detection by the host immune response, the parasite exports hundreds of effector molecules named exported proteins. These proteins remodel the host by changing its membrane's physical properties to promote cytoadhesion, mediated by the insertion of the *P. falciparum* erythrocyte membrane protein 1 (PfEMP1) protein into the host plasma membrane (Maier et al. 2009; de Koning-Ward et al. 2016). Parasite-induced host cell modifications will be discussed in detail later in the coming sections. During the blood-stage development (24–48 h depending on the species), the parasite undergoes the ring, trophozoite and schizont stages. Multiple replications (schizogony) result in 16-32 daughter merozoites ready to invade new RBC. Repeated rounds of invasion and growth lead to increased parasite population and destruction of erythrocytes, thereby enabling malaria-associated pathologies (Cowman and Crabb 2006). During each cycle, a proportion of blood-stage parasites commit to sexual development to form male and female gametocytes. For up to 11 days, the newly formed gametocytes sequester in the bone marrow to allow their maturation, thereby avoiding splenic clearance. Mature gametocytes circulate in the bloodstream while waiting to be taken up by the *Anopheles* mosquito during a blood meal (Joice et al. 2014; Sologub et al. 2011). The increase in pH and the presence of xanthurenic acid in the mosquito midgut activate the differentiation of gametocytes into a male microgamete and a female macrogamete (Sinden 2015). Fertilisation of male and female gametes results in the formation of a diploid zygote which matures into an invasive motile ookinete (Figure 2D). Then, this motile ookinete traverses the epithelial layer of the midgut wall and mature into an oocyst. In the oocyst, parasites undergo multiple asexual replications to generate thousands of sporozoites that are released into the haemolymph. These sporozoites then migrate to the mosquito's salivary gland, where they remain until the next female *Anopheles* mosquito's blood meal to start the cycle again (Venugopal et al. 2020).

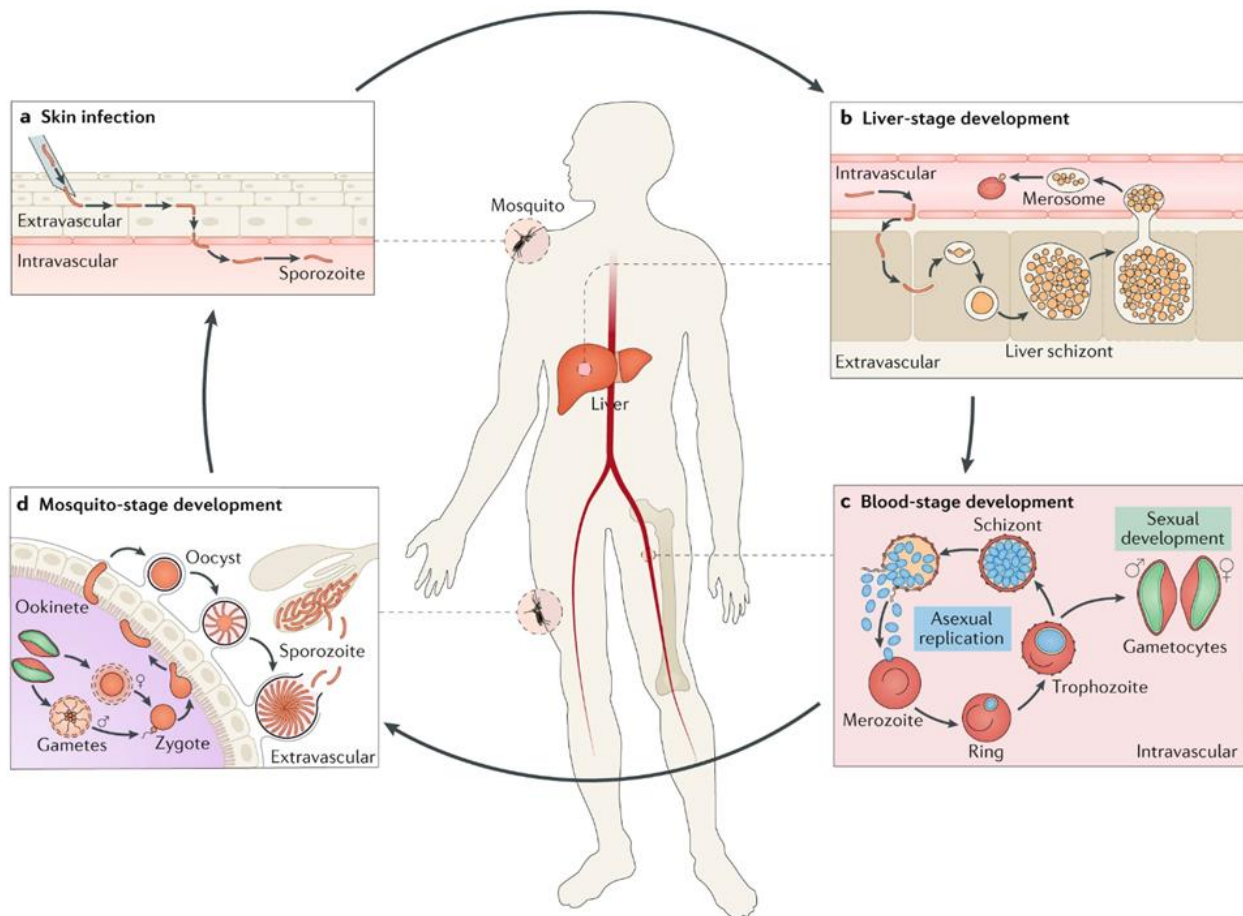


Figure 2: Life cycle of *Plasmodium falciparum* in humans and mosquitoes. The parasite has a complex life cycle alternating between human and *Anopheles* mosquitoes. A) *Plasmodium falciparum* sporozoites (orange) are introduced into the skin during an infected mosquito's blood meal. B) Sporozoites invade hepatocytes in which they undergo one asexual replication cycle to form liver schizonts containing thousands of merozoites (yellow). C) In the blood, *P. falciparum* parasites invade RBCs and undergoes asexual replications (blue). D) A female *Anopheles* mosquito ingests gametocytes which undergo gametogenesis within the midgut of the mosquito. (Venugopal et al. 2020).

1.4 The protein export pathway in *Plasmodium falciparum*-infected erythrocytes.

P. falciparum invades and resides within erythrocytes during its blood-stage development. Within these cells, the parasite is enclosed by the parasitophorous vacuole (PV) membrane, which is partially derived from the RBC membrane during the invasion. RBCs are small anucleated cells that have limited biosynthetic capacity. Therefore, to ensure its survival, the parasite exports effector proteins exported to the host cell, thereby contributing drastically to its host renovation. The parasite's habitation within the PV poses an extra challenge to the host cell makeover because all newly-synthesised exported proteins must reach the RBC membrane, be transported

beyond the parasite plasma membrane (PPM), the PVM, and through the cytosol of the host cell (Figure 3). Additionally, exported parasite proteins must also be differentiated from the proteins that enter the secretory pathway and those whose final destination is the PV (Matthews, Pitman, and de Koning-Ward 2019; Przyborski, Nyboer, and Lanzer 2016).

1.4.1 The gateway to the host cell: directing parasite protein cargo for export.

A signal peptide (SP) mediates in other systems the entry to the secretory pathway. Generally, the SP is a hydrophobic region located at the N-terminus of nascent proteins. The signal peptidase recognizes and cleaves the SP to mediate co-translational entry of mature proteins into the endoplasmic reticulum (ER) (Blobel and Dobberstein 1975b, 1975a). In *P. falciparum*, proteins containing only the SP sequence appear to follow the secretory pathway as in other systems. These proteins are mainly secreted into the parasitophorous vacuole's lumen (Przyborski, Nyboer, and Lanzer 2016; Waller et al. 2000). Proteins destined for export possess an additional motif typically located few amino acids downstream of the SP sequence, allowing them to be licenced and exported to the host cell (Marti et al. 2004). These exported proteins are classified into two groups.

The first group are those containing a pentameric amino acid motif RxLxE/Q/D known as the *Plasmodium* export element (PEXEL) or host-targeting sequence. In this motif, X symbolizes an amino acid, and solidi denote alternative amino acids for that position (Hiller et al. 2004; Marti et al. 2004; Przyborski and Lanzer 2005). Some proteins in *P. falciparum* have been identified to have relaxed PEXEL motifs R/K/HXL/IXXE and RXLXXE (Boddey et al. 2013; Schulze et al. 2015). Around 8% of *P. falciparum* proteome is predicted to have more than 400 PEXEL-containing proteins (Hiller et al. 2004; Marti et al. 2004). Within the ER, the aspartyl protease plasmepsin V (PM5) recognises and proteolytically cleaves the PEXEL motif on the C-terminal side of the leucine amino acid residue, and the new N-terminus is acetylated (Ac-x/E/D/Q) (Boddey et al. 2009; Chang et al. 2008). A recent study suggests that the entry of PEXEL proteins into the ER requires the sec61 translocon, signal peptidase 25 (SPC25) and PM5 (sec61-PfSPC25-PM5) complex (Figure 3), whereas secreted proteins require only the sec61-PfSPC25 implication (Marapana et al. 2018).

The second group of exported proteins is the PEXEL-negative exported proteins (PNEPs), which lack a PEXEL motif (Spielmann et al. 2006). This group includes the PfEMP1 family of virulence proteins which consist of 60 copies of the *var* gene (Boddey et al. 2013). Most exported PNEP proteins contain an internal transmembrane domain that functions as an ER entry signal, albeit

some have been identified as having a regular SP sequence. The SP sequence and the TM of PNEPs seem to be what is required for protein export (Gruring et al. 2012; Heiber et al. 2013). However, some PNEP proteins, such as PfHsp70-x, require only the SP sequence to be exported to the host cell (Kulzer et al. 2012). The number of PNEPs remains unknown because they lack conserved motifs to identify them, as in the case of PEXEL proteins.

1.4.2 Crossing the PVM and requirement of a translocon complex.

The current understanding postulate that soluble PNEPs and PEXEL proteins are loaded into secretory vesicles at the ER and are subsequently released directly into the PV in chaperoned complexes. Subsequently, these proteins will be inserted into the PPM and traffic further to the PVM (Mesen-Ramirez et al. 2016). To enter the RBC, PNEPs and PEXEL proteins must cross the PVM. This membrane contains pores that allow free passage of metabolites up to 1,4 kDa (Desai and Rosenberg 1997). However, exported parasite proteins do not passively cross the PVM because they need a translocon complex. Hence, the *Plasmodium* translocon of exported proteins (PTEX), a ~1.6 mega dalton proteinaceous complex, allows proteins to cross the PVM in an unfolded state. *P. falciparum*'s PTEX complex comprises five components that include the AAA+ ATPase heat shock protein 101 (HSP101), the exported protein 2 (EXP2) and the PTEX150 as core components. Thioredoxin 2 (TRX2) and PTEX88 represent two additional components of the complex (Figure 3) (de Koning-Ward et al. 2009; Ho et al. 2018). The *P. berghei* TRX2 and the *P. falciparum* PTEX88 appeared to be nonessential for the parasite survival whereas knockouts of HSP101, EXP2 and PTEX150 have not been successful, suggesting that these proteins are essential for the survival of the parasite. Knockdown of HSP101 and PTEX150 expression provided the first functional evidence that the PTEX complex plays an important role in the export of PEXEL and PNEPs proteins (Beck et al. 2014; Elsworth et al. 2014; Garten et al. 2018; Matthews et al. 2013; Matz, Matuschewski, and Kooij 2013).

HSP101 is the PTEX motor made of six protomers utilising ATP to unfold and drive protein translocation across the PVM. Moreover, EXP2 made of seven protomers, oligomerises to form a funnel-shape structure through the PVM facing the PV and expanded until the RBC cytoplasm. At the PV side, the EXP2 oligomer is tied with the HSP101 hexamer through seven protomers of PTEX150, which provides a protected path to the cargo moving from HSP101 to EXP2. Consequently, the core components of the PTEX complex is made of the following promoters configuration 7 EXP2: 7 PTEX150: 6 HSP101 (Ho et al. 2018). TRX2 is predicted to play a role in reducing disulfide bonds of proteins during translocation. PTEX88 engages with chaperones

and another complex at the PVM named as exported protein-interacting complex (EPIC) (Figure 3). This complex at the PVM interacts with PfEMP1 and contributes to cytoadhesion properties and thus virulence of *P. falciparum*-infected RBCs (Batinovic et al. 2017; Chisholm et al. 2018). Therefore, PTEX88 likely contributes to the delivery of cargo that initially interacts with the EPIC complex to HSP101. Additionally, PTEX88 contributes to maintaining the cargo in a competent transport state whilst awaiting translocation (Matthews, Pitman, and de Koning-Ward 2019).

1.4.3 Transport of proteins in the host cell cytoplasm.

Upon access of exported parasite proteins to the RBC cytoplasm through crossing the PVM, these proteins must be trafficked to their final subcellular localizations, where they play their function. There are three main possible destinations for exported proteins within the infected RBC (iRBC): the RBC plasma membrane (PM) and the host cytoskeleton, the membrane-bound organelles called Maurer's clefts (MCs), and the RBC cytoplasm as soluble proteins (Figure 3). Proteins that are exported to the RBC plasma membrane appear to transit through the RBC cytoplasm as chaperone-associated transport complexes (Knuepfer et al. 2005). These chaperoned complexes made of PfHsp40s and exported proteins en route to their final destination are named J-dots (Kulzer et al. 2010). Exported proteins that remained in the RBC cytoplasm as their final destination are still poorly understood. However, PfHsp70-x, which is a parasite-exported protein, appears to form a complex with PfHsp40 within J-dots and thus localized in the RBC cytoplasm as a chaperoned complex. PfEMP1 associates with J-dots and HSP70-x in the erythrocyte cytoplasm before its insertion into erythrocyte PM to promote cytoadhesion of iRBCs on various receptors. This observation supports the concept that chaperones are engaged in the trafficking of PfEMP1 to MCs. (Kulzer et al. 2012). Another destination of proteins is Maurer's Clefts (MCs) which are flat and lamellae-shaped structures with translucent lumen connected to the erythrocyte membrane by tubular tethers. These closed cisternal compartments are the final location for some proteins and function as a sorting organelle for proteins *en route* to the RBC membrane. (Lanzer et al. 2006). Several proteins such REX1, SBP1 and PTP1 in the Maurer's clefts have essential roles in shaping these organelles and in the effective delivery of protein cargo to the RBC plasma membrane (Cooke et al. 2006; McHugh et al. 2015; Rug et al. 2014). Finally, proteins that remained in the RBC cytoplasm are not fully identified.

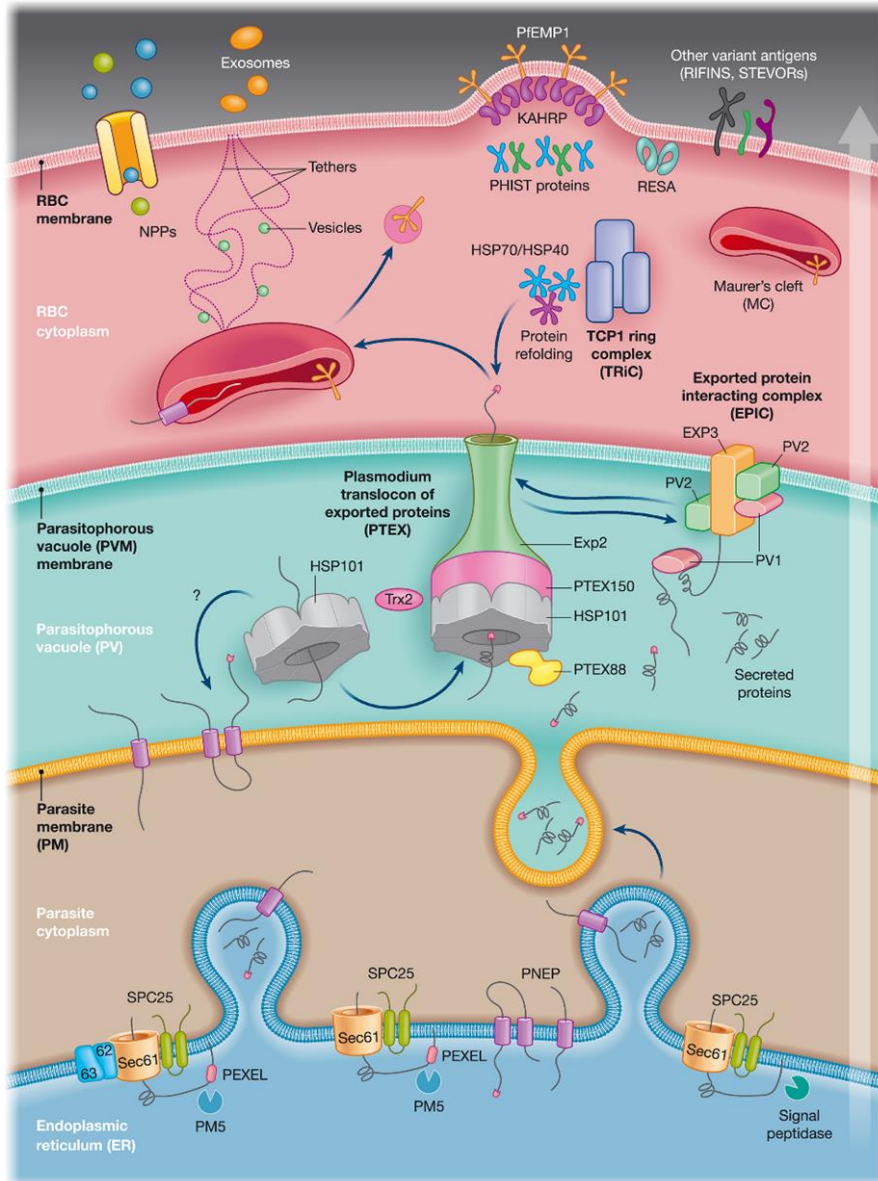


Figure 3: Schematic of the protein trafficking in *Plasmodium falciparum*-infected erythrocyte. Recognition of exported proteins begins at the endoplasmic reticulum (ER) through the Sec61/SPC25 pathway. Proteins destined to be exported to the host are released from the ER via cleavage of the *Plasmodium* export element (PEXEL) motif by the plasmepsin 5 protein, thereby initiating the export process. Soluble mature PEXEL proteins are loaded into the parasitophorous vacuole (PV). PEXEL proteins containing transmembrane (TM) domains and PEXEL-negative exported proteins (PNEPs) may be trafficked to the PV either as soluble chaperoned complexes or inserted into the parasite plasma membrane. Regardless of how cargo enters the PV, all trafficking pathways converge at the PV membrane (PVM). The *Plasmodium* translocon of exported proteins (PTEX) complex provides a portal through the EXP2 at the PVM and an energy force

motor protein (HSP101) to drive protein translocation. The PTEX150 protein serves a structural role in the PTEX complex. TRX2 and PTEX88 are accessory PTEX components that interact with the Exported Protein-Interacting Complex (EPIC), a complex that contributes to efficient cytoadherence and parasite virulence. Upon entry into the host cytoplasm, proteins are refolded with the help of parasite and/or host HSP70/40 proteins or the host TCP1 ring complex before being delivered to their final destinations at the Maurer's cleft or red blood cell membrane. HSP: heat shock protein; Sec61: Sec translocon 61; SPC25: signal peptidase complex (Matthews, Pitman, and de Koning-Ward 2019)

1.5 *Plasmodium falciparum*-induced host cell modifications and role of exported proteins in these renovations.

Understanding the parasite-induced host cell modifications requires the comprehension of the function and properties of the human RBC. Erythrocytes are simple 'sack' of haemoglobin, which are specialized in the transport of O₂ and CO₂ to human tissues. In their terminal differentiation, they lose their nucleus and their ability to synthesize new proteins. However, during their lifespan (120 days), their cytoskeleton enables them to move to different tissues through the blood circulation without any repair. To reach the inter-endothelial junctions (1–2 μm) that separate the splenic cords and venous sinuses, RBCs undergo remarkable deformation without fragmentation (An and Mohandas 2008). Three main components of the mature human erythrocyte are essential for the intracellular development of the parasite. These components include the plasma membrane, membrane skeleton (cytoskeleton), and cytosol. *P. falciparum* invades and develop within erythrocytes and undergo the ring, trophozoite and schizonts stages over a period ~48 hrs (Figure 4). This habitat represents a challenging environment for the parasite. Consequently, the parasite remodels the host to ensure its survival and propagation during its intraerythrocytic development. Upon completion of the intraerythrocytic cycle, ~16–32 merozoites are released from the RBC, and the infected RBC membrane and cytoskeleton are demolished. Each stage of the blood-stage development, thus, has its necessities, and through renovating the host cell, *P. falciparum* achieves those demands. Parasite exported proteins play a vital function in fulfilling different blood-stage growth necessities (Warncke and Beck 2019). These necessities, referred to as host cell modifications, will be discussed in detail in the subsequent sections.

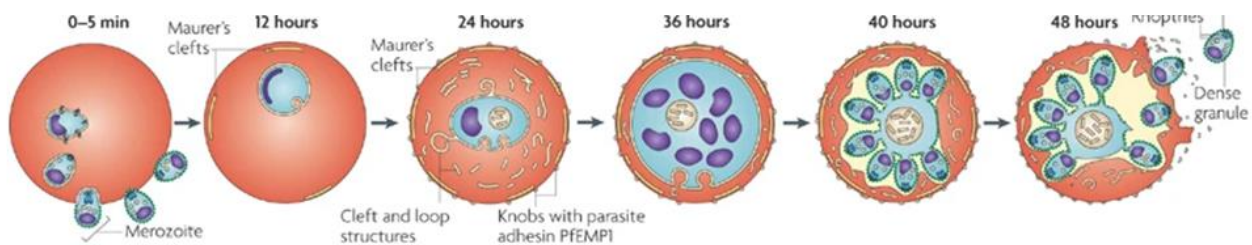


Figure 4: Development of *Plasmodium falciparum* in human erythrocytes. The parasite form known as merozoite attaches to and invades mature erythrocyte and develops in a parasitophorous vacuole over the ring (0–24 hours), trophozoite (24–36 hours) and schizont stages (40–48 hours) during the blood-stage development (Maier et al. 2009).

1.5.1 Host cell modifications during the invasion and ring stages.

Invasion of erythrocyte by the parasite is a fast and well-organised process that is completed within the first 5 min (Figure 3). The merozoite surface protein 1 (MSP1) mediates the primary binding between merozoites and the RBC plasma membrane. This contact is followed by the reorientation of the merozoite and stronger binding of the *P. falciparum* reticulocyte-binding (PfRh) protein to the complement receptor 1 (CR1) or to glycophorin A, B, or C on the RBC surface (Cowman et al. 2017). The merozoite pushes itself into a growing membrane sack through an actinomyosin-dependent force and a concerted interplay of proteins secretion. This sack which is thought to originate from the RBC plasma membrane, form the PVM in which the parasite develops during the intraerythrocytic life cycle (Koch and Baum 2016; Matz, Beck, and Blackman 2020). The majority of the host cytoskeleton remodelling happens during the contact phase between the merozoite and the RBC to smoothing the parasite's entry and the formation of the PVM. Upon successful invasion, the erythrocyte membrane is resealed and the cytoskeleton reinstated, thus, suggesting that the cytoskeleton modifications are reversible and non-destructive during the invasion. (Dasgupta et al. 2014).

1.5.1.1 Parasitophorous vacuole biogenesis and function.

The origin of the PVM has been widely investigated. However, this parasite's shelter and its rapid generation pose particular challenges to unravel its composition fully (Figure 5A). Nonetheless, fluorescent lipophilic probes introduced into the RBC membrane have been shown to be incorporated into the nascent vacuole. In addition, incorporated fluorescent lipids from the parasite were reported to be transferred to the vacuole, indicating that the host and parasite's membrane lipids contribute to the biogenesis of the PVM in iRBCs (Mikkelsen et al. 1988; Ward, Miller, and Dvorak 1993). The well-studied and abundant protein of the PVM is EXP1 which has emerged to have an essential function in the spatial organization of proteins embedded in the PVM (Matz, Beck, and Blackman 2020). Also, EXP1 was shown to function as a glutathione transferase (GST) because of its ability to detoxify haem *in vitro*, thereby supporting its redox protection function (Lisewski et al. 2014). A subsequent *in vivo* study showed that the GST activity of EXP1 is not critical for parasite growth and reported its implication in the parasite's uptake of nutrients across the PVM. However, it appeared that this protein does not contribute to protein export (Mesen-Ramirez et al. 2019).

1.5.1.2 Formation of a tubovesicular network (TVN) and its function.

The PV increases in size and complexity with parasite maturation, thereby leading to the development of large membranous loop extensions and whorls that originate from the PVM and extend far into the erythrocyte cytoplasm to form the tubulovesicular network (TVN) (Behari and Haldar 1994). Additionally, membranous tubules link the vacuole-derived vesicular structures and the whorls, indicating that the TVN is a convoluted and contiguous system of the PVM (**Figure 5B**). *P. falciparum* TVN is primarily comprised of large double-membrane whorls that occupy portions or the entire RBC's cytoplasm (Hanssen et al. 2010). The presence of TVN-derived rim-like compartments (autonomous double-membrane vesicles) in the host cytoplasm implicate the TVN to play a role as a 'molecular garbage bin' for incorrectly folded export cargo proteins. Furthermore, the *P. falciparum* TVN was shown to be involved in the sequestration of export- incompetent cargo proteins. The sequestered cargo contains proteins that have failed to unfold or which are not ready for export. Consequently, suggesting an essential role of the TVN to prevent the protein translocation machinery's exhaustion (Charnaud et al. 2018).

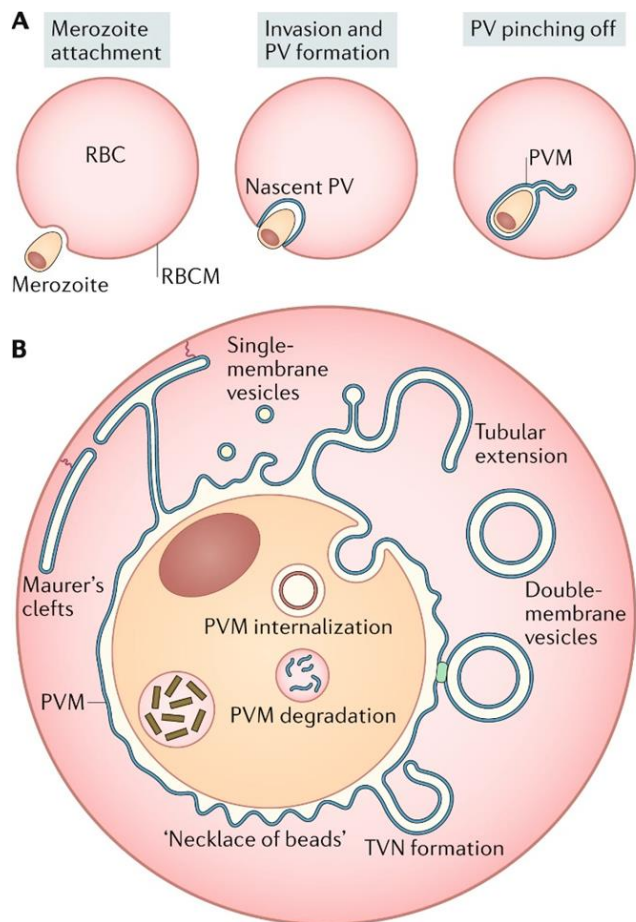


Figure 5: Biogenesis of the parasitophorous vacuole and the tubovesicular network. A) The merozoite induces invagination of the red blood cell membrane during the invasion. Active merozoite motility and subsequent membrane division result in the parasitophorous vacuole membrane (PVM) (blue) formation. B) Remodelling and trafficking of the PVM. The vacuole can form a continuous space around the parasite. The frequently observed 'necklace of beads' morphology reveals a constriction zone between the parasite and the PVM. Membrane whorls emerge from the PVM and envelop the erythrocyte cytoplasm, resulting in the formation of the tubovesicular network (TVN) and the release of double-membrane vesicles. The TVN also features distinct junctional sites (green) and partially interconnected tubular and vesicular compartments. (Matz, Beck, and Blackman 2020).

1.5.2 Host cell remodelling during the transition from ring to trophozoite stage.

Few hours after the invasion, the parasite establishes a fully functional protein-trafficking machinery and pathway, allowing the transport of its proteins to numerous localizations within the iRBC (Warncke and Beck 2019). At around 16 to 24 h post-infection, the transition from ring to trophozoite stage occurs and is marked by many changes in the infected erythrocyte. Exported proteins allow the parasite to change the properties and the structure cytoskeleton. These changes occur to prepare the growth and the formation of merozoites and to avoid splenic clearance through cytoadhesion. The changes known as parasite-induced host cell modifications with various proteins involved are described in detail as follow:

1.5.2.1 Formation and tethering of Maurer's Clefts (MC) to the host cell plasma membrane.

During the ring stage, structures such as Maurer's Clefts (MC) and other components are generated by the parasite. MCs are flat and lamellae-shaped organelles with a translucent lumen in the cytoplasm of infected erythrocytes (Lanzer et al. 2006). The structures are thought to arise from the PVM or the TVN. Their formation is completed during the early trophozoite stage (20-24 hours post-invasion) when they become tethered to the erythrocyte membrane or cytoskeleton through proteinaceous anchors. Tethering of MCs to the cytoskeleton is mainly mediated by a small exported protein called MC-associated histidine-rich protein 2 (MAHRP2) (Pachlatko et al. 2010; Tilley et al. 2008). Several proteins are exported to the Maurer's cleft, where they are kept until being further trafficked when needed to their final destination. Maurer's clefts appear to be more prominent during the ring stage than in the trophozoite stage, indicating a possible role as storage organelles within the iRBC (Mundwiler-Pachlatko and Beck 2013). At the MCs, Pf332 and the PfEMP1 transport protein 1 (PfPTP1) proteins have been found to be necessary for the attachment of the remodelled actin filament to the cytoskeleton. The skeleton-binding protein 1 (SBP1) protein, an MC-resident marker, shares almost the same expression profile and localization with Pf332 and PfPTP1. It was postulated that these three proteins form a complex at the MCs (Rug et al. 2014; Nilsson et al. 2012). Also, SBP1 has been suggested to play a role in linking Maurer's clefts to the erythrocyte membrane skeleton (Maier et al. 2007). Another MC protein, the parasite-infected erythrocyte surface protein 2 (PIESP2), has been shown to interact with the MC-associated histidine-rich protein 1 (MAHRP1), Pf332 and SBP1 (Figure 6) (Tilley et al. 2008; Zhang, Faou, et al. 2018).

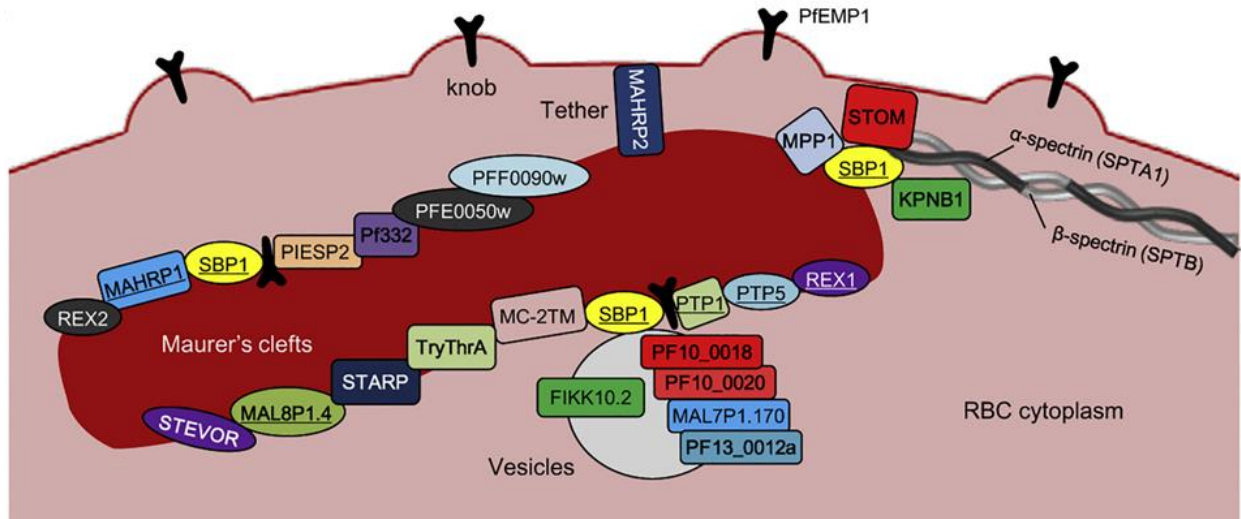


Figure 6: Structure of a Maurer's cleft and its protein contents. Overview of the protein-protein interactions at the MCs uncovered by the SBP1 interactomes (Takano et al. 2019).

1.5.2.2 New permeability pathway (NPP).

Because of erythrocytes' limited anabolic activity, *P. falciparum* struggles to obtain enough nutrients for its biomass production. Consequently, the parasite digests the host haemoglobin to supply its amino acid demand (Liu et al. 2006). However, isoleucine is absent from human haemoglobin. Nutrients and numerous other amino acids are not well-distributed in the erythrocyte as well (Baumeister et al. 2010). Hence, the parasite obtains extra metabolites from the bloodstream by establishing the so-called new permeability pathways (NPP), mainly facilitated by nutrient transporters at the erythrocyte surface (Figure 7) (Baumeister et al. 2006; Matz, Beck, and Blackman 2020). Members of the high-molecular-weight protein family (RhopH) are released from the rhoptries during the invasion and are then present throughout the whole blood-stage growth at the infected erythrocytes periphery, thereby playing a role in nutrient uptake (Counihan et al. 2017; Sherling et al. 2017; Vincensini et al. 2008). After traversing the erythrocyte membrane, imported nutrients must cross the PVM in order to reach the parasite. Monosaccharides and amino acids smaller than ~1400 Da with an effective pore diameter of 23 Å can efficiently traverse the PVM (Desai, Krogstad, and McCleskey 1993; Desai and Rosenberg 1997). EXP2 of the PTEX complex at the PVM appears to form both a nutrient pore and a protein conducting channel (Garten et al. 2018). A rhoptry protein known as RON3 is secreted into the PV during *P. falciparum* invasion, and appears to be vital for protein export and small-molecule transport (Low et al. 2019).

Additionally, genetic inactivation of EXP1 impaired nutrient permeation at the PVM and led to parasite death, but most unexpectedly did not impact protein export, thereby supporting the role of EXP1 in nutrients uptake across the PVM (Figure 7B) (Mesen-Ramirez et al. 2019). The cation ATPase PfATP4, a Na⁺ efflux pump located at the parasite's plasma membrane (PPM), maintains Na⁺ homeostasis in the parasite cytoplasm exporting Na⁺ whilst importing H⁺ ions. Consequently, PfATP4 was reported to supply the parasite with Na⁺ ions imported through the RhopH2-regulated new permeability pathways (Figure 7A) (Spillman et al. 2013; Spillman and Kirk 2015; Gilson et al. 2019).

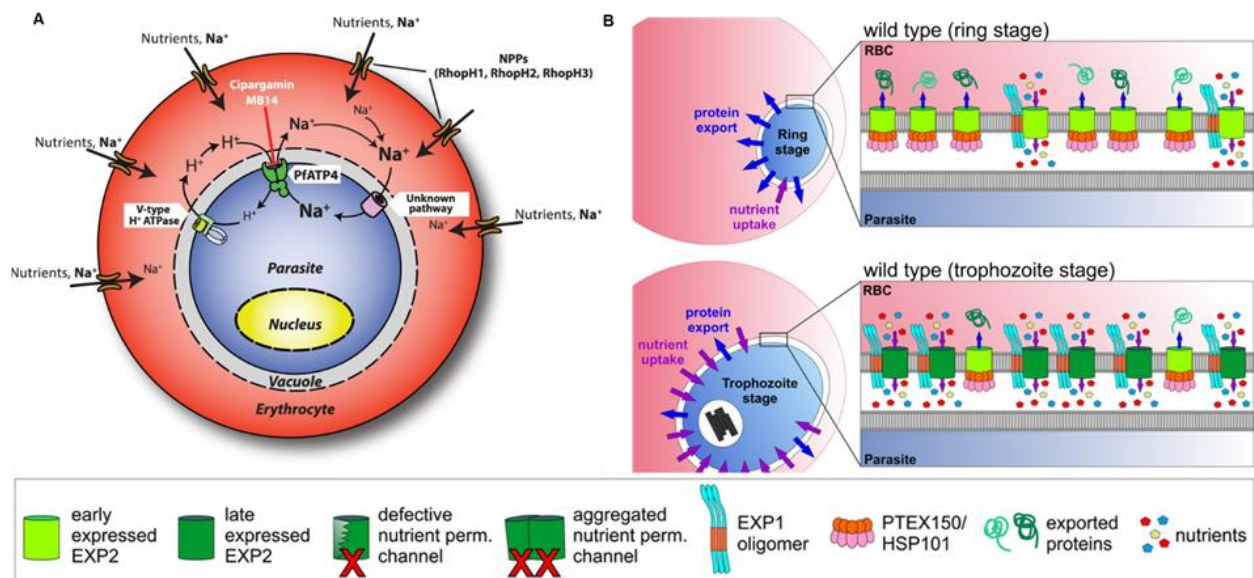


Figure 7: New Permeability Pathways (NPP) in the infected erythrocyte. A) NPP at the erythrocyte plasma membrane mainly mediated by RhopH1, RhopH2 and RhopH3 proteins. PfATP4 at the PPM supplies the parasite with Na⁺ ions mainly imported through the NPP (Gilson et al. 2019). B) Nutrients uptake across the PVM mainly facilitated by EXP2 of the PTEX complex and EXP1 (Mesen-Ramirez et al. 2019).

1.5.2.3 Altered deformability of the infected erythrocytes.

The RBC cytoskeleton's structural integrity and deformability are essential for the survival of the parasite and are stage-specifically controlled during each life cycle stage. A temporary increase in infected erythrocyte deformability during invasion is required but is quickly reverted to the original state upon successful entry of the parasite (Warncke and Beck 2019). There is limited cytoskeleton rigidification during the ring stage, mainly attributed to the interaction of RESA with the spectrin network (Mills et al. 2007). However, this appears not to be enough as infected erythrocytes circulate and pass through the spleen despite the reduced deformability (Nash et al.

1989). Over the late stages of the intraerythrocytic development, the shape of iRBCs changes and the deformability decreases, thereby allowing them to sequester to the endothelial capillary linings. Also, the parasite's metabolic products exert oxidative stress, which enhances the rigidification of the infected erythrocyte's cytoskeleton (Dondorp et al. 2000; Nash et al. 1989). Depletion of several exported proteins such as RESA, PFB0920w, GBP130, PF13_0073 and PTP3 showed a significant increase in membrane rigidity, thereby suggesting their implication in the resulting altered deformability of iRBCs during the *P. falciparum* infection (Silva et al. 2005; Maier et al. 2008).

1.5.2.4 J-dots and chaperones in the host cell remodelling.

Chaperones in a typical cellular environment play the role of preventing aggregation or misfolding of nascent polypeptides, thereby maintaining the entire proteome's integrity. *P. falciparum*'s genome encodes for many chaperones, including the Hsp90, Hsp70, Hsp60, and Hsp40 family members of heat shock proteins that were upregulated in the infected erythrocyte. (Watanabe 1997; Das et al. 1997; Kumar et al. 1991; Banumathy et al. 2003). The Hsp40 chaperones are classified into four types (I to IV), of which numerous are exported. These parasite's exported chaperones play essential functions in cellular processes such as protein translocation, folding, degradation, and translation, thus highlighting their importance in the parasite's biology (Botha, Pesce, and Blatch 2007). Hsp40s contain a highly conserved DnaJ domain and, in other systems, are molecular co-chaperones of Hsp70s (Hennessy et al. 2005). The *P. falciparum*-encoded exported Hsp70/Hsp40 chaperone/co-chaperone, and seven PHISTb proteins contain a DnaJ domain through which they interact with or recruit parasite proteins to contribute to the host cell renovation process (Gilson et al. 2017; Kulzer et al. 2012; Kulzer et al. 2010). A recombinant Hsp40 (PFA0660w) was found to significantly stimulate the ATPase activity of PfHsp70-x but not the *Plasmodium* Hsp70 (PfHsp70-1) or the human Hsp70, suggesting that the interaction of PFA0660w with PfHsp70-x most likely represent a co-chaperone/chaperone interaction (Daniyan et al. 2016). In addition, a study revealed that the SBD domain of PfHsp70-1 is important for several functional features of this molecular chaperone and that this protein facilitates the folding of plasmodial proteins (Lebepe et al. 2020). Moreover, PfHsp70-x was shown to support the parasite growth under elevated temperature conditions and especially when most of the host cell renovation takes place at the beginning of the parasite life cycle (Day et al. 2019). The exported PfHsp70-x and PfHsp40 chaperones (PFE0055c, PFA0660w) are present as large complexes with numerous other exported proteins in intracellular structures known as J-dots (Figure 8A) (Zhang et al. 2017; Kulzer et al. 2012). J-dots were shown to be implicated in the trafficking of

proteins from Maurer's clefts to the iRBC plasma membrane (Boddey and Cowman 2013). PfHsp70-x and PfHsp40s co-localized with PfEMP1, and depletion of PfHsp70-x delayed the export of PfEMP1, suggesting a role of these chaperones in the transport of PfEMP1 to the host cell plasma membrane. In addition, RBCs infected with parasite line deficient in Hsp70-x exhibited higher retention rates in microfiltration, indicating a decreased deformability, thus implying that chaperones might play a role in the renovation of the host cell cytoskeleton (Charnaud et al. 2017). Recently, inactivation of an exported Hsp40 member named PFA66 led to aberrant knob morphology on the iRBC surface, disrupted presentation of the cytoadherence molecule PfEMP1, and a lack of cytoadherence, despite the presence of the knob associated protein KAHRP (Diehl et al. 2021).

1.5.2.5 Reorganization of the infected erythrocyte cytoskeleton.

The parasite starts to export proteins into the host cell minutes after the invasion and throughout the whole blood-stage development (Boddey and Cowman 2013). The ring-infected erythrocyte surface antigen (RESA) protein from the *Plasmodium* helical interspersed subtelomeric (PHIST) multigene families is one of the first exported proteins discharged from dense granules into the PV and then exported to the erythrocyte cytoskeleton. Malaria pathology is associated with fever episodes due to the rupture of iRBCs. As temperature increases, the stability of the RBC's spectrin network decreases. Therefore, binding of RESA to the repeat 16 of β -spectrin provides protection against the thermal denaturation of the infected erythrocyte (Pei, Guo, Coppel, Bhattacharjee, et al. 2007; Silva et al. 2005). RESA seems to protect and stabilize the iRBC cytoskeleton against thermally-induced denaturation during the ring stage and might not be required any longer during the trophozoite stage. The transition from ring to trophozoite stage is marked by the binding of MESA (also known as PfEMP2) to the spectrin-actin network stabilizing protein of RBCs named band 4.1R (Lustigman et al. 1990). MESA and 13 exported parasite proteins were found to contain a band 4.1R-binding motif suggesting that MESA is likely not the only protein involved in renovating the cytoskeleton infected erythrocytes (Kilili and LaCount 2011). The large and highly charged *Plasmodium falciparum* erythrocyte plasma membrane 3 (PfEMP3) protein was shown to be associated with iRBC cytoskeleton (Pasloske et al. 1993). Through its 60-residue fragment, this protein binds to spectrin at a 4.1R protein junction, thereby probably contributing to the loss of the deformability of the membrane in the late stage of parasite development (Figure 8A) (Pei, Guo, Coppel, Mohandas, et al. 2007).

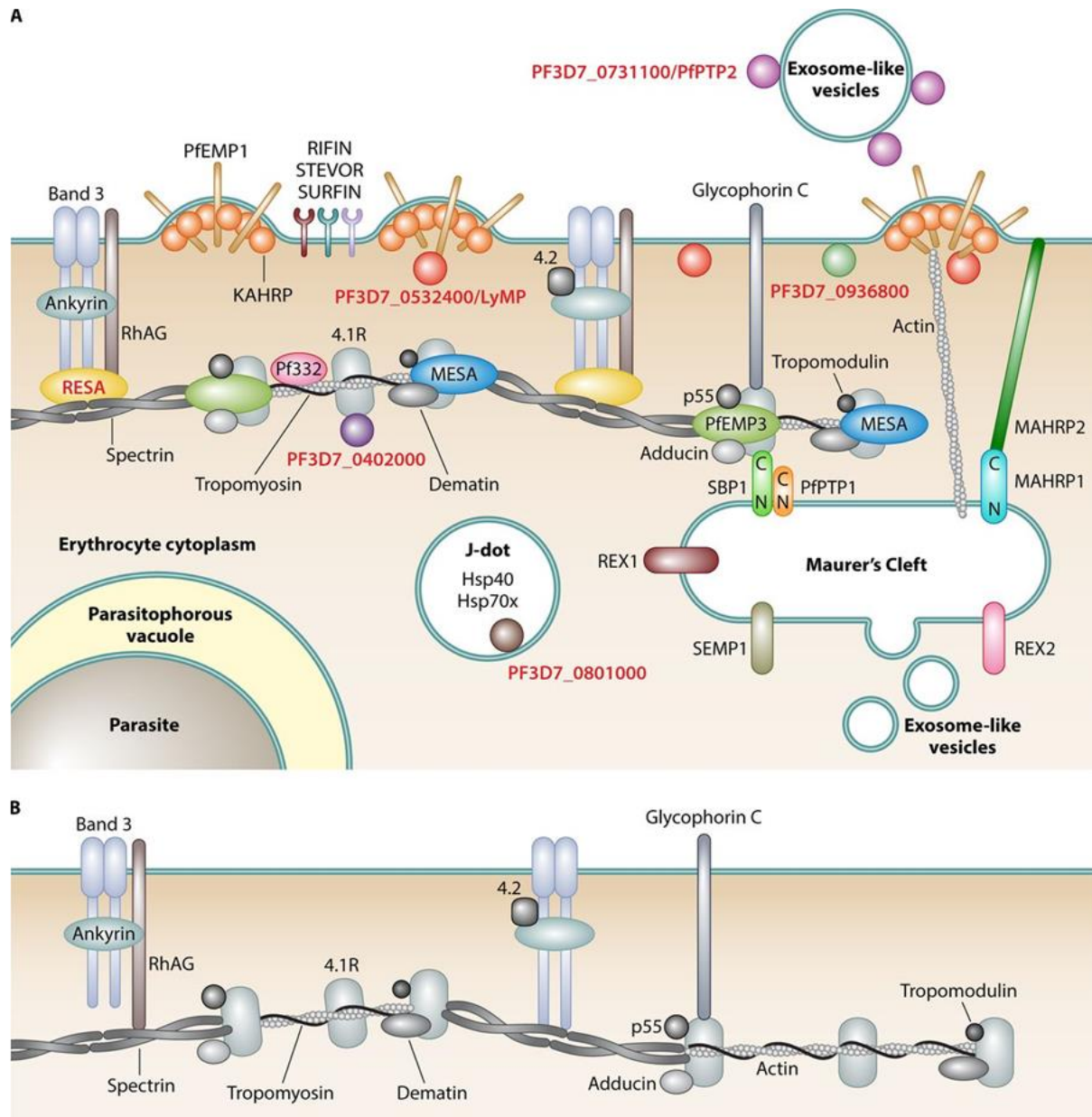


Figure 8: Various host cell modifications. A) infected erythrocyte displaying its renovation. B) Uninfected erythrocyte cytoskeleton (Warncke, Vakonakis, and Beck 2016).

1.5.2.6 Formation of knobs on the iRBC plasma membrane.

Approximately 20 hours post-invasion (hpi), electron-dense layers protrusions known as knobs begin to form underneath the infected erythrocyte membrane. A spiral scaffold underlies these membrane elevations which are made of a protein complex mainly dominated by the knob-associated histidine-rich protein (KAHRP) (Watermeyer et al. 2016; Rug et al. 2006). KAHRP is

essential for knob formation (Crabb et al. 1997) and was found to self-assemble underneath the iRBC membrane as well as to bind spectrin, actin, and band 4.1R (Looker et al. 2019). Probably, the primary function of knobs is to anchor the PfEMP1 protein, which accumulates at around 16 to 20h hpi at the iRBC surface. PfEMP1 mediates the adhesion of iRBCs to endothelium receptors. Sequestration of infected erythrocytes is connected to severe malaria, making PfEMP1 the main virulence factor of malaria (Wahlgren, Goel, and Akhouri 2017a). Knobs were reported to contain 3.3 ± 1.7 PfEMP1 molecules, principally placed on the knobs' tip in infected erythrocytes (Sanchez et al. 2019). Several other exported proteins localize close to the knobs and might play a role in maintaining the structural integrity and shape of knobs. These exported proteins are linked to the host cytoskeleton through the PHIST proteins. A protein of the PHIST family known as PFI1780w (LyMP) has been shown to only interact with the acidic terminal segment (ATS) domains of PfEMP1, whereas PFE1605w interacts with ATS domains and band 3 of the iRBC cytoskeleton (Oberli et al. 2016; Warncke and Beck 2019). As shown in Figure 9, the knob assembly complex formation requires a concerted array of parasite exported proteins which remain, up to this date, not all identified. Therefore, future in-depth studies are required to resolve the biological process underlying the formation of knobs on the iRBCs surface.

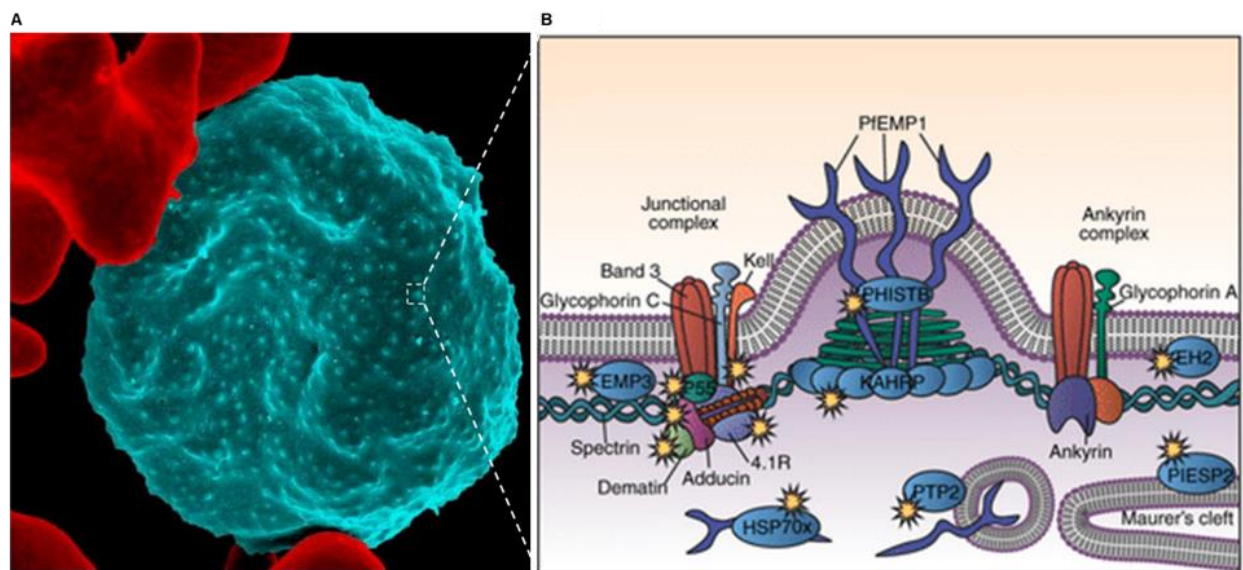


Figure 9: Structure of knobs in the infected erythrocyte. A) Colourized (blue) scanning electron microscopy picture of red blood cell infected with the malaria parasite in the image area's centre. To the left are uninfected cells with smooth red surfaces coloured in red (NIH 2020). B) Model of the final knob assembly complex characterized by high protein density due to KAHRP self-association and the formation of spiral assemblies. PHIST proteins may further connect PfEMP1 and the cytoskeleton. The yellow stars represent the FIKK4.1 kinase substrates identified by mass spectrometry (Davies et al. 2020).

1.5.2.7 Cytoadhesion and immune evasion of iRBCs.

PfEMP1 mainly mediates the cytoadhesion iRBCs. This process seems to increase underflow conditions when the parasite matures over its late intraerythrocytic development stages (Dasanna et al. 2017). The PfEMP1 antigen is made of three core regions. The acidic terminal segment (ATS) at the cytoplasmic tail, which anchors the protein into the knobs. A transmembrane (TM) region that traverses the iRBC membrane (Waller et al. 1999). Finally, the cysteine-rich interdomain regions (CIDRs) and an N-terminal segment composed of Duffy-binding-like domains (DBLs), which mediate the binding to various receptors such as CSA, ICAM and EPCR (Figure 8A) (Smith 2014). Per genome, PfEMP1 is encoded by ~60 copies of var multigene family, of which only one is expressed (Fernandez et al. 2002). This contributes to a constant antigenic variation, thus enabling *P. falciparum* to evade the host's immune system. In many parasites, PfEMP1 is expressed together with the repetitive interspersed family (RIFIN) proteins and/or subtelomeric variable open reading frame (STEVOR) family, consequently indicating these adhesins collectively induce the sequestration of iRBCs (Wahlgren, Goel, and Akhouri 2017b). RIFIN and STEVOR proteins contain a basic terminal segment (BTS) in their C termini and are both rich in cysteine residues (Joannin et al. 2011).

Similarly to RIFINs, STEVORs seem to affect the RBC membrane deformability (Sanyal et al. 2012). Additionally, RIFINs adhere to iRBCs by binding to sialic acids on glycophorin A while STEVORs bind to glycophorin C. Furthermore, RIFINs have been shown to mediate rosetting, a process by which iRBC adheres to multiple uninfected RBCs in order to evade the host immune system (Figure 8C) (Goel et al. 2015; Mancio-Silva and Mota 2015). PfEMP1 is primarily expressed at the late stages (trophozoite and schizont), whereas RIFINs and STEVORs are expressed at different stages of parasite development. RIFINs are mainly expressed during the merozoite and late schizont stages. Interestingly, PfEMP1 is downregulated in gametocytes whilst both RIFINs and STEVORs are expressed commonly (Tiburcio et al. 2013). Among the ~150 variants of RIFIN and STEVOR proteins, only a few of them have been studied so far. Consequently, future studies are required to resolve and unravel their function in the parasite's survival mechanism (Wahlgren, Goel, and Akhouri 2017b).

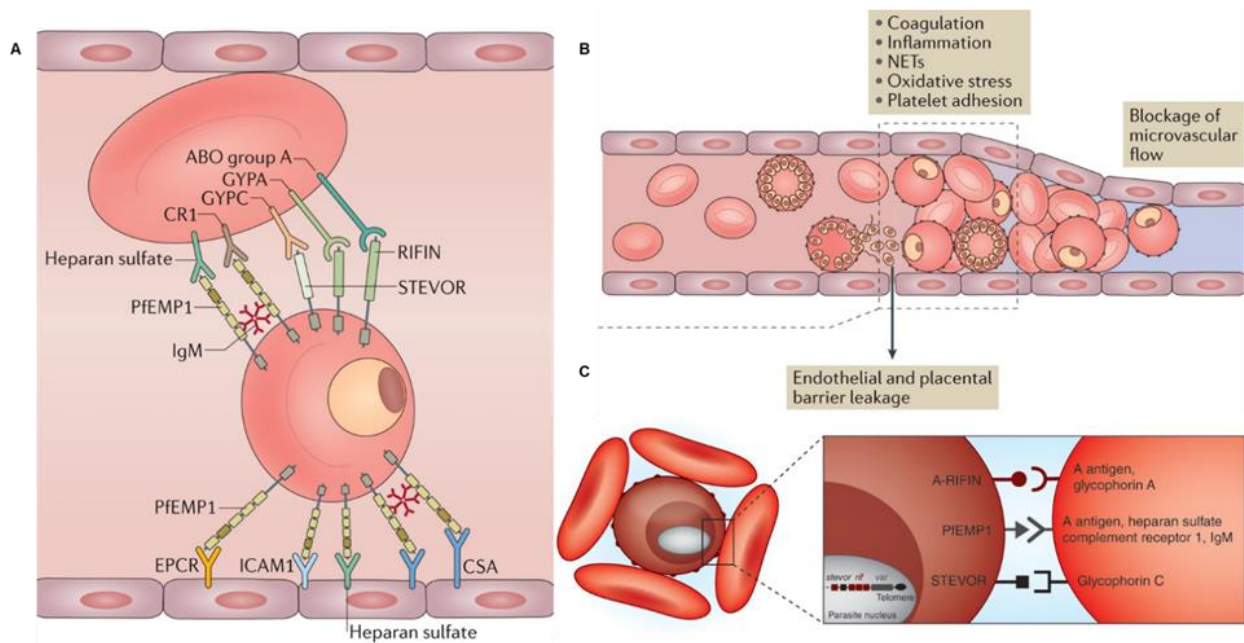


Figure 10: Cytoshesion of infected erythrocytes on various receptors. A, B) Binding of iRBCs to human endothelium receptors in the microvasculature is mediated by PfEMP1, RIFIN and STEVOR proteins. Through PfEMP1, infected erythrocytes that adhere to cells in the placenta bind to chondroitin sulfate A (CSA). In addition, PfEMP1 is known to interact with such as immunoglobulin M (IgM) and many other receptors such as heparan sulfate, complement receptor 1 (CR1), the intercellular adhesion molecule 1 (ICAM1) and the endothelial protein C receptor (EPCR). RIFINs are known to interact with type A blood group antigen and glycophorin A. STEVORs interact with glycophorin C. Neutrophil extracellular traps (NETs) (Wahlgren, Goel, and Akhouri 2017b). C) A-RIFIN is responsible for the rosetting phenotype (binding of iRBCs to uninfected RBCs) in A blood group. Other protein-carbohydrate interactions are thought to be possibly involved (Mancio-Silva and Mota 2015).

1.5.2.8 The parasite's exported kinases involved in the Host cell remodelling.

P. falciparum exports into the host cell some of its kinases. At least 20 parasite kinases mostly belonging to the FIKK family are thought to be exported (Nunes et al. 2007). The FIKK4.1 was shown to regulate the rigidification of the RBC cytoskeleton and trafficking of PfEMP1. This kinase associate with Maurer's clefts and was found to phosphorylate *in vitro* the human erythrocyte cytoskeleton protein known as dematin (Figure 9B) (Davies et al. 2020; Nunes et al. 2007; Brandt and Bailey 2013). Deletion of FIKK4.2 showed reduced knob number on the iRBC surface, increased iRBCs rigidity, and impaired host cell renovation (Kats et al. 2014). The FIKK9.3, FIKK9.6 and FIKK10.1 associate with Maurer's clefts, with the FIKK10.1 being localized in the J-dots. Additionally, conditional knockout of FIKK8 impaired the parasite's growth, thus suggesting its role in the asexual proliferation of the parasite (Davies et al. 2020; Nunes et al. 2007). Several

other FIKK kinases have been shown to contribute to various host cell modifications (Adderley, Williamson, and Doerig 2021).

1.5.3 Host cell remodelling during the trophozoite and schizont stages.

As previously described above, most host cell modifications occur during the ring stage and the transition from the ring to the trophozoite stage. However, few significant changes to the host cell seem to occur during the trophozoite stage. This stage is the most metabolically active phase of the parasite during the blood-stage development, and it prepares the parasite for multiple replications and, thus, the formation of merozoites (Bannister and Mitchell 2003). Although most host cell modifications occur during the transition, many of these changes appear to continue throughout the late stages and possibly even until the egress of daughter cells. This constant renovation indicates that protein export still occurs and contribute to the maturation of the parasite within the infected erythrocyte (Warncke and Beck 2019). During the schizont stage, merozoites are formed, which later will reinvade new RBCs. Protein synthesis throughout this phase is focused on merozoite proteins required for invasion and proteins that will be stored and exported right after the invasion to initiate the host cell makeover of the new intraerythrocytic cycle (Bozdech et al. 2003). *Plasmodium falciparum* devotes 8-10% of its genome to proteins that are exported to the host cell. Several of these proteins have been shown to remarkably contribute to various host cell modifications during the intraerythrocytic parasite development (de Koning-Ward et al. 2016; Matthews, Pitman, and de Koning-Ward 2019; Maier et al. 2009). This highlights the need of exported proteins in ensuring the survival of the parasite within the erythrocytes. However, the function of a lot these proteins remain unknown due the lack of the adequate genetic system but nowadays the availability of new genetic tools enable the functional characterization of these proteins. Thus, making possible to further understand the biology of the parasite and consequently contribute to malaria eradication.

1.6 Genetic systems to study *Plasmodium falciparum* genes.

Tremendous progress has been made in the development of genetic tools to study *Plasmodium* spp. genes. The advent of transfection in the *Plasmodium falciparum* system made possible the expansion of genetic tools necessary to study the function of many parasite's genes (Wu et al. 1995; Crabb et al. 1997; Wu, Kirkman, and Wellems 1996). Since the first transfection was established, significant progress has been achieved in developing genetic systems to study *Plasmodium* spp. In 2015, de Koning-Ward and colleagues already reported more than 440 peer-

reviewed publications that have used transfection methods to successfully target ~500 *Plasmodium* genes (mainly those of *P. berghei* or *P. falciparum*) for inactivation (de Koning-Ward, Gilson, and Crabb 2015). Although this appeared to be a massive progression in characterising the *Plasmodium* spp. genome (~5,200 genes), there are still many genes that remain annotated as unknown function. Several factors have hampered a faster progression in genetic manipulations. These factors include poor transfection efficiencies, the paucity of robust selectable markers and the lack of a robust system to regulate gene expression levels (de Koning-Ward, Gilson, and Crabb 2015). However, many genetic tools have been developed and/or optimised in recent years, thereby enabling many genes' functional characterisation. Genetic tools developed or optimised over the past seven years are presented in the coming sections.

1.6.1 Direct genes' inactivation systems.

1.6.1.1 The clustered regularly interspaced short palindromic repeats/Cas9 (CRISPR/Cas9)

Previously, gene inactivation in *P. falciparum* involved lengthy cell culture periods of assessing a random integration via double or single crossover homologous recombination of an episomal plasmid, impeding fast genome manipulation efforts. Using the prokaryotic viral defence gene-editing tool known as clustered regularly interspaced short palindromic repeats (CRISPR/Cas9) has circumvented this problem because it allows scientists to specifically cleave a DNA sequence in the genome containing a protospacer-adjacent motif (PAM) (Figure 11). *Plasmodium* spp. possesses only homologous recombination (HC) as a DNA repair mechanism. Therefore, high-fidelity HC between the cleaved genomic sequence and a donor DNA template enables the integration of the donor DNA (Lee et al. 2019; Ghorbal et al. 2014). For examples, the *P. falciparum* GEXP07 protein's role in the Maurer's Cleft architecture, knob morphology, and PfEMP1 trafficking was unravelled based on its inactivation via the CRISPR/Cas9 editing tool (McHugh et al. 2020). Additionally, this editing tool was used to introduce the 3xFLAG epitope tag onto the PTEX complex, which enabled its affinity purification and consequently unravelled its native structure by cryo-electron microscopy. This understanding of the structure of the PTEX complex provided insights into the unique interactions between the HSP101, PTEX88, EXP2 and the cargo of protein ready to be translocated across the PVM (Ho et al. 2018).

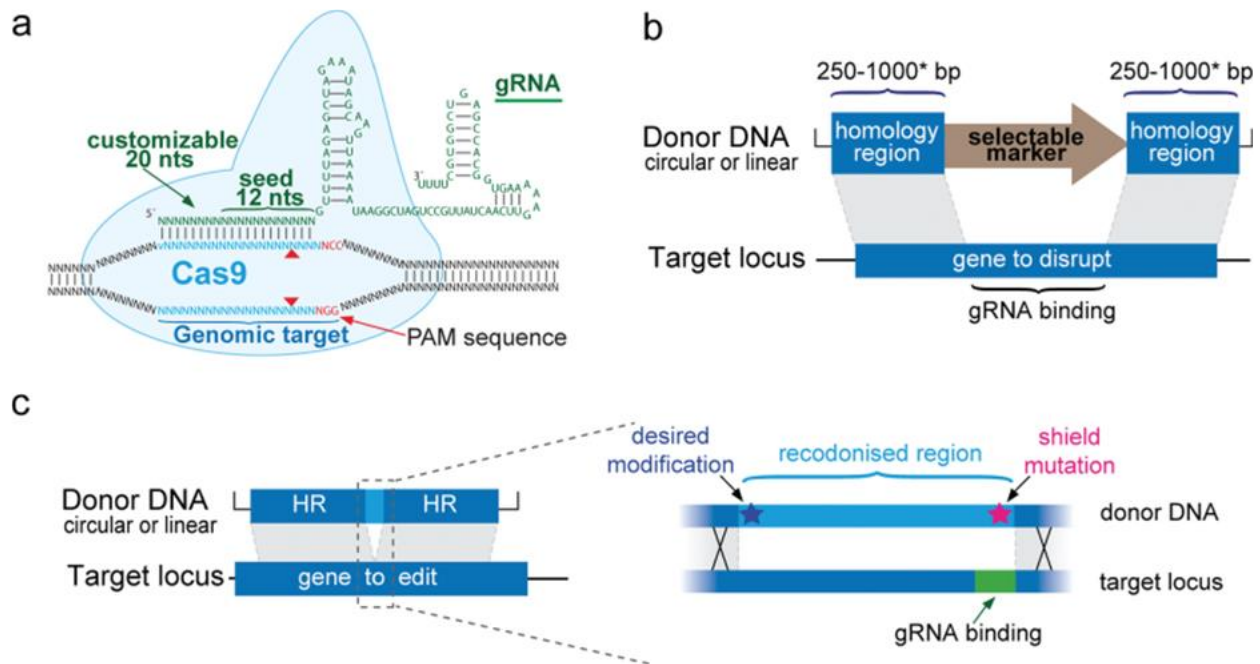


Figure 11: CRISPR/Cas9 editing system. A) The Cas9 nuclease protein is directed to a specific genomic target by the first 20 nucleotides of the guide RNA (gRNA), resulting in the generation of a double-strand break (red triangles). B) Donor design for a typical gene-inactivation approach in *P. falciparum*. C) Marker-free genome editing of a point mutation. Silent 'shield mutations' prevent Cas9-gRNA cleavage of the edited locus. (Lee et al. 2019).

1.6.1.2 Selection-linked integration (SLI) targeted gene disruption.

Over the past decades, the selection of rare integration events for the generation of parasite lines deficient of a gene of interest was time-consuming and labour-intensive. However, the recent development of the selection-linked integration (SLI) approach allowed the rapid generation of parasite mutants with targeted genomic integration events. In this approach, the targeting region on the vector does not contain a promoter and is separated from a second selectable marker by a 2A skip peptide that allows the expression of two polypeptides from one mRNA (Birnbaum et al. 2017). The additional selectable marker can only be expressed upon successfully integrating the target region on the plasmid behind the target gene's promoter. Therefore, parasites carrying correct integration can be selected using the second resistance marker, thus enabling a rapid selection of the desired parasite population. The robustness of the SLI strategy was validated through its application in genes' disruption, functional analyses of proteins, and knocking in of an allele conferring artemisinin (ART) resistance (Birnbaum et al. 2020; Birnbaum et al. 2017).

1.6.2 Conditional gene expression systems.

1.6.2.1 Glucosamine-6-phosphate activated ribozyme (*glmS*) system.

Usually, gene knockouts can only be applied to characterize nonessential genes. Conditional gene expression systems that allow inducible mRNA regulation and protein can be utilised as alternatives to studying essential genes. As shown in (Figure 12A), target genes containing in their 3' untranslated region (UTR) the glucosamine-6-phosphate activated ribozyme (*glmS*) sequence can be efficiently knocked down at the protein levels in response to a glucosamine-6-phosphate inducer (Prommana et al. 2013). This system has enabled the knockdown of essential PTEX components (HSP101 and PTEX150) proteins, thereby showing direct evidence of the PTEX complex's role and scope in proteins translocation across the PVM (Elsworth et al. 2014). In addition, this system was used to downregulate the PfSPC25 and the *P. falciparum* Plasmeprin V proteins, thus establishing their concerted interaction to license PEXEL proteins for export to the infected erythrocytes (Marapana et al. 2018).

1.6.2.2 The DiCre/*loxP* recombinase system.

Conditional gene modifications can also be achieved using the Cre recombinase, which recognizes two *loxP* sites of 34 nucleotides that flank the target gene sequence. The Cre/*loxP* system primarily involves expressing two inactive Cre polypeptide moieties fused to the FK506-binding protein 12 (FKBP) and an FKBP rapamycin-binding (FRB) protein. Upon addition of the rapamycin inducer, the two inactive Cre components get activated and dimerize (DiCre), thereby mediating the excision or inversion of the target sequence depending on the orientation of the *loxP* sites (Figure 12B) (Collins et al. 2013). Despite the robustness of the DiCre excision system, the low transfection efficiency in *P. falciparum* makes the introduction of the two *loxP* sites that flank the desired target time-consuming and labour intensive. Recently, silent synthetic introns (*loxPint*) have been developed, which allows the introduction of *loxP* sites anywhere in open reading frames without compromising the desired target protein expression (Jones et al. 2016). The large-scale quantitative phosphoproteomics of the study of Davie and colleagues leveraged the DiCre/*loxPint* innovation to conditionally delete 18 *P. falciparum* exported FIKK serine/threonine kinases. This resulted in revealing FIKK kinases' function in various host cell modifications (Davies et al. 2020).

1.6.2.3 The knock-sideways (KS) approach.

The function of desired proteins can be elucidated by using the knock-sideways (KS) approach. In this approach, the target is fused with FKBP, and the FRB is fused to a signal that will mediate the mislocalization of the target in a different cellular compartment. The addition of rapamycin induces the dimerization of the FRB and FKBP, thus directing the target protein away from its usual site of action (Figure 12D). Birnbaum et al. utilised the KS approach to achieve the mislocalization of the artemisinin resistance marker PfKelch 13, thereby enabling its inactivation. Furthermore, in combination with the BioID, this approach was used to identify proteins located at the Kelch13-defined compartment essential for the parasite's survival (Birnbaum et al. 2017; Birnbaum et al. 2020).

1.6.2.4 Destabilization domain (DD) system.

Regulation of genes at the protein level can also be achieved by introducing into the target protein an unstable destabilizing domain, such as the FKBP-based destabilization domain (DD) or an *Escherichia coli* DHFR destabilizing domain (DDD) (Okombo et al. 2021). The destabilizing domains activate proteasomal degradation and thus knockdown of the target protein. Compounds such as Shield-1 for DD and trimethoprim fusion proteins for DDD are used to stabilise the complex, thereby allowing turnable expression of the target protein (Figure 12C). This conditional knockdown approach was used to identify the PfCRK4 kinase as the key cell-cycle regulator that orchestrates multiple DNA replication rounds throughout schizogony in *P. falciparum* infection (Ganter et al. 2017). Also, using the DDD, *glmS* and CRISPR/Cas9 systems, Cobb et al. showed that the *P. falciparum* exported Hsp70x is not essential for the parasite intraerythrocytic development (Cobb et al. 2017).

1.6.2.5 The TetR-DOZI aptamer system.

Protein regulation can also be achieved by hindering the transcription of a target gene. The tetracycline repressor (TetR) protein, through allosteric interaction with tetracycline or its analogue anhydrotetracycline (aTc), induces repression of transcription. This system was modified into the TetR-DOZI aptamer approach in which the TetR-DOZI fusion protein binds to a 10xTetR RNA aptamer sequences placed in the 3' untranslated region (UTR) of the target gene, thus causing the inhibition of the translation upon removal of aTc (Figure 12E) (Okombo et al. 2021). For example, the *P. falciparum* EXP1 knockdown using this system displayed profound changes in

the vacuole ultrastructure, including increased separation of the PVM from the parasite plasma membrane and abnormal membrane structures (Nessel et al. 2020).

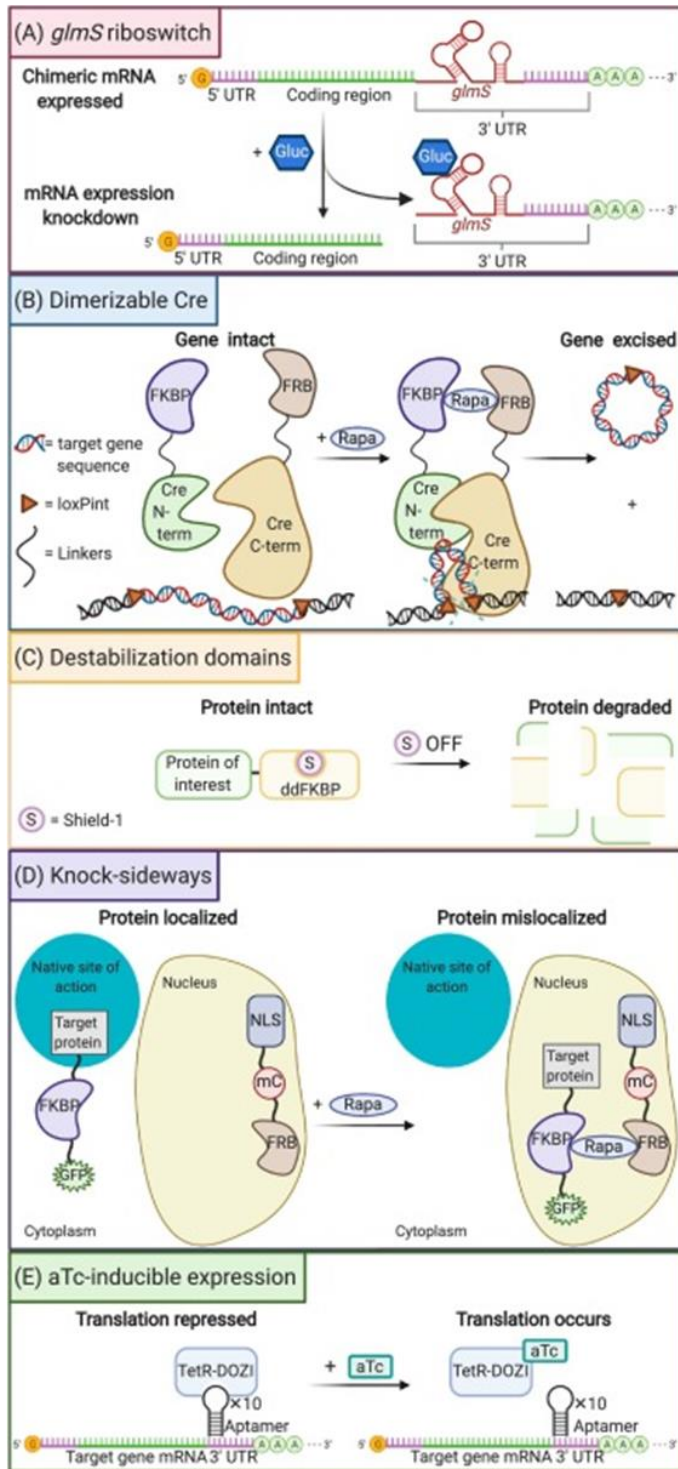


Figure 12: Schematic of genetic systems for conditional gene expression in *Plasmodium*. A) Glucosamine-6-phosphate activated ribozyme (*glmS*) system: the targeting vector construct contains the *glmS* molecule at the 3' UTR end of the target gene. Addition of glucosamine activates the *glmS* ribozyme, leading to its self cleavage and thus knockdown of the target protein. B) DiCre/*loxP* recombinase system: Rapamycin induces the FKBP12 and FRB dimerisation, leading to the excision (or inversion) of the *loxP* flanked DNA segments. C) Destabilization domain (DD) system: Shield 1-protected protein-ddFKBP fusion proteins degrade upon removal of Shield-1 and consequently knockdown of the protein. D) Knock-sideways system: FRB-mCherry fusion is localized in one subcellular compartment while the desired protein, tagged with a FKBP-GFP fusion, is elsewhere. Addition of rapamycin activates the heterodimerization of FKBP and FRB and results in mislocalization of the protein of interest. E) TetR/DOZI aTc-inducible system: Addition of the anhydrotetracycline (aTc) induces reversible allosteric interaction with the TetR/DOZI protein disrupting the TetR-DOZI– aptamer interaction, and enables mRNA expression of the target gene. Abbreviations: Rapa, rapamycin; NLS, nuclear localization signal; S, Shield-1; FRB, the binding domain of the FKBP-rapamycin-associated protein; FKBP, FK506-binding protein; *loxP* site encoded in a synthetic intron; mC, mCherry aTc, anhydrotetracycline; *loxPint*. (Okombo et al. 2021).

1.7 Rational and aim of the study.

Malaria is an infectious disease caused by *Plasmodium* spp., responsible for more than 387,000 deaths annually worldwide. *Plasmodium falciparum* is the most prevalent and dangerous among the five human malaria species (WHO 2020). The disease is transmitted when a female *Anopheles* mosquito injects sporozoites, which infect the liver in a human host. The parasite enters the bloodstream from the liver and infects circulating red blood cells, thereby starting the asexual intra-erythrocytic cycle. Having invaded the red blood cell, *P. falciparum* begins to renovate the erythrocyte to ensure its survival, changing the biochemical and biophysical properties of the host cell. Host cell modification is essential for parasite survival in cell culture and *in vivo* (Maier et al. 2009; Maier et al. 2008). However, such modifications are also responsible for much of the pathology associated with malaria infection. Many, if not all of these host cell modifications are mediated by parasite-encoded proteins that are exported to the host cell following parasite entry. Conservative estimates suggest that over 400 proteins are trafficked to the host cell, with more being identified every year (Matthews, Pitman, and de Koning-Ward 2019). Although much progress has been made in understanding protein transport to the *P. falciparum*-infected host cell, some fundamental questions remain unanswered, especially the role of many exported proteins in parasite survival. The identification of such proteins has been hampered in the past by the lack of a conditional knockout genetic systems in this model organism. However, recent advances in technology now allow a systematic analysis of exported proteins' essentiality (de Koning-Ward, Gilson, and Crabb 2015; Okombo et al. 2021).

In this project, we aimed to fill this knowledge gap by identifying and characterizing exported proteins essential for the parasite's survival and propagation during its blood-stage development. In reaching this objective, we used a rapid knockout strategy approach called selection linked integration targeted gene disruption (SLI-TGD) (Birnbaum et al. 2017) to quickly screen 15 selected genes that are predicted to be exported to the host cell. Additionally, the glucosamine-6-phosphate activated ribozyme (*glmS*) system was used to analyse and characterize essential genes that could not be disrupted in the SLI-TGD approach.

Objectives and work programme.

1. To determine which exported proteins are essential for the survival of the parasite. This was completed by targeting the 15 genes of interest for disruption via the selection linked integration targeted gene disruption strategy (SLI-TGD).
2. To find out at what point in the parasite blood-stage lifecycle, the selected exported parasite

proteins are essential. This was investigated by performing growth assays.

3. To determine various processes in which the selected proteins are involved. This was investigated by analysing the morphology, the localisations, and cytoadherence phenotype of parasite mutants with depleted genes (via the SLI-TGD) or with a downregulated (knockdown via the *glmS*) exported protein.

RESULTS

2 Results

2.1 Knockout screening of *P. falciparum*'s genes encoding for exported proteins using the selection integration targeted gene disruption (SLI-TGD).

2.1.1 Selection of the gene candidates.

The Pathogenicity of *Plasmodium falciparum* infection during the blood-stage development is mediated by a plethora of parasite-induced host cell modifications taking place on the molecular level and mainly driven by parasite exported proteins. These exported proteins ensure the survival of the parasite (Boddey and Cowman 2013). There are predicted to be over 400 parasite genes encoding for exported proteins (having a PEXEL motif), but few of these genes have been characterized (see section 1.5 of the introduction). When knocked out, many of them resulted in being possibly or not essential for the parasite *in vitro* growth (Maier et al. 2008; Zhang, Wang, et al. 2018). It is imperative to characterize these genes since they may contribute to finding an effective therapy. The inherent difficulty to genetically manipulate these parasite genes renders large-scale screening impractical. For this reason, we used a bioinformatics pipeline approach to prioritize gene targets to a manageable number and increased the likelihood of discovering novel genes essential for parasite survival. We aimed to identify genes that fulfilled the following criteria 1) Predicted to be exported to the host cell (according to *PlasmoDB*). 2) Not part of the STEVOR, RIFIN or var multigene families (due to mutually exclusive expression of only one family member per parasite). 3) Refractory to knockout. 4) Evidence for high transcript levels at 0-16 or 44-48 hours post-invasion (as most proteins involved in host cell modifications are expressed at this time). 5) A coding sequence of at least 600bp to allow a single crossover recombination. The query generated a list of 15 genes (Table 1) that of which 11 are annotated as having "unknown function" and four with "putative functions". We focused on these genes and targeted them for disruption using the selection linked integration targeted gene disruption (SLI-TGD) strategy (Birnbaum et al. 2017).

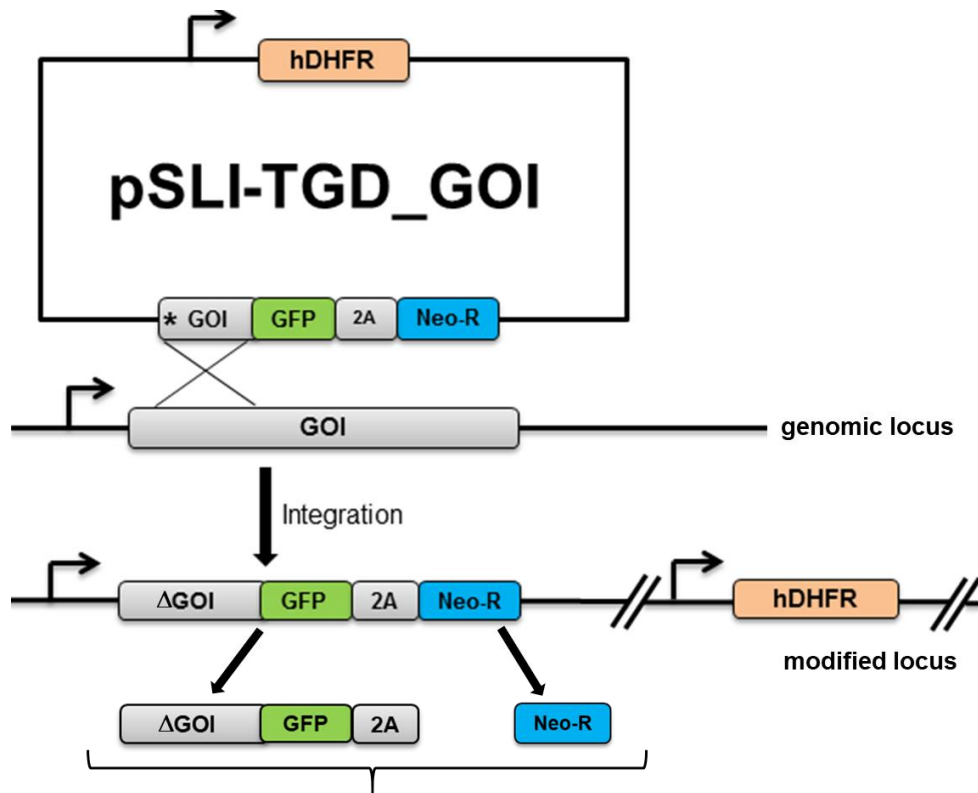
Table 1: List of gene candidates.

GeneID	Product
PF3D7_0113300	<i>Plasmodium</i> exported protein (hyp1), unknown function
PF3D7_0220300	<i>Plasmodium</i> exported protein, unknown function
PF3D7_0220600	<i>Plasmodium</i> exported protein (hyp9), unknown function
PF3D7_0220700	<i>Plasmodium</i> exported protein (hyp9), unknown function
PF3D7_0221200	<i>Plasmodium</i> exported protein (hyp15), unknown function
PF3D7_0301600	<i>Plasmodium</i> exported protein (hyp1), unknown function (GEXP21)
PF3D7_0301800	<i>Plasmodium</i> exported protein, unknown function
PF3D7_0310400	parasite-infected erythrocyte surface protein (PIESP1)
PF3D7_0701900	<i>Plasmodium</i> exported protein, unknown function
PF3D7_1038600	<i>Plasmodium</i> exported protein, unknown function
PF3D7_1102600	<i>Plasmodium</i> exported protein, unknown function (GEXP14)
PF3D7_1149200	ring-infected erythrocyte surface antigen (RESA3)
PF3D7_1301200	glycophorin binding protein (GBPH2)
PF3D7_1401200	<i>Plasmodium</i> exported protein, unknown function
PF3D7_1001900	<i>Plasmodium</i> exported protein (hyp16), unknown function (Pfj23)

2.1.2 Generation of parasite mutants with disrupted genes of interest.

After reducing the pool of potentially interesting genes to 15, we wanted to investigate whether these genes are dispensable or not. Previously, a study used a transposon mutagenesis to saturate the whole genome of *P. falciparum* and randomly disrupt the expression of the majority of its genes. This study classified these genes as essential or nonessential for optimal parasite's growth during the blood-stage development (Zhang, Wang, et al. 2018). Although the study represented a comprehensive picture of the parasite's essential genes, it possesses a considerable amount of uncertainty since it reported many known and characterised essential genes as nonessential. Therefore, we independently validated our target gene list using the SLI-TGD strategy. In the SLI-TGD approach, a short sequence of each target gene (to allow a single crossover recombination) shortly downstream of the start codon was cloned into the pSLI-TGD vector (courtesy of Dr Tobias Spielmann). This vector contains the human dihydrofolate reductase (hDHFR) as the primary selectable marker for selection after the transfection. Also, each target gene insert was tagged with a green fluorescent protein (GFP) sequence and separated from an additional selectable marker (in this case, Neomycin-R) by a 2A skip peptide (Figure 13). Addedly, a stop codon was included at the beginning of each insert to prevent its random expression from the vector or after its integration. Since the resulted target region on the vector does not contain a promoter, the additional selectable marker can be expressed only upon integration (via a single crossover recombination) of the target locus behind the promoter of the target gene. During the

ribosome translation, the virus-derived 2A self-cleaving peptide in the system allows the expression of two polypeptides from one polycistronic mRNA (Straimer et al. 2012). In our case, the two polypeptides expressed are the truncated target protein and the aminoglycoside phosphotransferase protein conferring resistance to neomycin, G418 or kanamycin. Consequently, only parasites that successfully integrated the target region on the vector were neomycin/G418 resistant. This eliminates the need for long-term drug cycling of parasites to select rare integration events, as integrant parasites can be selected from the parasite population by applying selective drug pressure (in this case, G418).



Coexpression of the truncated protein of interest and the aminoglycoside phosphotransferase protein conferring resistance to Neomycin/G418.

Figure 13: Genetic strategy of the SLI-TGD system for gene disruption. G418 selection drives a single crossover recombination between the target region on the vector and the genomic locus, allowing its integration. Ribosome skipping during the translation driven by the 2A skip peptide leads to the synthesis of two proteins from one mRNA. In this case, the truncated protein of interest and the aminoglycoside phosphotransferase protein conferring resistance to neomycin/G418. Asterisks: Stop codons. 2A: skip peptide. Arrows: promoters. GOI: gene of interest. Δ GOI: disrupted gene. GFP: Green fluorescent protein. hDHFR: human dihydrofolate reductase as the first selectable marker. Neo-R: Neomycin resistance as the second selectable marker.

To generate all the constructs, specific forward and reverse primers (see 4.2.4) of each gene were used to generate via PCR an insert of ~250-600bp. All generated inserts and the pSLI-TGD plasmid were digested (NotI and MluI), ligated and transformed into the PMC103 *E. coli* cells. The resulting colonies were screened via colony PCR, and the positive colonies were grown in a liquid SB media for mini preparation and later for maxi preparation. The resulted constructs were verified via restriction digestion and DNA sequencing. All 15 generated constructs were transfected into the CS2 (wild type) strain and selected with WR99210 (WR) over the first six days and cultured without drug until parasites were seen (~21-40 days). The reappeared parasites named as transfectants with episomal plasmids were subjected to the second selection using the G418 drug. For this purpose, transfectants in 5mL cultures in triplicates (in a six-well plate) were placed under the G418 selection pressure. These transfectant cultures were fed daily with G418 until parasites disappeared (up to 10 days) and cultured until reappearance of the parasites, or over 60 days if no parasite growth was observed (Figure 14 Figure 15). If reappeared, these parasites named integrants were inspected for integration via PCR and tested for the leftover unmodified locus to exclude the presence of wild type or incorrect integration.

15 genes' constructs

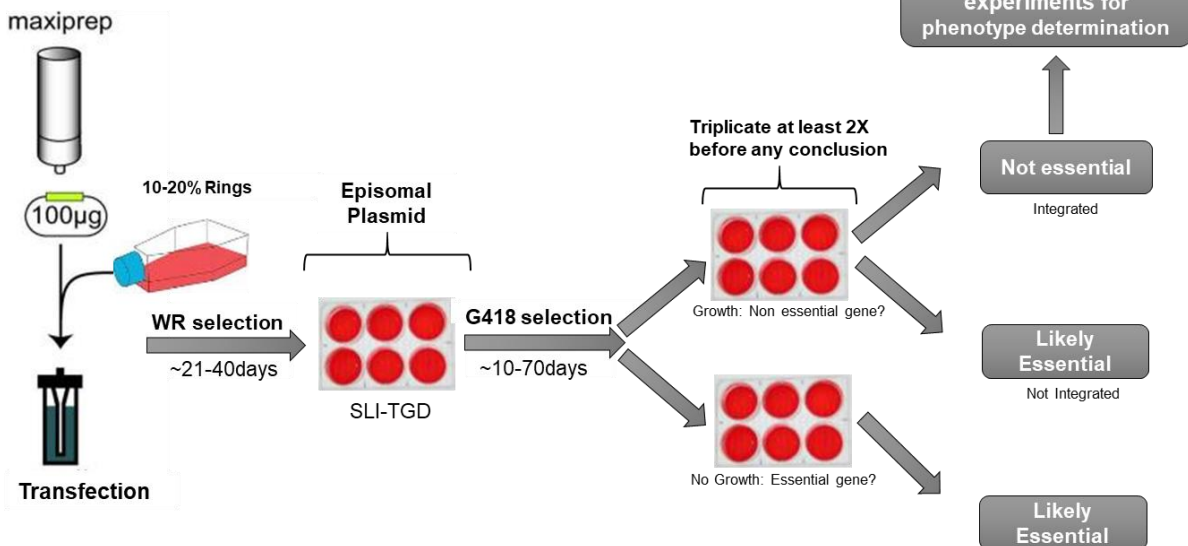


Figure 14: Experimental design and workflow for the disruption of the 15 genes of interest via the SLI-TGD approach. Drug selection with WR99210 (WR) and G418. The G418 selection was performed in triplicates of the 5 mL six-well plate culture. Rings: represent the first developmental stage of *P. falciparum* during its blood-stage growth. 10 to 20 % of Rings of a wild type culture was used to perform the transfection. SLI-TGD: selection linked integration targeted gene disruption.

2.1.3 Gene candidates classification after the SLI-TGD screening.

The selection using G418 after the transfection was performed to determine which parasite line will grow after the truncation of the respective target protein. Upon two rounds of selection in triplicate resulting in a total of six attempts, the obtained parasites were classified as likely essential or nonessential according to the following criteria: 1) If no growth was observed after 60 days of G418 selection, the gene was classified as likely essential. 2) If, after parasite growth, no correct integration (via PCR) was seen, the gene was classified as likely essential. 3) If, after parasite growth, a correct integration (via PCR) was obtained, the gene was classified as nonessential (Figure 14). During all selections, transfectants with known nonessential genes were treated in parallel as controls to exclude any technical difficulties during the process. Of the 15 genes we targeted for gene disruption, 14 could not integrate. Interestingly, only one gene (*pfj23*) could be disrupted (Table 2). To exclude any technical pitfall or in-system defect in our approach, such as a mutation in the vector sequence, we cloned a fragment of a nonessential gene named *PFA0660w* (Diehl et al. 2021) into the vector backbone from the *PF3D7_0220300* gene construct classified as likely essential in our screening. This resulted in parasites' growth after the G418 selection, indicating that our system was working correctly. This verification allowed us to confidently conclude that 14 of our genes are likely essential for *in vitro* blood-stage growth of *P. falciparum* (Table 2).

2.2 Phenotypic characterisation of Pfj23.

2.2.1 Pfj23 is nonessential for parasite survival during the blood-stage development.

Our screening revealed that 14 of our gene candidates did not show any parasite growth, and only one parasite integrant line (Pfj23) showed growth upon G418 selection. The truncation of Pfj23 using the SLI-TGD led to the loss of both putative transmembrane domains and left only 27 amino acids after its PEXEL motif at the N-terminus (Figure 15C). The reappeared Pfj23 integrants, referred to now as Δ Pfj23 was subjected to a limiting dilution subcloning to obtain a pure parasite population. The DNA from the Δ Pfj23 parasites was extracted, and a diagnostic PCR was performed to verify the correct integration. In parallel, the DNA from CS2 was extracted and used as a control to verify the presence of the unmodified locus. Agarose gel electrophoresis of the PCR products from Δ Pfj23 showed correct integrations (5' and 3') at the expected sizes with no wild type locus remaining in the culture (Figure 15A, B).

Table 2: Essentiality classification of the gene candidates.

Genes of interest	Constructs	Transfectants	Integrated 2X G418 selection	(Prediction)
<i>PF3D7_0113900 (cbp1)</i>	Yes	Yes	No	Likely Essential
<i>PF3D7_0220300</i>	Yes	Yes	No	Likely Essential
<i>PF3D7_0220600</i>	Yes	Yes	No	Likely Essential
<i>PF3D7_0220700</i>	Yes	Yes	No	Likely Essential
<i>PF3D7_0301600 (gexp21)</i>	Yes	Yes	No	Likely Essential
<i>PF3D7_0301800</i>	Yes	Yes	No	Likely Essential
<i>PF3D7_0310400 (piesp1)</i>	Yes	Yes	No	Likely Essential
<i>PF3D7_0701900</i>	Yes	Yes	No	Likely Essential
<i>PF3D7_1038600</i>	Yes	Yes	No	Likely Essential
<i>PF3D7_1102600 (gexp14)</i>	Yes	Yes	No	Likely Essential
<i>PF3D7_1149200 (resa3)</i>	Yes	Yes	No	Likely Essential
<i>PF3D7_1301200 (gbph2)</i>	Yes	Yes	No	Likely Essential
<i>PF3D7_1401200</i>	Yes	Yes	No	Likely Essential
<i>PF3D7_0113300</i>	Yes	Yes	No	Likely Essential
<i>PF3D7_1001900 (pfj23)</i>	Yes	Yes	Yes	Nonessential

As the Δ Pfj23 parasite line showed correct integration, we expected the truncated Pfj23 protein to be expressed. To verify the expression of the truncated protein, we performed a western blot (WB). For this purpose, Late-stage parasites of Δ Pfj23 and CS2 were purified using magnetic cell sorting (MACS), then protein extracts were separated on a polyacrylamide gel. Proteins in the sample were detected using primary antibodies such as the mouse anti-GFP (to detect the truncated Pfj23), the rabbit anti-Aldolase (as the loading control) and the anti-mouse/rabbit-HRP as secondary antibodies. In comparison to CS2, the Δ Pfj23 cell line showed a band at the molecular weight of ~35kDa, most likely representing the truncated Pfj23 (Figure 15C, D).

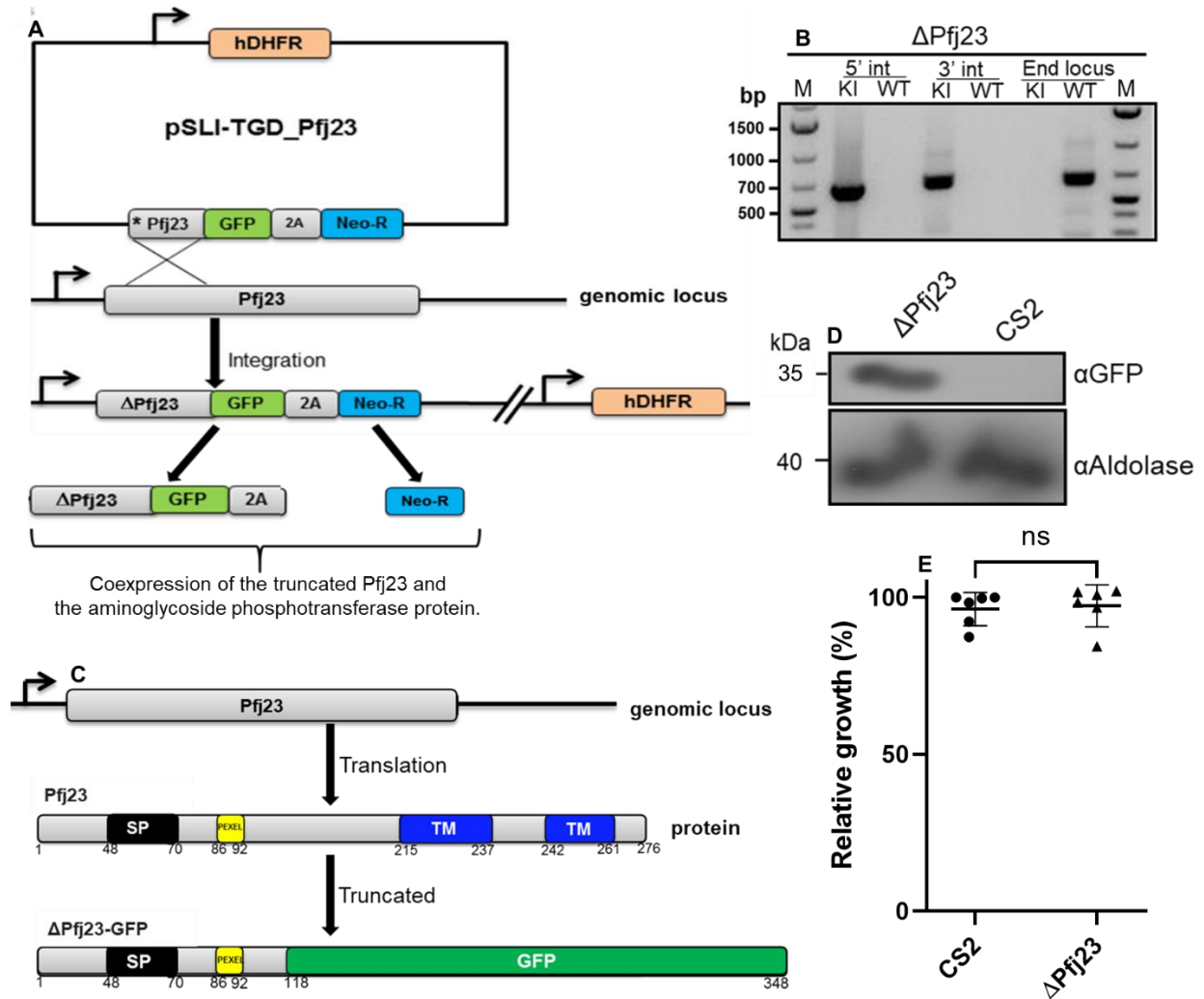


Figure 15: Pfj23 is nonessential for the parasite blood-stage growth A) Genetic manipulation strategy used to generate the Δ Pfj23 truncated cell line. 2A skip peptide; NeoR neomycin resistant marker; Arrows promoters; Asterisks stop codon. B) PCR verification for correct integrations indicated as 5' int expected size ~700bp and 3' int ~750bp. The absence of the original locus (End locus) shows that no wild type parasites remained in the population. KI: Knock in cell line WT: CS2 wild type, M: Marker. C) representation of the truncation of Pfj23 at the protein level. SP signal peptide; PEXEL motif: RxLxQ/E/D in yellow. D) Western blot showing the expression of the truncated Δ Pfj23 using GFP antibody (expected size 35kDa) and Aldolase as a loading control. E) Growth of CS2 and Δ Pfj23 over 72 hours measured using the Clario plate reader of Sybr green-stained parasites. No significant growth difference. Student's t-test, two independent experiments.

Next, we were interested in finding whether Pfj23 truncation could affect the parasite growth. For this purpose, a growth assay was carried out to investigate a potential growth defect of the Δ Pfj23 line compared to CS2. Ring stage Δ Pfj23 and CS2 parasites at the parasitemia of 0,2% were cultured for 72 hours, then stained with Sybr green, and measured on a plate reader to assess the growth rate of parasites. In comparison to CS2, Δ Pfj23 parasites did not display any significant growth difference (Figure 15E). Altogether, our PCRs, WB and growth assay results strongly indicate that Pfj23 is nonessential for the *in-vitro* growth of the parasite during the blood-stage development. Therefore, further experiments were performed to investigate if Pfj23 is involved in various parasite-induced host cell modifications.

2.2.2 Investigation of the effect of Pfj23 truncation on the distribution of various exported protein markers within the infected red blood cells (iRBCs).

Previous studies have shown that interfering in protein traffic to the host cell or knockout of genes causes a change in the distribution of marker proteins for specific subcellular structures within the infected host cell (Beck et al. 2014; Elsworth et al. 2014; Maier et al. 2008). These markers represent various localisations and membrane association and include SBP1, a marker of the Maurer's clefts (MC) and integral membrane (Cooke et al. 2006; Maier et al. 2007). Also, REX1, a marker of Maurer's clefts and peripheral membrane protein (Hanssen et al. 2008). KAHRP and EMP3, markers of Maurer's clefts, host cell plasma membrane, knobs and peripheral membrane protein (Crabb et al. 1997; Waterkeyn et al. 2000; Rug et al. 2006). As we were interested in finding if there is an effect of *pfj23* disruption on these markers, we performed indirect immunofluorescence assays (IFA) using specific antibodies against these protein markers. The primary antibodies include the rabbit anti-KAHRP, anti-REX1, anti-EMP3, anti-SBP1, and the secondary antibody used was the rabbit-Cy3. Additionally, DAPI was used to stain the parasite nucleus.

2.2.2.1 Truncation of Pfj23 does not impair KAHRP, REX1 and EMP3 distributions.

First, we investigated the distributions of KAHRP, REX1 and EMP3 proteins in the CS2 (as control) and Δ Pfj23 parasite-infected red blood cells. The IFA was performed on acetone/methanol fixed cells, stained using respective antibodies and imaged on an epifluorescence microscope. Our data showed no significant difference observed in the distributions of REX1, KAHRP and EMP3 upon *pfj23* disruption.

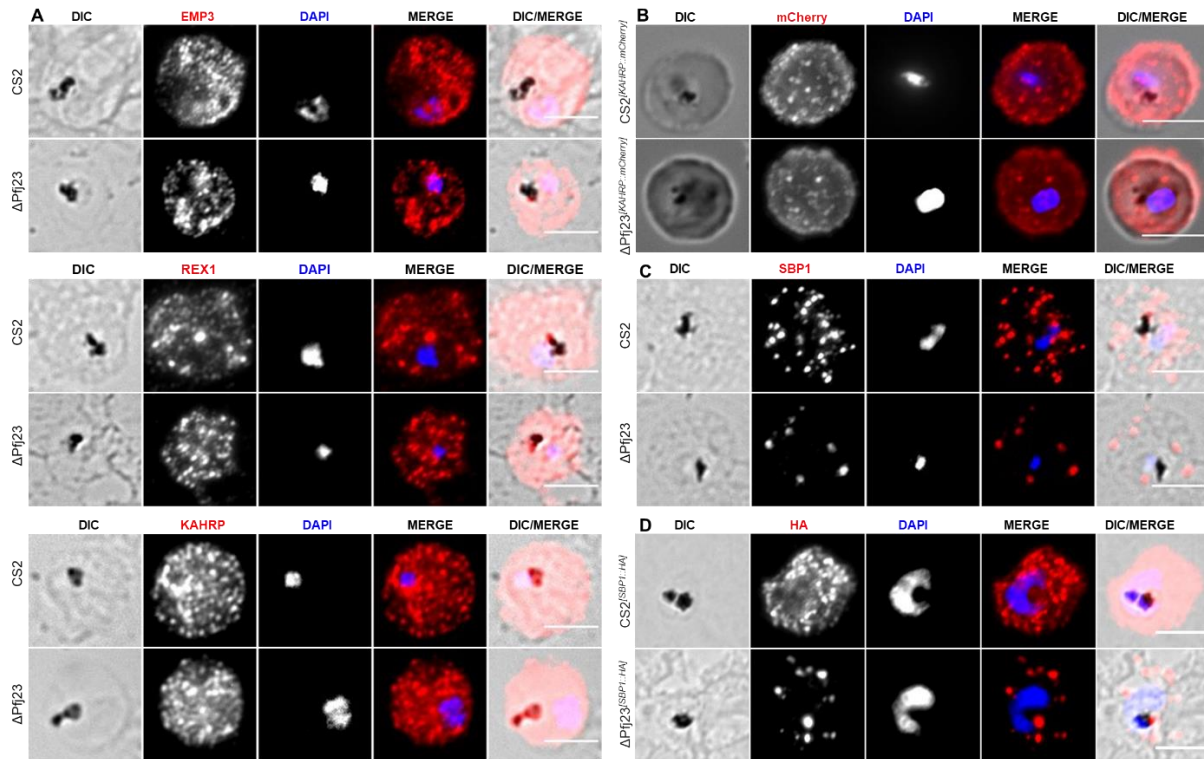


Figure 16: Indirect immunofluorescence assay (IFA) analysis on various exported protein markers localisations. A) EMP3, REX1 and KAHRP antisera in MeOH acetone-fixed $\Delta Pfj23$ and CS2 parasites. No significant difference in their localisations. B) Maximum fluorescence intensity of Z-stacks from the Live-cell imaging in the mCherry channel on $\Delta Pfj23^{[KAHRP::mCherry]}$ and $CS2^{[KAHRP::mCherry]}$ parasite lines. C, D) Aberrant SBP1 distribution in the $\Delta Pfj23$ cell line when compared to CS2. DAPI was used for nucleus staining, Scale bar $5\mu m$.

2.2.2.2 Truncation of PfJ23 impairs the distribution of SBP1.

As we did not see any effect of *pfj23* disruption on the distributions of REX1, EMP3 and KAHRP, we further investigated the distribution of SBP1. Compared to CS2, $\Delta Pfj23$ parasites revealed aberrant SBP1 distributions (Figure 16C). Furthermore, we episomally expressed the *SBP1::HA* fusion in the $\Delta Pfj23$ ($\Delta Pfj23^{[SBP1::HA]}$) and CS2 ($CS2^{[SBP1::HA]}$) parasite lines to validate the observed difference. An IFA using the anti-HA antibody on $\Delta Pfj23^{[SBP1::HA]}$ parasites showed an impaired distribution of SBP1 when compared to $CS2^{[SBP1::HA]}$ (Figure 16D). Consequently, our data strongly indicate that *pfj23* disruption leads to aberrant SBP1 distributions within the iRBCs. Knowing that SBP1 is a Maurer's Cleft (MC) resident protein, this observed phenotype on its distribution led us to investigate the morphology and architecture of MCs upon *pfj23* disruption.

2.2.3 Truncation of Pfj23 displays altered Maurer's clefts ultrastructure.

Maurer's clefts play an essential role in protein traffic to the host cell plasma membrane. Knockout of several genes, including SBP1, showed severe morphological defects in Maurer's clefts morphology and subsequent delivery of proteins to the host cell membrane (Rug et al. 2014; Spycher et al. 2008; Cooke et al. 2006). Transmission electron microscopy (TEM) on the wild type and the Δ Pfj23-infected erythrocytes was performed to investigate the ultrastructure of MCs. In doing so, late-stage Δ Pfj23 and CS2 iRBCs were MACS purified, fixed and prepared for TEM imaging. The CS2 line displayed typical single lamellae with translucent lumen MCs, whereas the Δ Pfj23 line revealed aberrant globular shaped MCs morphology randomly distributed through the iRBC cytoplasm (Figure 17). Hence, our results suggest that Pfj23 contributes to the structural integrity of MCs. Next, we investigated the morphology of knobs on the iRBC plasma membrane upon truncation of Pfj23.

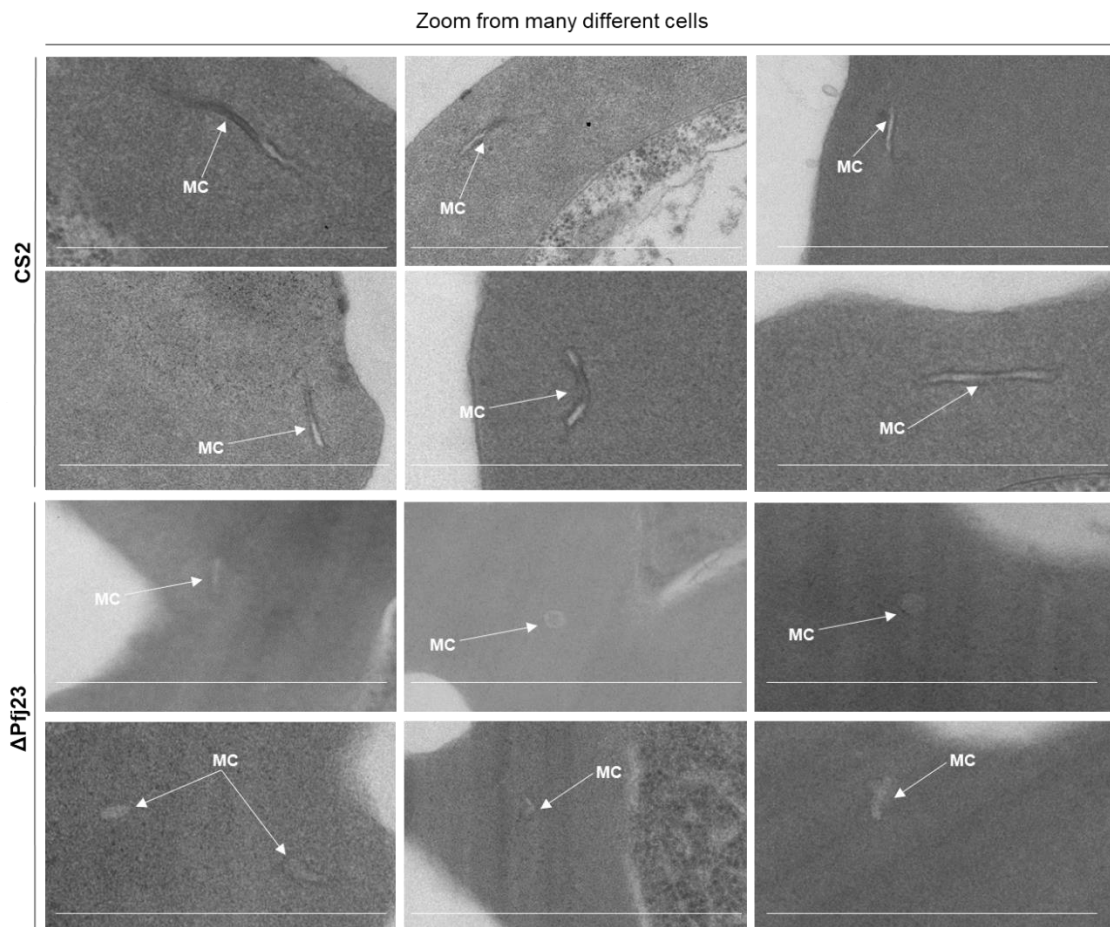


Figure 17: Transmission electron microscopy (TEM) of CS2 and Δ Pfj23 parasite-infected erythrocytes. The upper panel (CS2) showing typical MCs, and the lower panel (Δ Pfj23) displaying distorted globular MCs morphology. MC: Maurer's Clefts, Scale bar 1 μ m.

2.2.4 Δ Pfj23 parasite-infected RBCs display deformed and elongated worm-like knobs morphologies.

During its blood stage development, *P. falciparum* induces elevations beneath the RBC plasma membrane known as knobs. Previous studies have shown that genes' disruption leads to aberrant knobs morphologies (Maier et al. 2008; McHugh et al. 2020; Diehl et al. 2021). Therefore, we used scanning electron microscopy (SEM) to investigate the effect of Pfj23 truncation on knobs morphology. Late-stage Δ Pfj23 and CS2 parasite-infected erythrocytes were MACS purified, fixed and prepared for SEM imaging. CS2 displayed regular knobs in contrast to deformed, enlarged and elongated worm-like knobs morphologies in the Δ Pfj23 cell line (Figure 18A and Appendix 1). Furthermore, transmission electron microscopy (TEM) revealed regular knobs with electrons dense coat for CS2, whereas the Δ Pfj23 line displayed deformed and elongated knobs as seen on SEM (Figure 19 and Appendix 2). To quantify the observed phenotype, we classified the SEM knobs morphologies into three categories: 1) normal, 2) deformed, enlarged and 3) elongated worm-like. For this purpose, approximately 3500 knobs were counted from 17 infected erythrocytes deriving each from the SEM images of the parental and truncated lines. While CS2 showed around 95% normal knobs, Δ Pfj23 showed over 70% of deformed, enlarged and elongated worm-like knobs morphologies (Figure 18B). Our results indicate that Pfj23 contributes to the proper formation of knobs on the *P. falciparum*-infected RBCs plasma membrane. Next, we evaluated whether Pfj23 truncation could affect the adhesion capabilities of Δ Pfj23 parasite-infected erythrocytes to receptors such as chondroitin sulfate A (CSA).

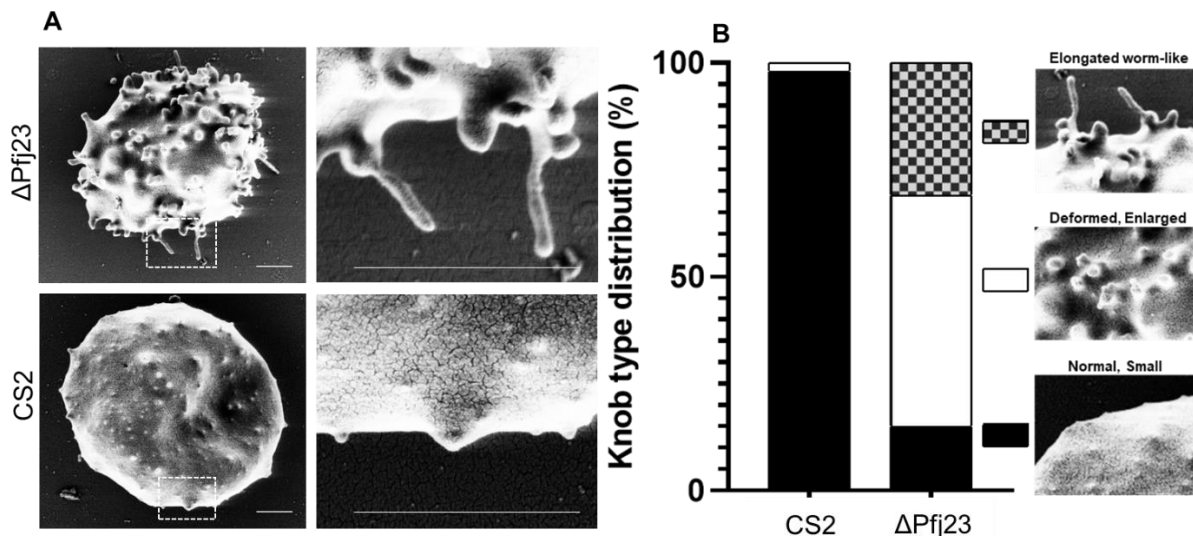


Figure 18: Pfj23 truncation leads to aberrant knobs morphologies. A) Scanning electron microscopy (SEM) showing normal knobs in CS2 and aberrant knobs morphologies in Δ Pfj23 parasite-infected erythrocytes.

B) Quantification of different knobs morphologies. 1) Normal small 2) Deformed elongated 3) Elongated worm-like. A total number of 17 cells were counted from each cell line (CS2 and Δ Pfj23). Scale bar 1 μ m.

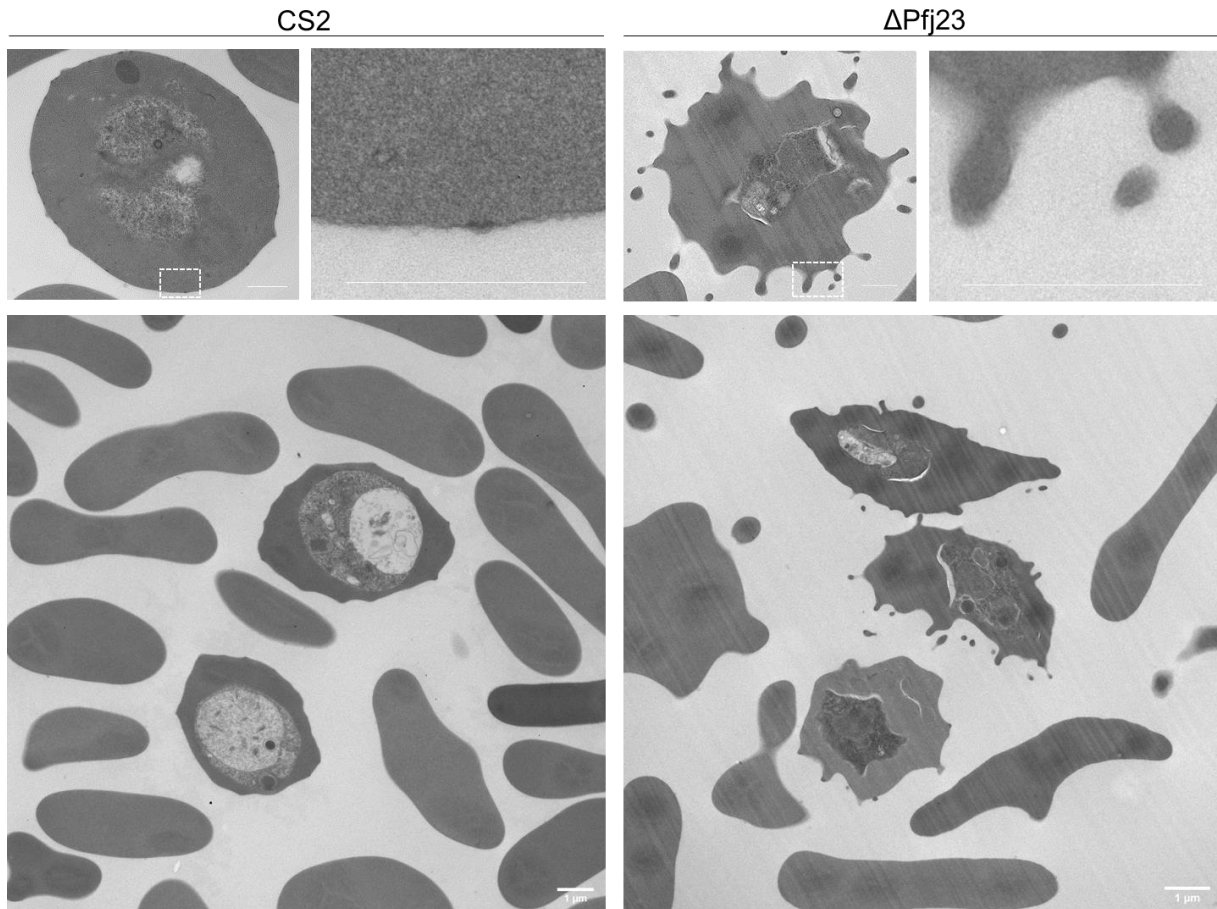


Figure 19: Pfj23 truncation leads to aberrant knobs morphologies. Transmission electron microscopy (TEM) depicting normal knobs in CS2 and aberrant knobs morphologies in Δ Pfj23 parasite-infected erythrocytes. Scale bar 1 μ m.

2.2.5 Δ Pfj23 parasite-infected RBCs result in reduced binding to Chondroitin Sulfate A (CSA) under static binding conditions.

Knobs are important for the effective presentation of proteins involved in the cytoadherence of iRBCs. Cytoadhesion allows *P. falciparum*-infected RBCs to sequester within the host's microvasculature, thereby avoiding clearance in the spleen and consequently contribute to parasite virulence. The process is mainly mediated by a family of proteins called PfEMP1 encoded by the *var* multigene family (Kraemer and Smith 2006; Smith et al. 1995). Insertion of PfEMP1 into the RBCs membrane can mediate binding of iRBCs to various vascular endothelium receptors such as ICAM, CD36 and CSA on placental receptors (Fried and

Duffy 1996; Wahlgren, Goel, and Akhouri 2017b). Our CS2 parental line was selected to express the PfEMP1^{var2CSA} variant, thereby enabling the parasites to bind to CSA. Hence, we evaluated under static conditions the binding capability of Δ Pfj23 parasite-infected erythrocytes to CSA. In doing so, late-stage CS2 and Δ Pfj23 parasite-infected RBCs were purified using gelatine and applied on petri dish spots previously incubated with the ligand CSA. Subsequently, cells were allowed to cytoadhere to these spots, and non-bound cells were washed away while CSA-bound iRBCs remain. In parallel, PBS coated spots were used as a negative control. Also, parasites in solution with CSA (CSASOL) were applied onto CSA coated spots to control the binding specificity during the assay (Diehl 2019). Then, the petri dish containing all spots was fixed, stained and imaged on a microscope to evaluate the binding efficiency. Compared to the CS2 parental line, Δ Pfj23 parasites-infected RBCs displayed a significantly reduced binding to CSA (Figure 20). As expected, CS2 and Δ Pfj23 in solution with CSA showed reduced binding to CSA when compared to CS2(CSA). Therefore, our results indicate that Pfj23 contributes to the binding of iRBCs to endothelium receptors.

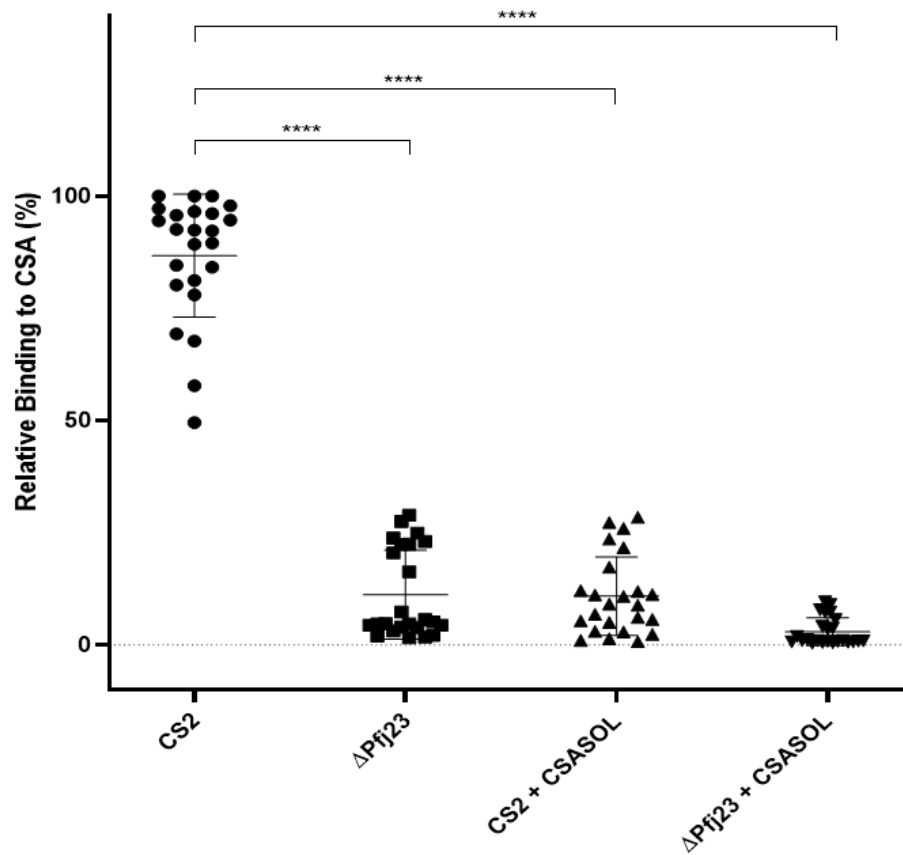


Figure 20: Pfj23 truncation reduces binding to Chondroitin sulfate A (CSA). Binding of CS2 and Δ Pfj23 to CSA. As control binding of CS2(CSASOL) and Δ Pfj23(CSASOL) to CSA. CSASOL: CSA in solution; Student's t-test, ****P-value < 0.0001; three independent biological replicates.

2.3 Analysis of gene candidates using the *glmS* ribozyme system.

The screening of the 15 selected genes revealed that 14 of them were likely to be essential (Table 2). So, a possible way to characterise these genes would be through a conditional knockout system or a knockdown approach. We used a conditional knockdown approach known as glucosamine-6-phosphate activated ribozyme (*glmS*) system to characterise four selected genes *PF3D7_0301800*, *PF3D7_0310400* (*PIESP1*), *PF3D7_1401200* and *PF3D7_0113900* (*CBP1*). The *glmS* riboswitch is an RNA molecule structure from Gram-positive bacteria that catalyses its self-cleavage upon glucosamine-6-phosphate (GlcN6P) activation (Winkler et al. 2004). In our approach, the addition of glucosamine activates the *glmS* ribozyme and causes the cleavage of the mRNA of the target gene, consequently leading to the knockdown of the protein expression (Prommana et al. 2013). To characterize the above mentioned four genes, we used the *glmS* ribozyme coupled with the selection linked integration (SLI) described above in the SLI-TGD approach. The resulting system named SLI-*glmS* contains the *glmS* ribozyme sequence at the 3' UTR of the target gene in the SLI-*glmS* vector (Figure 21).

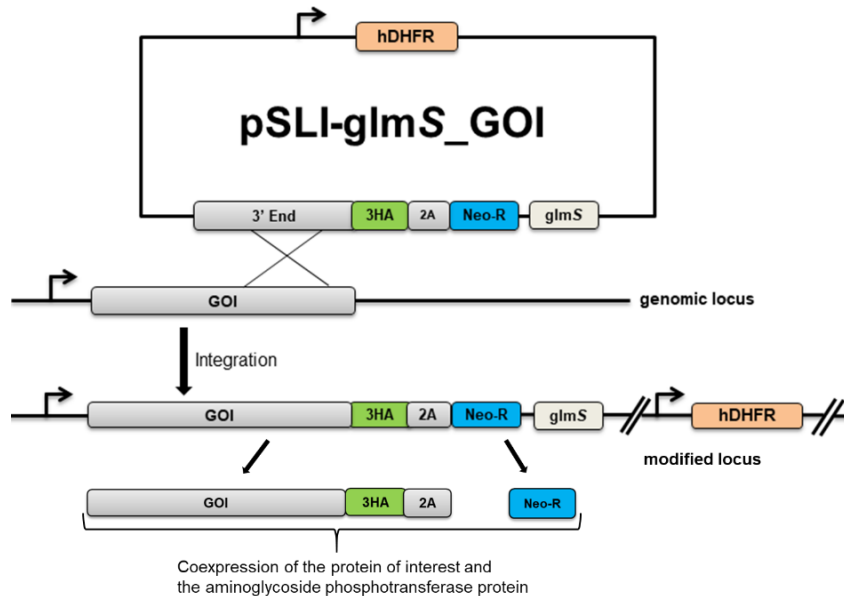


Figure 21: Selection linked integration (SLI) glucosamine-6-phosphate activated ribozyme system (SLI-*glmS*) for conditional protein downregulation. G418 selection drives a single cross-over recombination between the target region on the vector and the genomic locus, allowing its integration. Ribosome skipping during the translation driven by the 2A skip peptide leads to the synthesis of two proteins from one mRNA. In this case, our protein of interest (POI) and the aminoglycoside phosphotransferase protein conferring resistance to neomycin/G418. 2A: skip peptide. Arrows: promoters. GOI: gene of interest. Arrows: promoters. GOI: gene of interest. 3HA: 3xHA hemagglutinin tag. hDHFR: human dihydrofolate reductase as the first selectable marker. Neo-R: Neomycin as the second selectable marker.

2.3.1 Generation of the SLI-*glmS* transfectants.

SLI-*glmS* constructs and transfectants were generated as described in the SLI-TGD approach. Specifically, 600-1000bp of the 3' end (without the stop codon) of each target gene was cloned into the plasmid pSLI-*glmS* (courtesy of Dr Markus Ganter) to allow a single cross-over homologous recombination with the genomic locus of the gene of interest (GOI). All cloned inserts were tagged with a 3xHA (hemagglutinin) sequence, and the vector backbone contained the same selectable markers as in the SLI-TGD approach (Figure 21). The generated constructs were transfected into the CS2 wild type and selected over six days with WR and cultured until reappearance of transfectant parasites. As a control for phenotypic characterization, we generated an *M9* (mutated *glmS*) transfectant of each target gene representing the inactive version of each *glmS* line. The *M9* control was used to avoid drawing any conclusion from a phenotype not resulting from the knockdown of the protein of interest (POI) but instead resulting from the cytotoxicity of the glucosamine concentration or any other unknown factors. As a result, we were able to generate both *glmS* and *M9* transfectants of the four selected genes (Table 3).

Table 3: List of the generated transfectants using the SLI-*glmS* approach.

Genes of interest	SLI-TGD	SLI- <i>glmS</i>	
	prediction	Constructs <i>glmS</i> / <i>M9</i>	Transfectants <i>glmS</i> / <i>M9</i>
<i>PF3D7_0301800</i>	Likely Essential	Yes	Yes
<i>PF3D7_0310400 (PIESP1)</i>	Likely Essential	Yes	Yes
<i>PF3D7_1401200</i>	Likely Essential	Yes	Yes
<i>PF3D7_0113900 (CBP1)</i>	Likely Essential	Yes	Yes

As we became aware that Prof Leann Tilley's research group in Australia was working on analysing the *CBP1* gene using an inducible knockout system, we decided not to continue its analysis (Personal communication). Due to the available time at our disposal, the analysis of *PF3D7_0310400 (PIESP1)* and *PF3D7_1401200* were assigned to another student in our Lab. Hence, we remained with the characterisation of *PF3D7_0301800*, as it will be described in the coming sections.

2.4 Phenotypic characterisation of PF3D7_0301800.

2.4.1 Generation of parasite-infected erythrocytes with a *glmS* regulatable copy of the PF3D7_0301800 protein.

2.4.1.1 Generation of the *glmS* and *M9* parasite lines of PF3D7_0301800.

After generating the *glmS* and *M9* transfectants of the PF3D7_0301800 gene, parasites were subjected to the second selection using G418 over ten days and cultured without drug until regrowth of parasites (Figure 22).

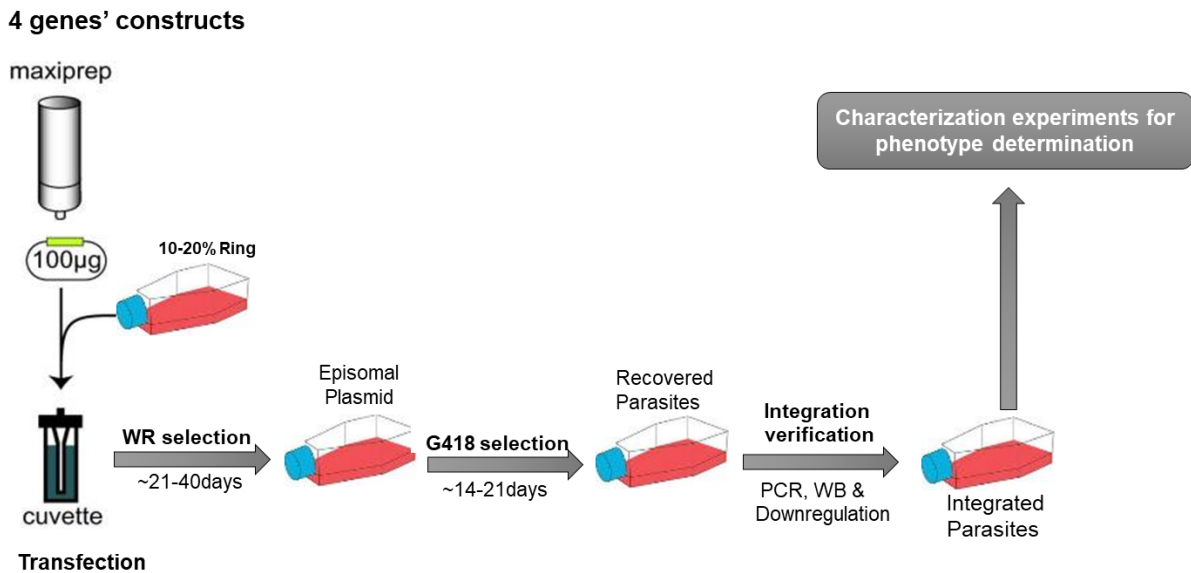


Figure 22: Experimental design and workflow strategy for generating the *glmS* and *M9* cell lines of PF3D7_0301800. Drug selection with WR99210 (WR) and G418. Rings: represent the first developmental stage of *P. falciparum* during its blood-stage growth. 10 to 20 % of Rings of a wild type (CS2) culture was used to perform the transfection. The G418 selection of the *glmS* and *M9* transfectants was performed over three weeks. Verification of integration was done using PCR and protein expression and downregulation via western blot (WB).

Reappeared parasites after G418 selection were subjected to a limiting dilution subcloning. The resulted parasite integrants were verified for correct integration using PCR. Both cell lines (*glmS* and *M9*) showed correct integrations and no wild type locus, resulting in a pure parasite population (Figure 23C, D). Furthermore, a western blot (WB) was performed to verify the expression of the POI. Late-stage parasites (*glmS*, *M9* and CS2) were enriched using magnetic purification. Then protein extracts were separated on a polyacrylamide gel electrophoresis. Detection was done using the anti-HA (detection of the POI) and anti-Aldolase as the loading control. As expected, PF3D7_0301800 was detected at ~35kDa, and no detection was seen in the CS2 parental line

(Figure 23E). Lengthy cell culture of *P. falciparum* is known to permit deletion of the subtelomeric arm of chromosome 2. The potential breakage leads to the loss of three potential genes *kahrp*, *emp3* and *kahsp40*, resulting in a “knobless” phenotype (Polog and Ravetch 1986). The *emp3* gene is located between *kahrp* and *kahsp40*. Its detection in our parasites would indicate the stability of the chromosome 2 arm. As a result, *emp3* was detected in both *glmS* and *M9* cell lines (Figure 23B). These parasites lines, referred to now as *CS2PF800^{glmS}* and *CS2PF800^{M9}*, were further analysed to evaluate a possible knockdown of the PF3D7_0301800 protein.

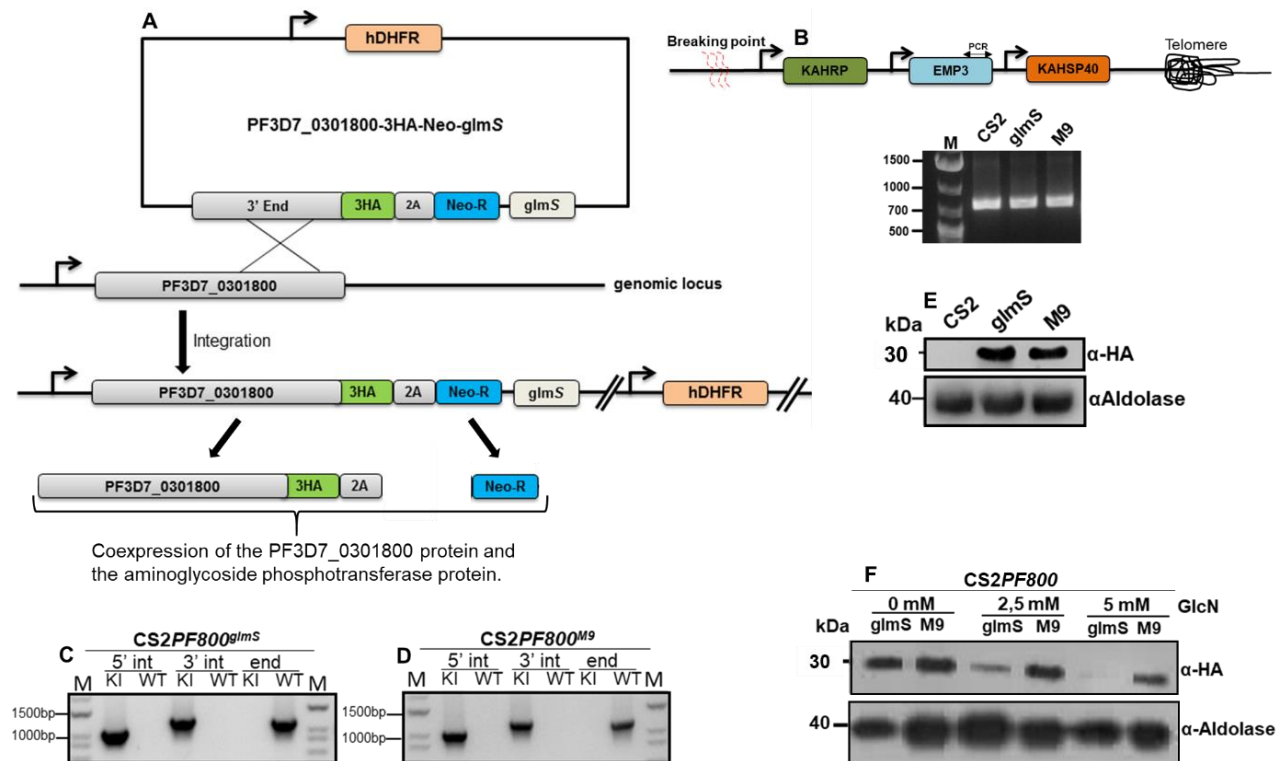


Figure 23: Generation of a *glmS* regulatable copy of the PF3D7_0301800 protein. A) Genetic manipulation strategy used to generate the *CS2PF800^{glmS}* and *CS2PF800^{M9}* cell lines. 2A skip peptide. NeoR neomycin resistant marker. Arrows promoters. B) overview of the architecture of the *P. falciparum* chromosome 2 and a PCR result from the amplification of the *EMP3* gene. Expected size~800bp. C,D) PCR verification for correct integrations indicated as 5' int expected size ~1040bp and 3' int ~1240bp. The absence of the original locus (End locus) shows that no wild type parasites remain in the population. KI: Knock in cell line WT: CS2 wild type, M: Marker. E) Western blot showing the expression of PF3D7_0301800 in the *glmS* and *M9* cell line. F) Downregulation of PF3D7_0301800 using different concentrations of glucosamine (GlcN). Anti-HA antibody (expected size ~30kDa) to detect the POI and Aldolase as a loading control.

2.4.1.2 PF3D7_0301800 protein is downregulated via glucosamine (GlcN).

After generating the CS2PF800^{gImS} and CS2PF800^{M9} cell lines, the POI should be downregulated via glucosamine (GlcN). Starting with 1% ring-stage parasites (*gImS* and control *M9*), the culture was split and incubated for 72 hours under different concentrations (0mM, 2,5mM and 5mM) of glucosamine (GlcN). Western blot was performed as described above using the anti-HA antibody (to monitor the POI's downregulation) and anti-Aldolase as the loading control. As expected, protein downregulation was seen in the CS2PF800^{gImS} cell line and no regulation in the CS2PF800^{M9} cell line (Figure 23F). These data show that the knockdown of the PF3D7_0301800 protein was successful using the SLI-*gImS* approach. Conditional regulation of CS2PF800^{gImS} parasites via glucosamine made possible the phenotypic characterisation of the *PF3D7_0301800* gene. To begin its analysis, we used a growth assay to investigate the downregulation effect of PF3D7_0301800 on the parasite's growth.

2.4.2 Downregulation of PF3D7_0301800 does not impair the growth of the parasite.

Parasite's growth upon protein downregulation was assessed via the Sybr green growth assay. For this purpose, parasites (CS2PF800^{gImS} and CS2PF800^{M9}) were incubated for 72 hours with different concentrations (0mM, 1,25mM, 2,5mM and 5mM) of GlcN. Then, the cells were stained with Sybr green and measured on a plate reader to assess the growth. In comparison to CS2PF800^{M9}, the downregulation of CS2PF800^{gImS} did not show any significant growth defect (Figure 24A). Surprisingly, a comparison between the nontreated (0mM GlcN) and treated (5mM GlcN) parasites showed a significant growth defect (Figure 24A). However, this observed effect is likely due to glucosamine's cytotoxicity as no significant growth difference was seen between CS2PF800^{gImS} and CS2PF800^{M9} at 5mM GlcN. For further characterisation experiments, we decided to use the 2,5 mM concentration of glucosamine. To start with the phenotypic characterization, we performed IFAs as described in the previous section to investigate the effect of PF3D7_0301800 downregulation on SBP1, REX1, EMP3 and KAHRP protein markers.

2.4.3 Downregulation of PF3D7_0301800 does not impair the distributions of SBP1, REX1 and EMP3.

To investigate the effect of the downregulation of PF3D7_0301800 on SBP1, REX1 and EMP3, we performed indirect immunofluorescence assays (IFAs) on the *CS2PF800^{gImS}* and *CS2PF800^{M9}* parasite lines. In doing so, ring-stage parasites (*gImS* and *M9*) were incubated with (+GlcN) and without (-GlcN) glucosamine for 72 hours and subsequently processed for IFAs exactly as described in the Pj23 analysis (see section 2.2.2). As a result, SBP1, REX1, and EMP3 distributions were not affected upon PF3D7_0301800 downregulation (Figure 24B, C, D). These data indicate that the downregulation of PF3D7_0301800 does not impair the localisations of SBP1, REX1 and EMP3 within the iRBC.

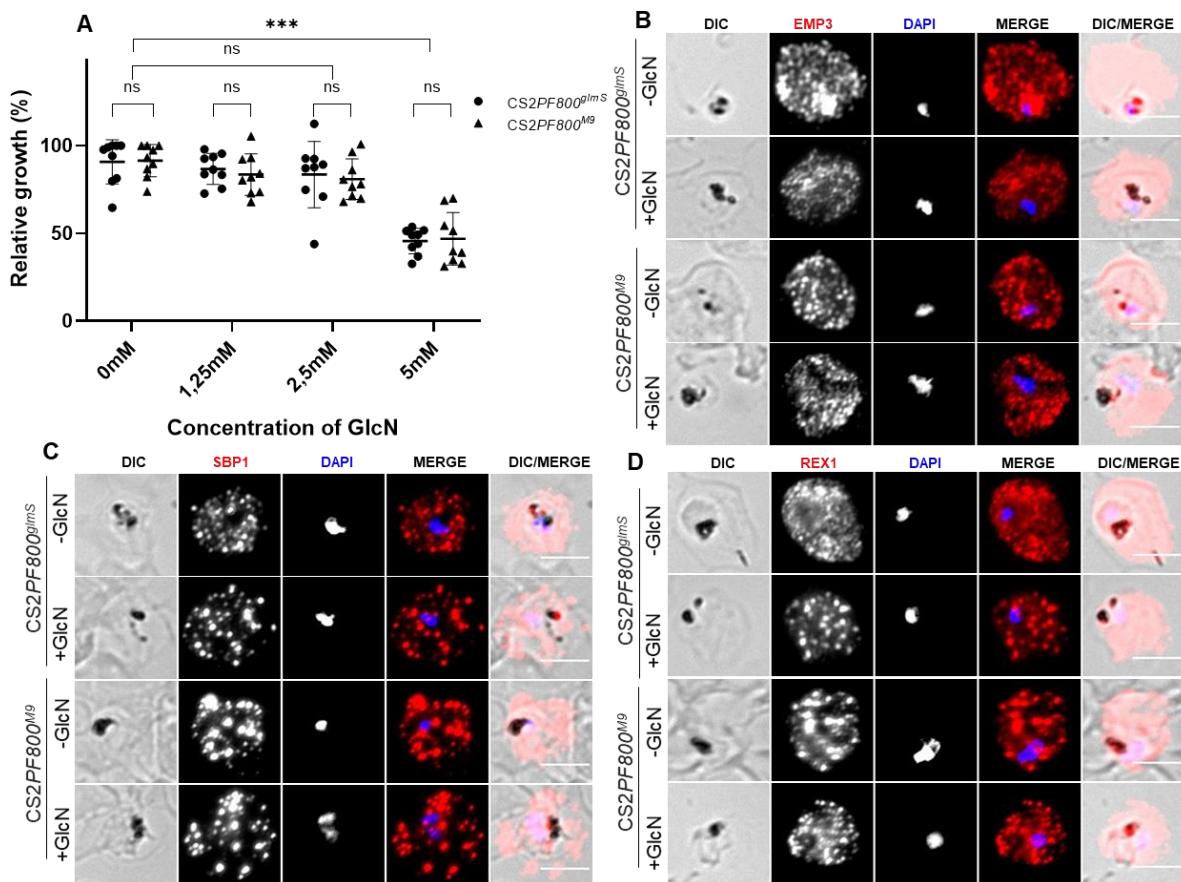


Figure 24: Knockdown of PF3D7_0301800 does not affect parasite's growth A) Growth assay Sybr green-stained of the *CS2PF800^{gImS}* and *CS2PF800^{M9}* parasites over 72 hours using different glucosamine concentrations (GlcN). No significant growth difference between *gImS* and *M9* at the same concentration of GlcN. Student's t-test. Significant growth difference between both cell lines at 0mM and 5mM GlcN, probably resulting from the GlcN cytotoxicity, two ways ANOVA test. Three independent experiments. B,C,D) EMP3, REX1 and SBP1 antisera in MeOH acetone-fixed *CS2PF800^{gImS}* and *CS2PF800^{M9}* parasites. No significant difference in their localisations. DAPI was used for the nucleus staining, Scale bar 5µm.

2.4.4 Downregulation of PF3D7_0301800 impairs the distribution of KAHRP.

In addition to SBP1, REX1 and EMP3, we investigated the distribution of KAHRP upon PF3D7_0301800 downregulation. Our preliminary data show that the punctate distribution of KAHRP was typically distributed across the cell in the treated CS2PF800^{M9} and non-treated *gImS/M9* lines. In contrast, these puncta were more concentrated in the middle of the cell in the treated CS2PF800^{gImS} line (Figure 25A). Additionally, to validate the observed effect, we episomally expressed the *KAHRP::mCherry* fusion in the CS2PF800^{gImS} parasite line, referred to now as CS2PF800^{gImS[KAHRP::mCh]}. Parasites were split and incubated with (+GlcN) or without (-GlcN) glucosamine for 72 hours. Live cell imaging in the mCherry channel (to monitor KAHRP) was performed on an epifluorescence microscope. Our preliminary data show that the distribution of KAHRP appears to be less abundant upon PF3D7_0301800 downregulation in the CS2PF800^{gImS[KAHRP::mCh]} cell line (Figure 25B). As these preliminary data represented the first trial of analysis, we will repeat them before drawing any firm conclusion (ongoing).

2.4.5 PF3D7_0301800 does not colocalise with KAHRP.

Based on the results from the analysis of KAHRP distribution, we hypothesised that PF3D7_0301800 might be exported to the same location as KAHRP. Therefore, we performed on the CS2PF800^{gImS[KAHRP::mCh]} line a colocalisation assay via IFA using anti-HA (POI detection) and mCherry (KAHRP detection). As a result, PF3D7_0301800 puncta distribution partially colocalised with KAHRP but were mainly distributed close to KAHRP puncta and not at the same location (Figure 25C). As a way forward, more colocalisation assays using different markers will be performed (ongoing). Next, we investigated the knobs morphologies upon PF3D7_0301800 knockdown.

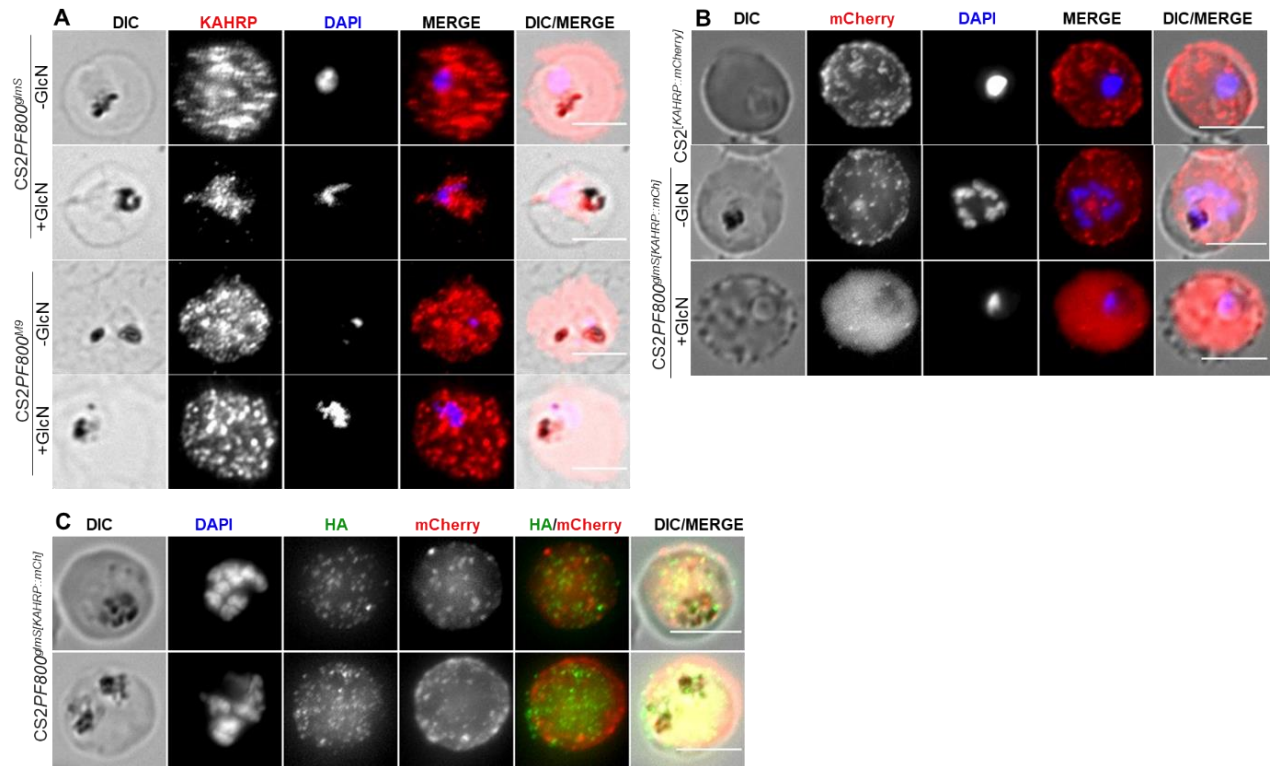
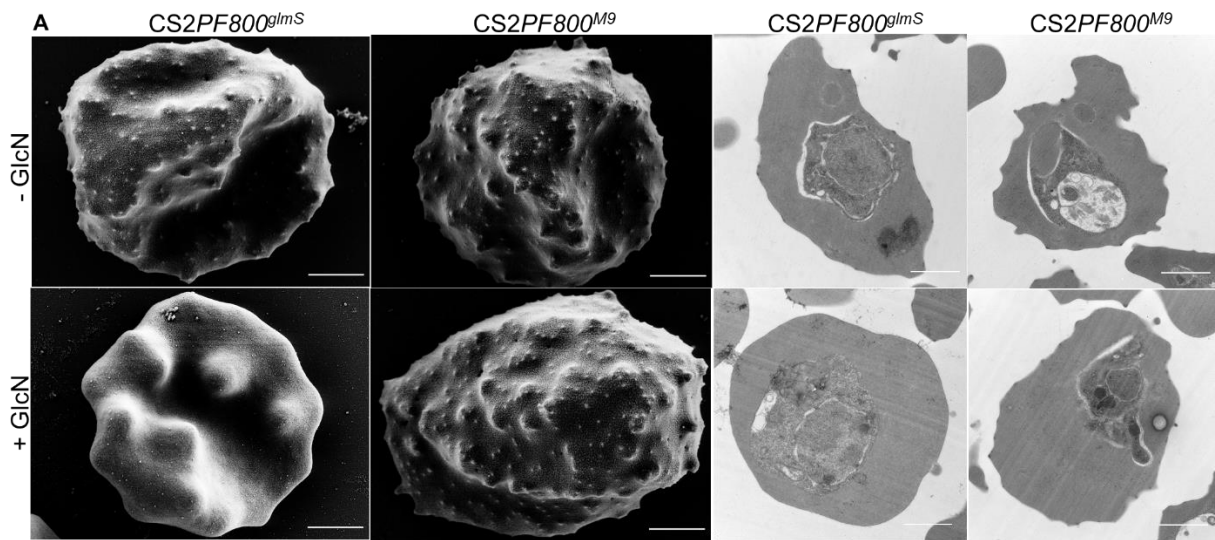


Figure 25: Immunofluorescence assays on KAHRP upon the knockdown of PF3D7_0301800 A) KAHRP antisera on MeOH acetone-fixed cells on the *CS2PF800^{gImS}* and *CS2PF800^{M9}* cell lines. B, C) Maximum fluorescence intensity of Z-stacks from the Live cell imaging in the m-Cherry channel on the *CS2[KAHRP::mCherry]* and *CS2PF800^{gImS}[KAHRP::mCh]* parasite lines. DAPI was used for the nucleus staining, Scale bar 5µm.

2.4.6 Downregulation of PF3D7_0301800 leads to a knobless phenotype.

KAHRP is essential for knobs formation on the infected erythrocytes plasma membrane (Crabb et al. 1997). The IFA data show that the downregulation of PF3D7_0301800 impairs KAHRP distribution. Consequently, we hypothesised that our POI, through its possible effect on KAHRP's distribution, might affect the knobs formation on the iRBC surface. We performed scanning and transmission electron microscopy (SEM and TEM) on the *CS2PF800^{gImS}* and *CS2PF800^{M9}* parasite lines to validate this hypothesis. Parasites were incubated (-GlcN and +GlcN) for 72 hours, and late-stage parasites were enriched using magnetic purification. Enriched cells were then processed for SEM and TEM as described in the analysis Pj23. As a result, nontreated *CS2PF800^{gImS}* and *CS2PF800^{M9}* displayed via SEM and TEM typical knobs with an electron-dense coat. Strikingly, the treated *CS2PF800^{gImS}* line displayed a smooth membrane surface with no knobs (“knobless”) when compared to the treated *CS2PF800^{M9}* line

(Figure 26A, B; Appendix 3 and Appendix 4). In addition, treated *CS2PF800^{glmS}* displayed infected erythrocytes with typical knobs (Appendix 3 and Appendix 4). Henceforth, we will perform more SEMs analyses to quantify this phenotype at different glucosamine concentrations. To do so, we would like to treat the *CS2PF800^{glmS}* and *CS2PF800^{M9}* cell lines with 0; 0,625mM; 1,25mM, and 2,5mM GlcN to quantify the influence of a gradual glucosamine concentration on the knobless phenotype observed upon PF3D7_0301800 knockdown. In conclusion, our data indicate that PF3D7_0301800 contributes to the formation of knobs on the infected erythrocytes plasma membrane. How it contributes to this process remain unknown and will be intensively investigated further (ongoing). Finally, we investigated via TEM the structure and the architecture of Maurer's upon PF3D7_0301800 knockdown. As a result, no difference was seen in the treated and non treated *CS2PF800^{glmS}* and *CS2PF800^{M9}* parasite lines (Appendix 5), suggesting that PF3D7_0301800 is not important for the formation and maintenance of the structure of MCs.



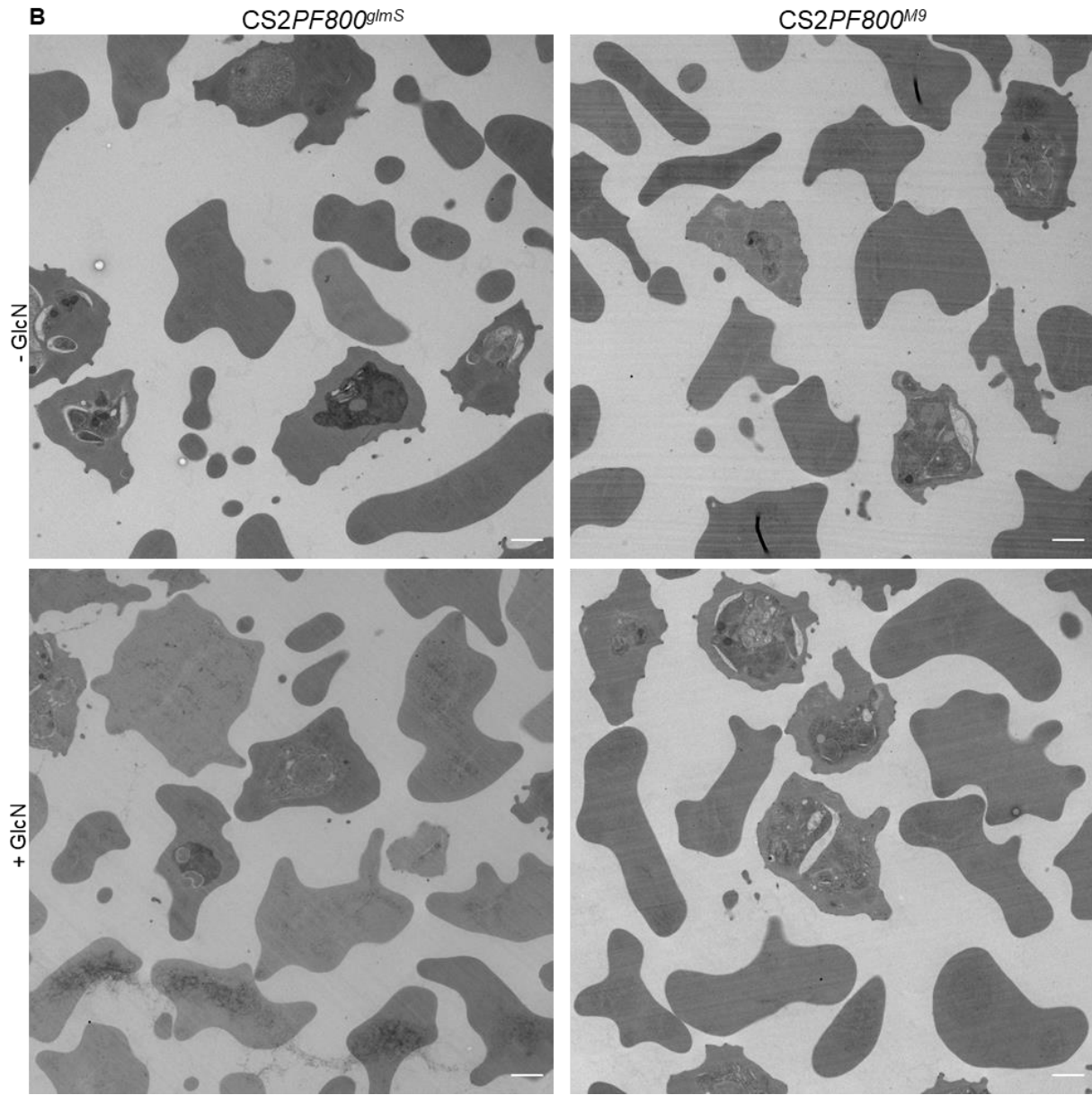


Figure 26: A) Scanning and transmission electron microscopy (SEM and TEM) depicting knobs morphologies in the CS2PF800^{gImS} and CS2PF800^{M9} cell lines C) TEM Overview. Scale bar 1 μ m

DISCUSSION

3 Discussion

3.1 Selection linked integration targeted gene disruption (SLI-TGD) screening.

Plasmodium falciparum parasite is the causative agent of the most devastating human malaria worldwide. Despite the intensive and continuous research work done by the research community over the years, many facets of the parasite's biology remain largely enigmatic. Genetic manipulation tools that have worked well in characterizing genes in other organisms are limited in their application to *P. falciparum* due to several reasons, leaving ~35% of malaria-parasite genes with no functional annotation (Oberstaller et al. 2021). The parasite undergoes the ring, trophozoite and schizont stages during its blood-stage development within the erythrocytes. During the maturation of erythrocytes in the bone marrow, these cells become anucleated and devoid of organelles as well as the protein synthesis and trafficking machinery (Maier et al. 2009). The environment within the host cell represents a challenging milieu for the parasite to develop and propagate easily. Therefore, to ensure its survival, the parasite export over 400 proteins to the host cell that induce various host cell modifications. These exported proteins are classified into two groups. Proteins that contain a conserved *Plasmodium* export element (PEXEL/HT) and those without this motif known as PEXEL-negative exported proteins (PNEPS) (Przyborski and Lanzer 2005; Marti et al. 2004; Spielmann and Gilberger 2010). The function of the majority of these exported proteins remains unknown. Unravelling their function is of utmost importance as a better understanding of parasite biology is needed to prioritize targets. In this project, we used a bioinformatics pipeline approach to select 14 genes encoding for exported PEXEL proteins and one gene encoding for a PNEP (PIESP1) protein (Table 1). These genes were subsequently targeted for disruption using the selection linked integration targeted disruption (SLI-TGD) (Figure 13). Conventional gene inactivation methods in the *Plasmodium* spp. system rely on rare integration events of the target region into the genetic locus of the desired gene. However, these approaches are labour-intensive, time-consuming and required a minimum of six months after transfection to generate a parasite mutant line. The advent of the selection linked integration (SLI) (Birnbaum et al. 2017; Birnbaum et al. 2020) considerably shortened the integration time to ~ two months, allowing us to perform our gene screening quickly.

The SLI-TGD is a robust and reliable genetic approach for genes screening and was utilised to target 18 *Plasmodium falciparum* genes for disruption, thereby classifying them as likely essential and nonessential (Birnbaum et al. 2017). In addition, this approach is faster for gene screening than the targeted gene disruption approach based on the double cross-over recombination used

in previous studies to disrupt 51 parasite genes encoding for exported proteins (Maier et al. 2008) and 13 potential SBP1-interactor proteins (Takano et al. 2019). Of the 15 genes candidates we screened in our study, 14 genes could not be disrupted, but only one gene (*pfj23*) could be knocked out. (Table 2). Using in our experimental procedures a control with a known dispensable gene (*PFA0660w*) (Diehl et al. 2021) allowed us to exclude any technical pitfalls in our approach. Therefore, the 14 genes that could not be disrupted were classified as likely essential for parasite survival during the blood-stage development. A large scale screening of the *P. falciparum* genome using a random transposon-mediated insertional mutagenesis classified the majority of the parasite genes as essential and nonessential (Zhang, Wang, et al. 2018). In comparison to this latter study, the screening study of Maier et al. (2008) and other studies, the classification of our 15 gene candidates revealed similarities and discrepancies (Table 4) described as follows.

The gene *PF3D7_0220300* could not be disrupted in our SLI-TGD approach and was shown through its C>T allele variant at position 814,288 of the genome to confer a protective effect of sickle cell haemoglobin against severe malaria patients in Africa (Band et al. 2021). In agreement with our study, Maier et al. (2008) could not inactivate *PF3D7_1149200* and *RESA3* but were categorised as nonessential in the Zhang et al. (2018) screening. Interestingly, the data from the Zhang et al. (2018) and Maier et al. (2008) studies were consistent with our screening in classifying *piesp1* and *gbph2* genes as likely essential for parasite survival. Finally, the classification of eight genes (*PF3D7_0220600*, *PF3D7_0220700*, *PF3D7_0301800*, *PF3D7_1038600*, *GEXP14*, *PF3D7_0113300*, *PF3D7_1401200* and *cbp1*) as likely essential in our study was congruent with the study of Zhang et al. (2018). Recently, knockdown of *PF3D7_1401200* was shown to significantly reduce the parasite growth, thereby suggesting that *PF3D7_1401200* is likely essential for the parasite's survival (Jonsdottir et al. 2021). Additionally, *cbp1* was refractory to CRISPR/Cas9 knockout, indicating that *cbp1* is likely an essential gene (personal communication: Olivia Carmo, PhD student of Prof Leann Tilley at the University of Melbourne). Unexpectedly, *pfj23* could be disrupted in our SLI-TGD approach but could not be inactivated in the study of Maier et al. (2008). Although *pfj23* could not be inactivated in the study of Maier et al. (2008), our results in agreement with the study of Zhang et al. (2018) strongly indicate that *pfj23* is a nonessential gene.

In summary, we found that one gene (*pfj23*) was nonessential and that 14 genes were classified as likely essential for parasite survival during the intra-erythrocytic development. In comparison to other studies, our data show similarities and discrepancies likely due to many possible reasons. These reasons could include the genetic approach used, the target gene, technical pitfalls or

many unknown factors to our knowledge. In regards to these observations, it would be difficult to predict what method will be the best to classify and characterize a particular gene. However, looking at our approach and all the controls done during our experimental analyses, we think our data are reliable. In conclusion, we would suggest that only upon successfully characterising a gene of interest using a particular method in the *Plasmodium* system should a researcher draw a firm conclusion.

Table 4: Comparison of SLI-TGD screening with other studies.

Genes of interest	SLI-TGD screening	(Zhang, Wang, et al. 2018) screening	Other studies
<i>PF3D7_0113900 (cbp1)</i>	Likely Essential	Essential	Refractory to CRISPR/Cas9 knockout (Personal communication: Olivia Carmo, PhD student of Prof Leann Tilley, University of Melbourne, Australia)
<i>PF3D7_0220300</i>	Likely Essential	Non essential	<i>Pf3D7_0220300</i> at position 814,288 of the genome confers through the <i>P.f</i> allele C>T variant, a protective effect of sickle cell haemoglobin against severe malaria in Africa (Band et al. 2021).
<i>PF3D7_0220600</i>	Likely Essential	Essential	NA
<i>PF3D7_0220700</i>	Likely Essential	Essential	NA
<i>PF3D7_0301600 (gexp21)</i>	Likely Essential	Nonessential	NA
<i>PF3D7_0301800</i>	Likely Essential	Essential	NA
<i>PF3D7_0310400 (piesp1)</i>	Likely Essential	Essential	The <i>Plasmodium</i> -infected erythrocyte surface protein 1 is highly conserved among the <i>P. falciparum</i> specie (Florens et al. 2004). Refractory to disruption (Maier et al. 2008).
<i>PF3D7_0701900</i>	Likely Essential	Nonessential	Refractory to inactivation (Maier et al. 2008).
<i>PF3D7_1038600</i>	Likely Essential	Essential	NA
<i>PF3D7_1102600 (gexp14)</i>	Likely Essential	Essential	NA

<i>PF3D7_1149200</i> (<i>resa3</i>)	Likely Essential	Nonessential	Homology with DNAJ/PHIST proteins and refractory to inactivation (Maier et al. 2008).
<i>PF3D7_1301200</i> (<i>gbph2</i>)	Likely Essential	Essential	Refractory to inactivation (Maier et al. 2008).
<i>PF3D7_1401200</i>	Likely Essential	Essential	Knockdown of <i>PF3D7_1401200</i> resulted in a delayed growth phenotype. <i>PF3D7_1401200</i> strongly associate with the RhopH components but is localised within parasite structures that partially co-localise with MCs and J-dots in the iRBC (Jonsdottir et al. 2021).
<i>PF3D7_0113300</i>	Likely Essential	Essential	NA
<i>PF3D7_1001900</i> (<i>pfj23</i>)	Nonessential	Nonessential	Refractory to inactivation (Maier et al. 2008).

3.2 Truncation of P*pfj23* and its phenotypic characterization.

The *P. falciparum pfj23* (*PF3D7_1001900*) gene is located on chromosome 1, and its encoding exported protein (~32 kDa) has two putative transmembrane domains (according to *PlasmoDB*). In our SLI-TGD screening, the G418 selection of *pfj23* transfectants led to parasites mutant with truncated P*pfj23*. In our *pfj23* disruption design, integration of the target region on the plasmid led to the truncation of P*pfj23* at position 118th amino acid. Considering that P*pfj23* is a protein of 276 amino acids with the plasmepsin 5 (PM5) cleavage taking place at position 91 of the PEXEL motif, the resulting truncated P*pfj23* possesses only 27 amino acids followed by a GFP sequence (Figure 15C). Integration PCRs and western blot verification confirmed correct integrations and disruption of the *pfj23* gene (Figure 15B, D). The generated Δ P*pfj23* cell line expresses few amino acids of the P*pfj23* protein lacking its two putative transmembrane (TM) domains. Growth assay of the truncated line in comparison with the CS2 wild type did not show any growth defect (Figure 15E), thereby strongly suggesting that P*pfj23* is nonessential for parasite growth during the blood-stage development. We used indirect immunofluorescence (IFA) analyses to investigate the potential effect of the truncation of P*pfj23* on various exported protein makers within the iRBCs. The marker proteins KAHRP, EMP3 and REX1 were found to be normally trafficked to their respective localizations in the absence of P*pfj23* function. Interestingly, the truncation of P*pfj23* revealed aberrant SBP1 distribution (Figure 16). SBP1 is a Maurer's Cleft resident protein (Cooke et al. 2006; Maier et al. 2007). Inactivation of several Maurer's Cleft proteins such as MAHRP1, REX1

and PTP1 displayed similar aberrant SBP1 distribution in the iRBCs as in our study (Rug et al. 2014; Spycher et al. 2008; McHugh et al. 2015). Consequently, our results suggest that Pfj23 is important for SBP1 localization at the MCs. Moreover, using an *in-vitro* biochemistry approach, a recombinant Pfj23 protein showed a possible interaction with SBP1 and PfEMP1 (Kaur et al. 2018). We have not performed further analyses to validate this observation. However, considering the SBP1 distribution phenotype from our IFA, it is likely possible that there is an unknown functional relationship between SBP1 and Pfj23. Co-immunoprecipitation using Pfj23 antibody could be able to reveal its possible interactors and its location. Additionally, an SBP1 immunotEM analysis could help to have a detailed observation of the localisation of SBP1 upon Pfj23 truncation.

Investigation of the Maurer's Clefts architecture using transmission electron microscopy (TEM) revealed segmented MCs structure with globular shape upon *pfj23* disruption (Figure 17). Similar MCs morphology with globular shape was obtained in iRBCs with depleted PTP1 (Rug et al. 2014). Additionally, knockout of several genes encoding for MCs resident proteins (GEXP07, REX1, MAHRP1, Pf332 and SBP1) displayed severe aberrant MCs morphologies in iRBCs (Figure 27) (McHugh et al. 2020; McHugh et al. 2015; Spycher et al. 2008; Cooke et al. 2006; Glenister et al. 2009). Similar to these studies, our data indicate that Pfj23 contributes to the structural integrity of the MCs architecture. The PEXEL motif of Pfj23 allows this protein to be exported to the red blood cell during the parasite blood-stage development. Additionally, the two putative TM domains of Pfj23 is a feature that could predict its localization either at the MCs, RBC plasma membrane or the parasitophorous vacuole (PVM) of the parasite-infected RBCs (iRBCs). Previous studies using a co-immunoprecipitation approach reported Pfj23 to be localized at the Maurer's Clefts (Das et al. 2019; McHugh et al. 2020; Vincensini et al. 2005). Considering our SBP1 distribution and MCs morphology phenotype upon Pfj23 truncation, it is likely possible that Pfj23 is an MC resident protein. However, its localisation remains to be validated in our study using the Pfj23 complementation cell line (ongoing). Although MCs were segmented upon Pfj23 truncation, the distribution of REX1, which is another MC protein (Hanssen et al. 2008), was not impaired (Figure 16). An explanation could be that despite the aberrant morphology of MCs in our Pfj23 truncated line, REX1 is still trafficked properly to the MCs. Our observation is consistent with previous studies where distorted MCs morphologies upon MAHRP1 and PTP1 inactivation did not show aberrant REX1 distribution (Spycher et al. 2008; Rug et al. 2014).

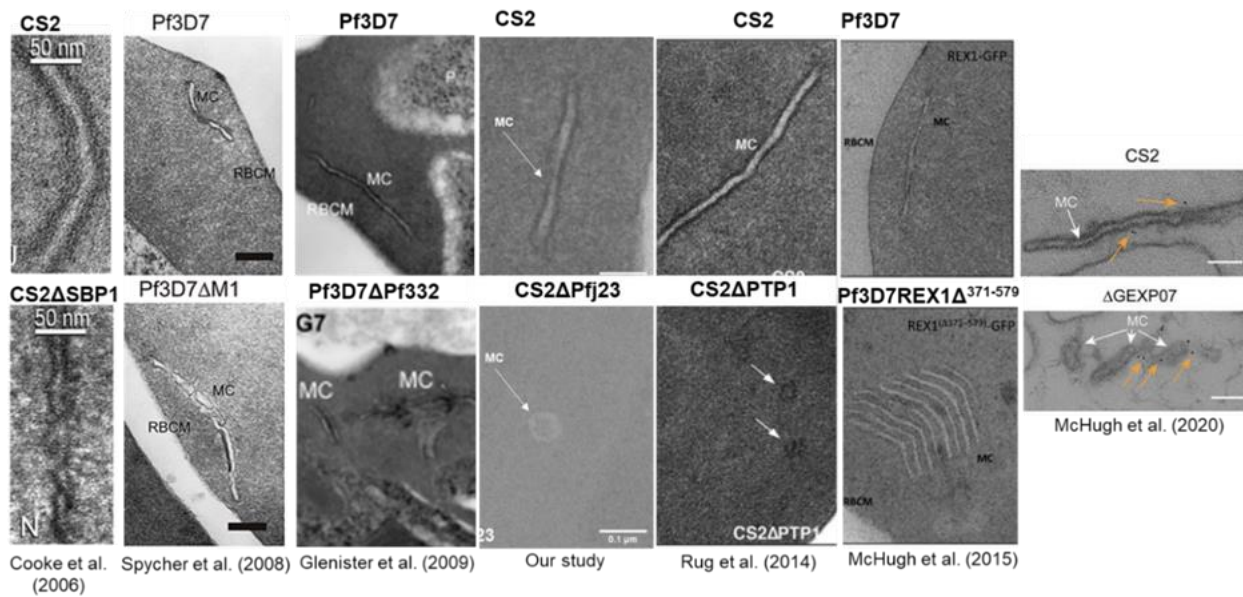


Figure 27: Comparison of our study with other aberrant Maurer's clefts (MCs) morphologies phenotype resulted from the knockouts of several genes (SBP1, MAHRP1, Pf332, PTP1, REX1 and GEXP07) encoding for proteins located at the MCs. These phenotypes were observed from various studies over the past 20 years.

Electron-dense protrusions known as knobs begin to form ~20 hrs post-invasion on the iRBCs membrane mediated by a protein complex mainly dominated by KAHRP (Rug et al. 2006). Scanning and transmission electron microscopy revealed distorted knobs morphologies upon Pfj23 truncation (Figure 18, Figure 19, Appendix 1 and Appendix 2). These aberrant knobs appeared to be deformed, enlarged and elongated with a worm-like shape. Our result is similar to recent studies, which reported aberrant knobs morphologies upon *PFA66Aw* and *gexp07* disruption (Diehl et al. 2021; McHugh et al. 2020). Therefore, our data suggest that Pfj23 contributes to the correct formation of knobs on the parasite-infected erythrocytes membrane. KAHRP is essential for knob formation (Crabb et al. 1997), but despite the observed knob phenotype in our study, KAHRP distribution on IFA was not affected upon Pfj23 truncation (Figure 16). Hence, It remains obscure the way Pfj23 exactly exerts its contribution to the knob formation. Nonetheless, investigation using KAHRP immuno-TEM and tomography could be helpful to reveal more details about the knobs and the localisation of KAHRP in these structures upon Pfj23 truncation.

The virulence of *P. falciparum* infection is partly due to its ability to traffic PfEMP1 to the RBC membrane, whereby it mediates the sequestration of iRBCs within the microvasculature of the host. Moreover, this cytoadhesive property of iRBCs seems to be a process that increases when the parasite matures during the late stage of its intraerythrocytic development (Wahlgren, Goel, and Akhouri 2017b; Dasanna et al. 2017). We evaluated a possible contribution of Pfj23 to this process using a static binding assay to chondroitin sulfate A (CSA). Infected erythrocytes with parasites depleted of Pfj23 exhibited reduced binding to CSA (Figure 20). Our result is similar to the findings of Diehl and colleagues, along with the study of McHugh and colleagues, where parasites mutants depleted of PFA66Aw and GEXP07 showed reduced binding to CSA, respectively (McHugh et al. 2020; Diehl et al. 2021). Our data suggest that Pfj23 contribute to the ability of iRBCs to bind endothelium receptors. According to *PlasmoDB*, Pfj23 is the only homologue of the PTP5 protein, which has been shown to be involved in PfEMP1 export (Maier et al. 2008). Additionally, recombinant Pfj23 protein was shown *in vitro* to interact with PfEMP1 and SBP1 (Kaur et al. 2018). Although our data showed that Pfj23 plays a role in promoting the binding of parasite-infected erythrocytes, the mechanism by which Pfj23 contribute to this process remains enigmatic. It is known that PfEMP1 is trafficked first to the MCs and then transferred to the erythrocyte membrane (Voigt et al. 2000). Furthermore, alterations in MCs architecture were postulated to indirectly or directly affect the efficiency of PfEMP1 trafficking to the erythrocyte membrane (McHugh et al. 2015). It is possible that Pfj23, through its contribution to the structural integrity of MCs, influences the efficient trafficking of PfEMP1 to the MCs *en route* to the RBC membrane, thereby leading to the observed reduced binding. In addition, disruption of SBP1 revealed a loss of PfEMP1 trafficking to the RBC membrane (Maier et al. 2007; Cooke et al. 2006). Using IFA, the truncation of Pfj23 showed an aberrant distribution of SBP1. Hence, it could also be possible that Pfj23 influences the trafficking of PfEMP1 through its effect on SBP1. A recent study reported a reduced binding of parasite depleted of PFA66Aw to CSA and suggested that PfEMP1 is exported correctly to the surface but is either not correctly presented or not correctly folded (Diehl et al. 2021). Besides, another possible explanation of the reduced binding phenotype could be that PfEMP1 is trafficked correctly to the iRBC surface but fails to anchor properly in the aberrant knobs morphologies observed upon Pfj23 truncation. Further experiments such as an IFA staining using anti-EMP1 and a flow cytometry analysis will help to understand if PfEMP1 is still trafficked to iRBC membrane in the parasite mutants depleted of Pfj23.

In summary, using the SLI-TGD approach, we were able to target 15 genes for disruption and classified 14 genes as likely essential and *pfj23* as nonessential. Characterization of the *pfj23* gene revealed that its encoding exported protein contributes to the SBP1 localisation and the structural integrity of Maurer's clefts. Also, we showed that Pfj23 plays a role in the correct display of knobs on the parasitized erythrocyte membrane. Finally, we showed that Pfj23 contributes to the binding of iRBCs to the endothelium receptors. Further analysis of the function of Pfj23 could provide an important new insight to combat the *Plasmodium falciparum* malaria infection.

3.3 Selection linked integration glmS (SLI-glmS) approach.

Plasmodium falciparum genes encoding for exported proteins induce host cell modifications in the infected erythrocytes (Matthews, Pitman, and de Koning-Ward 2019). Parasite genes encoding for exported proteins essential for its survival could only be characterized using an inducible knockout system or a conditional knockdown approach at a protein level. Our screening data revealed that 14 genes encoding for exported proteins are likely essential for parasite survival. With the aim to characterize these genes, we introduced a *glmS* ribozyme sequence in the 3' UTR of the gene of interest (GOI), which allows the knockdown of the protein of interest (POI) upon glucosamine treatment (Prommana et al. 2013). Additionally, an inactivated version of *glmS* here named *M9* was generated as a control for each gene of interest. The *glmS* system, in combination with the selection linked integration (SLI-*glmS*) (Birnbaum et al. 2017), was used to quickly generate parasite lines with a regulatable copy of each GOI (Figure 21). The SLI-*glmS* transfectants of *PF3D7_0301800*, *PIESP1*, *PF3D7_1401200* and *CBP1* (Table 3) were generated, but only *PF3D7_0301800* was further analysed.

3.4 Generation of the SLI-*glmS* regulatable copy of the PF3D7_0301800 protein and phenotypic characterization.

In our SLI-TGD screening, we classified *PF3D7_0301800* as likely essential for parasite survival (Table 2). Our result was consistent with the *P. falciparum* large genome screening study of Zhang et al. in 2018. According to *PlasmoDB*, *PF3D7_0301800* is a ~31 kDa exported protein with an unknown function and having neither a putative transmembrane domain nor a predicted GPI anchor. Using the selection linked integration (Birnbaum et al. 2017), we generated parasite integrants with a *glmS* regulatable copy of the *PF3D7_0301800* protein (Figure 23A). The generated *glmS* line of *PF3D7_0301800* protein named *CS2PF800^{glmS}* and the control line as

CS2PF800^{M9} were successfully verified for correct integration via PCR and protein expression through western blot (Figure 23C, D, E). Glucosamine treatment showed a successful knockdown of PF3D7_0301800 in the CS2PF800^{glmS} line and, as expected, no downregulation in the CS2PF800^{M9} control line (Figure 23F). These results show that PF3D7_0301800 is conditionally regulated via the *glmS* ribozyme system, thereon enabling us to characterize this protein. We were not able to quantify the knockdown efficiency of our protein of interest (POI) because the blots from the western blot data were overexposed. However, previous studies using the *glmS* ribozyme system reported a phenotype upon achieving more than 50% reduction of PTEX150 and PfDHFR-TS (Elsworth et al. 2014; Prommana et al. 2013). The usage of the 2A skip peptide in our SLI approach allows, through a process called ribosome skipping (Straimer et al. 2012), the expression of two individual proteins (in our case, PF3D7_0301800 and the protein conferring resistance to neomycin/G418) from one polycistronic mRNA (Figure 23A). The 2A skip peptide-mediated ribosome skipping is not always fully efficient, thereby leading to the synthesis of a skipped product (both proteins separately) and an unskipped product (both proteins together as one chimaera) (Matthews, Kalanon, and de Koning-Ward 2019). Although the skip inefficiency did not significantly affect the finding in the latter study, both of our cell lines (*glmS* and *M9*) did not show any unskipped product (Appendix 6). Moreover, a previous study used the SLI-*glmS* strategy to generate a regulatable copy of the *P. falciparum* lipocalin (PfLCN) protein and did not report any skip inefficiency (Burda et al. 2020). Thus, our strategy is robust and efficient for characterizing PF3D7_0301800 encoding for an unknown exported protein likely essential for the survival of *P. falciparum* during the blood-stage development.

Downregulation of PF3D7_0301800 using various concentration (0mM, 1,25mM, 2,5mM and 5mM) of glucosamine (GlcN) did not show any significant growth defect. However, a growth defect was seen with 5mM GlcN treatment when compared to 0 mM GlcN (Figure 24A). The observed growth phenotype was likely due to the cytotoxicity of the GlcN concentration as the comparison between CS2PF800^{glmS} and the control CS2PF800^{M9} at 5mM GlcN treatment did not show any growth defect (Figure 24A). Hence, optimum downregulation of our protein of interest with no cytotoxicity effect was achieved using a concentration of 2,5 mM GlcN, resulting in no growth defect over a period of 72 hours (1,5 cycles) GlcN treatment. Not seeing a growth phenotype upon our POI knockdown does not indicate that the protein is not important for the parasite survival. An explanation to this resulting observation could be that the remaining PF3D7_0301800 upon its knockdown is still enough to ensure the parasite's growth during the blood-stage development. Recently, downregulation of the exported protein PF3D7_1401200 (classified as likely essential

in our screening) did not show any significant growth effect over two cycles but resulted in a 50% reduction of parasite growth on the third cycle of 2,5mM GlcN treatment (Jonsdottir et al. 2021). Addedly, the *P. falciparum* lipocalin (PfLCN) knockdown showed more than 50% reduction of parasite growth after 96 hours (2 cycles) of 2,5mM GlcN treatment (Burda et al. 2020). In comparison with our results, it could be possible that the 72 hours (1,5 cycles) of GlcN treatment was not enough to see a potential growth difference. Hence, a longer GlcN treatment for the knockdown of PF3D7_0301800 may reveal a potential parasite growth defect. Nonetheless, a growth assay resulting in no parasite growth defect does not always translate that PF3D7_0301800 is not important for other parasite cell biology processes. Therefore, further analyses were performed to characterize the POI.

We performed immunofluorescence assays (IFA) to investigate the effect of PF3D7_0301800 knockdown on several exported protein markers. Our preliminary data show that downregulation of the POI did not impair the distributions of SBP1, REX1 and EMP3, thereby possibly suggesting that PF3D7_0301800 does not have an effect on their localizations (Figure 24B, C, D). Strikingly, our results showed aberrant KAHRP distribution upon PF3D7_0301800 downregulation (Figure 25A). Moreover, expression of a *KAHRP-mCherry* fusion in the *CS2PF800^{gImS}* (*CS2PF800^{gImS}[KAHRP::mCh]*) resulted in aberrant KAHRP distribution upon knockdown of the POI (Figure 25B). At this stage of the project, we did not draw any firm conclusion from this observation as these data represent preliminary results and thus will require additional reevaluation. Previous studies showed similar aberrant KAHRP distribution on IFA upon truncation of several KAHRP domains (Looker et al. 2019; Rug et al. 2006). Hence, repeated and further analyses will be carried out with the aim to unravel the potential role of PF3D7_0301800 in KAHRP trafficking and localization. The KAHRP protein has been shown to be essential for knobs formation on the plasma membrane of iRBCs (Crabb et al. 1997). Accordingly, the potential observed effect on KAHRP distribution (IFA data Figure 25A, B) allowed us to hypothesized that PF3D7_0301800 might colocalize with KAHRP in the knobs. As a result, PF3D7_0301800 appeared to be exported to the RBC cytoplasm but mainly does not colocalize with KAHRP (Figure 25C). Henceforth, colocalization assays with other marker proteins will be performed with the purpose to reveal the precise localization of PF3D7_0301800 in the iRBC cytoplasm.

Investigation of knobs morphologies upon PF3D7_0301800 knockdown via scanning and transmission electron microscopy revealed a smooth plasma membrane of infected erythrocytes deficient of knobs (knobless) (Figure 26A, B; Appendix 3 and Appendix 4). So, this phenotypic observation indicates that our POI through an unknown mechanism contributes to the formation

of knobs on the plasma membrane of iRBCs. Although we have not yet been able to quantify the knockdown efficiency of our POI, two cell populations (with knobs and knobless) were found in iRBCs with downregulated PF3D7_0301800 (Appendix 3 and Appendix 4). The control *M9* line did not display iRBCs with a knobless phenotype upon glucosamine treatment. Thus, the infected erythrocytes with knobs seen in the downregulated *glmS* line were likely from the residual PF3D7_0301800 protein as a complete knockdown could not be attained. Our finding is similar to previous studies whereby iRBCs with KAHRP truncation displayed a knobless phenotype (Crabb et al. 1997; Rug et al. 2006; Looker et al. 2019). We have not yet quantified this phenotype because many SEM pictures (minimum of 15 from each condition) need to be taken in order to evaluate how many cells have a knobless phenotype in our study (ongoing). Future work will be focused on titrating the effect of the different GlcN concentrations (0mM, 0,75mM, 1,25mM and 2,5mM) on the observed knobless phenotype. Knob assembly complex formation is a multifaceted process requiring a concerted array of exported proteins mainly dominated by KAHRP (Cutts et al. 2017). A spiral scaffold underlies the shape of knobs with five KAHRP units connected and maintained together in a knob by an unknown protein (Looker et al. 2019). We first hypothesized that the unknown protein was PF3D7_0301800, but our localization assay data showed that our POI does not colocalize with KAHRP (Figure 25C). Therefore, considering all our data, we postulate that PF3D7_0301800 could directly or indirectly, through an unknown mechanism, plays a role in the trafficking of KAHRP to the knob. Further investigation such as KAHRP immuno-TEM will help to reveal the localization of KAHRP upon PF3D7_0301800 knockdown. Additionally, a binding assay as performed in the analysis of Pfj23 will be carried out to evaluate the cytoadhesion phenotype of infected erythrocyte with downregulated PF3D7_0301800.

In summary, we were able to generate a regulatable *glmS* cell line of the exported PF3D7_0301800 protein in this second part of the project. Additionally, we showed that its downregulation neither affects the parasite growth nor displays aberrant distributions of SBP1, REX1, and EMP3 exported protein markers. Furthermore, our preliminary data showed an aberrant KAHRP distribution upon PF3D7_0301800 knockdown. Finally, iRBCs with downregulated PF3D7_0301800 protein displayed a knobless phenotype. Further analysis will be performed to investigate the potential role of PF3D7_0301800 in the knobs assembly complex formation. Deciphering the function of PF3D7_0301800 will contribute to the understanding of the malaria parasite biology

MATERIAL AND METHODS

4 Material and Methods

4.1 Methods

4.1.1 Molecular and biochemical based methods.

4.1.1.1 Polymerase chain reaction (PCR).

The polymerase chain reaction (PCR) is a method that allows a specific amplification of a DNA template using two oligonucleotides called primers. The latter flank the DNA fragment region to be amplified through multiple rounds of amplification by the enzyme called DNA polymerase. The reaction involves repeated cycles of heat denaturation of the DNA, annealing of the primers to their complementary sequences, and extension of the annealed primers (Figure 28). The newly DNA synthesis by the polymerase starts with the 3' end leading to the amount of DNA doubling in each successive cycle. The KOD polymerase possesses a proof-reading activity causing fewer errors in the amplification process. Therefore, it was used to amplify inserts for cloning. Regular PCR diagnostic checks such as colony PCRs, integration PCRs were performed using the Taq polymerase.

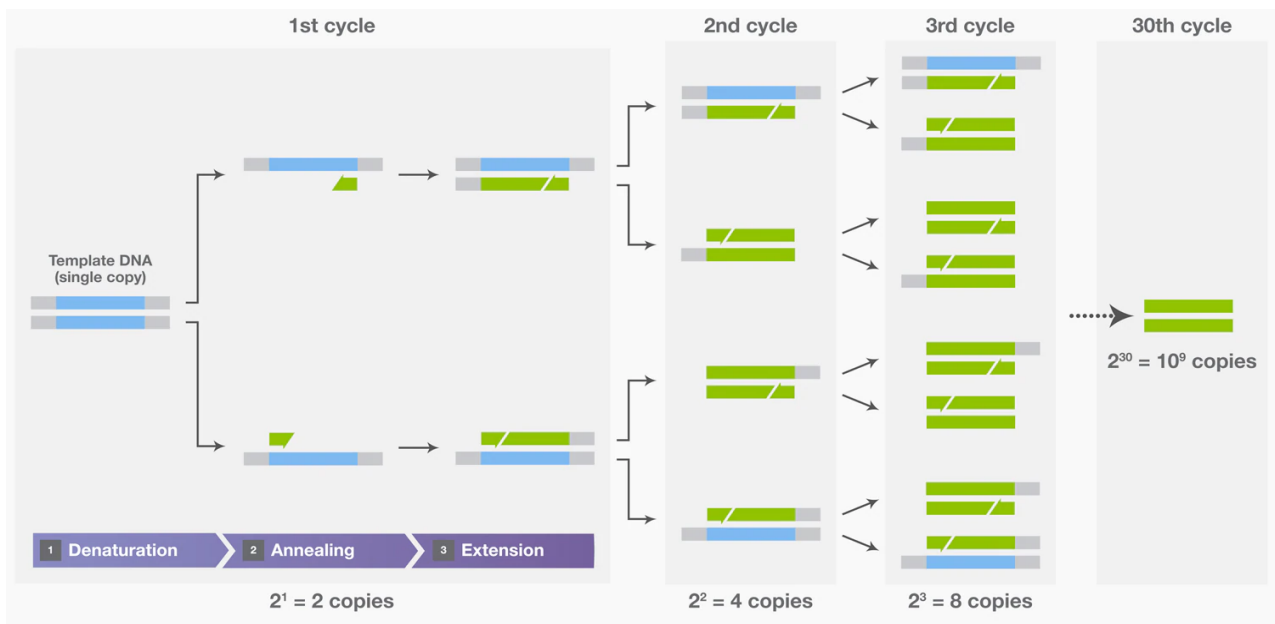


Figure 28: Three steps of the PCR reaction. Denaturation, annealing, and extension as shown in the first cycle, and the exponential amplification of target DNA with repeated cycling. (ThermoFisher Scientific).

KOD reaction components

5 units KOD Hot-Start polymerase
5 µl KOD buffer 10x
5 µl dNTPs (2 mM each; final conc. 10mM)
3 µl MgSO₄ (25 mM; final conc. 1.5 mM)
1 ng Template DNA
0,5 µl forward primer (final conc. 0,5 pmol/µl)
0,5 µl reverse primer (final conc. 0,5 pmol/µl)
filled up to 50 µl with ddH₂O

KOD PCR program: 30 cycles

1) Initial denaturation	95°C	5 min
2) Denaturation	95°C	1 min
3) Annealing*	50°C	1 min
4) Elongation	70°C	30s/kb
5) Final elongation	70°C	10 min
6) Storage	4°C	∞

Taq: Typical reaction

2.5 µl of 10xTaq Buffer
2 mM dNTP-mix
0,5 µl forward primer (final conc. 5 pmol/µl)
0,5 µl reverse primer (final conc. 5 pmol/µl)
1 µl self-made Taq polymerase
Filled up to 25 µl with with ddH₂O

Normal Taq PCR program: 35 cycles

1) Initial denaturation:	95° C, 6 min
2) Denaturation	95°C, 1 min
3) Annealing*	45°C, 1 min
4) Elongation	68°C, 60s/kb
5) Final elongation:	68°C, 10min
6) Storage	4°C, ∞

IntegrationTaq PCR program: 50 cycles

- 1) Initial denaturation: 95° C, 10 min
- 2) Denaturation 95°C, 1 min
- 3) Annealing* 45°C, 1 min
- 4) Elongation 60°C, 8 min
- 5) Final elongation: 60°C, 10min
- 6) Storage 4°C, ∞

* Annealing temperature is dependent on the lowest melting temperature of the used primers. Typically, a temperature 5-10 °C below was chosen to get a high specificity of primer annealing.

4.1.1.2 Colony PCR.

Colony PCR screening was used to verify which colony from the previous transformation contains the correct plasmid. One specific forward primer was used for the insert and the reverse primer for the plasmid. Single *E. coli* colonies were picked with a pipette tip, replicated on an LB agar plate (backup plate), and then resuspended in the reaction mix.

Colony PCR reaction

25 µl Colony mix
0,5 µl forward primer (final conc. 5 pmol/µl)
0,5 µl reverse primer (final conc. 5 pmol/µl)
5 units Taq polymerase

COL PCR program: 35 cycles

1) Initial denaturation	95°C	10 min
2) Denaturation	95°C	1 min
3) Annealing	50°C	1 min
4) Elongation	68°C	1 min/kb
5) Final elongation	68°C	10 min
6) Storage	4°C	∞

Colony mix

1 ml Cresol red solution
600 µl Taq polymerase buffer 10x
120 µl dNTPs (10mM each)
fill up to 6 ml with ddH₂O

Cresol red solution

0,1 g/10 ml O-Cresolsulfonephthalein
60% (v/v) Sucrose in ddH₂O

Taq polymerase buffer 10x

200 mM Tris
100 mM KCl
100 mM (NH₄)₂SO₄
20 mM MgSO₄
1% (v/v) Triton-X-100
pH 8,8

4.1.1.3 Preparation of plasmid DNA.

The QIAGEN Plasmid Maxi Kit was used for the generation of large amounts of DNA (300-600 ng/µl) for transfection. 4 ml SB medium with 50 µg/ml Ampicillin was inoculated with a single E. coli colony and incubated at 37°C in the shaking incubator for 6 hours. The preculture was transferred to 400 ml SB medium with 50 µg/ml Ampicillin for incubation overnight at 37°C in the shaking incubator. Plasmid DNA was then prepared according to the provided QIAGEN Plasmid Maxi Kit protocol. For smaller amounts of DNA (100-300 ng/µl) preparation for test after ligation, 3 ml SB medium with 50 µg/ml Ampicillin was inoculated with a single colony and incubated overnight at 37°C in the shaking incubator. The plasmid DNA was prepared with the peqGOLD Plasmid Miniprep Kit I according to the provided protocol. All purified DNAs were stored at -20°C in the TE buffer.

Tris-EDTA (TE) buffer

10 mM Tris/HCl
1 mM EDTA
pH 8.0

4.1.1.4 Restriction digestion of DNA.

Many different restriction enzymes recognise various restriction sites and produce blunt ends or 3' and 5' overhangs. In cloning a new construct, the vector was digested overnight (6 hours and kept at 4°C), and the new amplified insert was digested with specific enzymes for 2 hours at 37°C. The digested vector was dephosphorylated by Antarctic phosphatase for 30 min and deactivated at 80°C for 2 minutes to prevent the vector's religation without the insert. The concentration of both digests was measured on a nanodrop, and the DNA was purified using the peqGOLD Cycle-Pure Kit or the peqGOLD Gel Extraction Kit and eluted in 30 µl ddH₂O. For regular restriction digestion test after miniprep or maxiprep preparation, respective enzymes were used to digest the DNA for 30-60 min at 37°C. A typical reaction contains:

Vector digest

2 µg DNA
5 µl buffer 10x (NEB)
20 units each enzyme
filled up to 50 µl with ddH₂O

Insert digest

15 µl DNA
3 µl buffer 10x (NEB)
5 units each enzyme
filled up to 30 µl with ddH₂O

Vector dephosphorylation

50 µl vector digest mix
5 µl Antarctic phosphatase buffer 10x
10 units Antarctic phosphatase

Test digest

5/2 µl mini/maxi
1 µl buffer 10x (NEB)
1 unit each enzyme
filled up to 10 µl with ddH₂O

4.1.1.5 Agarose gel electrophoresis.

This method was used to separate DNA fragments according to their size. It permits analysis if fragments have the wanted size following a DNA restriction or PCRs. Because DNA molecules are negatively charged, they migrate to the positively charged anode. The separated DNA fragments were visualised by gel staining with ethidium bromide or UV light exposure (in Gießen) An agarose gel was prepared by solving and boiling the respective amount of agarose in the 1x TAE buffer in the microwave. Then, 50 ng/µl ethidium bromide or the DNA staining dye (Gießen) was added, and the solution was poured into a gel chamber. A comb was applied to form the wells for the samples. After solidification at room temperature, the gel was transferred to a gel chamber and covered with 1x TAE. The DNA sample was mixed with a loading dye and transferred into a well of the agarose gel on the cathode site. A DNA size standard (1 kb+) was placed into a well next to the sample as a standard of comparison. An electric field (90-120 V, 400 mA) was then applied to the DNA samples for 30-90 minutes.

Tris-Acetate-EDTA (TAE) buffer 50x

2 M Tris
2 M Acetic acid
50 mM EDTA

DNA loading dye 6x

50 mM Tris/HCl
5 mM EDTA
30% (v/v) Glycerol in ddH₂O
1% (v/v) Bromophenol blue
pH 8.0

1 kb+ DNA size standard

940 µl TE buffer 1x
200 µl DNA loading dye 6x
60 µl 1 kb+ DNA ladder

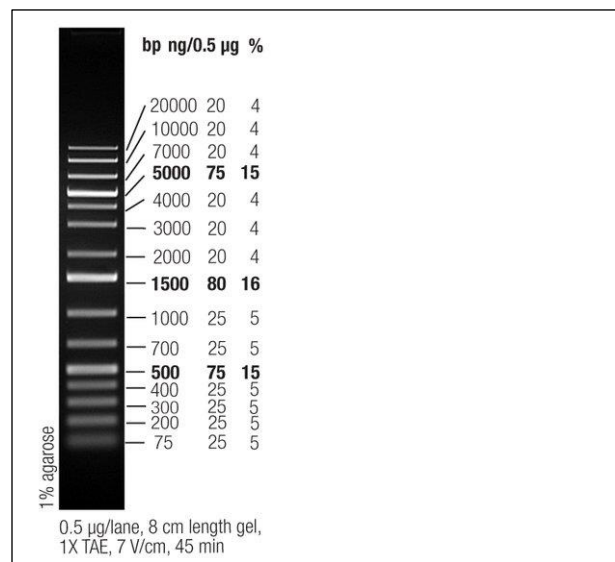


Figure 29: 1kb+ DNA size standard (ThermoFisher Scientific).

4.1.1.6 Ligation of DNA fragments.

The Ligase enzyme catalyzes the joining of multiple DNA fragments with 5' and 3' end (overhangs or blunt) by covalently forming new phosphodiester bonds between the 3' hydroxy and the 5' phosphate end of a double-stranded DNA. This method was used to ligate the digested insert into a digested vector, which resulted in a component called constructs. The insert and vector were ligated in a 3:1 molar ratio and incubated for 2 hours at RT or left at 16°C overnight.

Ligation

3:1 insert : vector

2 µl T4 ligase buffer 5x

1 unit T4 ligase

Filled up to 10 µl with ddH₂O

4.1.1.7 Transformation of electrocompetent *E. coli* PMC103

Transformation via electroporation was done using precipitated DNA in 10 µl ddH₂O. Then 50 µl thawed electrocompetent PMC103 cells were added, mixed, and transferred to an electroporation cuvette followed by electroporation at 2kV, 25 µF and 200 Ω. 1 ml SOC medium was added to the cells immediately and cooled down for 2 min on ice. After incubation for 1 hour at 37°C in the shaking incubator, cells were plated on an LB-agar plate containing Ampicillin for vector selection.

Super Optimal Broth (SOB) medium

20 g/l Peptone

5 g/l Yeast extract

10 mM NaCl

2,5 mM KCl

20 mM MgCl₂

Luria-Bertani (LB) agar

35 g/l LB agar

Ampicillin

final concentration: 50 µg/ml

Super Optimal Broth with Catabolite repression (SOC) medium

SOB medium

20mM Glucose

4.1.1.8 Transformation of chemocompetent cells.

A quantity of DNA was mixed with a respective *E. coli* strain and incubated for 5 min on ice. The mixture was then heated shock at 42°C for 45 seconds and 1 ml SOC medium was added and cooled down for 2 min on ice. After incubation for 1 hour at 37°C in the shaking incubator, cells were plated on an LB-agar plate containing Ampicillin.

4.1.1.9 DNA sequencing

For verification of completed constructs, DNA samples and primers were send to Eurofins for sequencing.

Plasmid

20 µl DNA sample (30-100 µg/mL)

Fill up to 20 µl ddH₂O

Primer

4 µl Primer (5 pmol/µl)

16 µl ddH₂O

4.1.1.10 SDS PAGE.

Sodium Dodecyl Sulfate polyacrylamide gel electrophoresis (SDS-PAGE) allows the separation of proteins according to their molecular weight. SDS is an anionic detergent that linearises polypeptides and adds negative charges in proportion to the molecular weight of the proteins. Protein samples were resuspended in a 2x loading buffer containing the reducing agent dithiothreitol (DTT), which breaks the disulphide bonds within the proteins, followed by denaturation at 100°C for 10 minutes. The protein samples were centrifuged at 20000g for 10 minutes at 4°C, and a volume equal to a certain number of infected cells (10⁷ cells per well) was loaded onto a discontinuous SDS-polyacrylamide gel. Due to the different pH of the stacking and separating gel, a more precise separation of the proteins is achieved. The gel was run at 90 V in SDS running buffer until the proteins passed the 5% stacking gel. Once the proteins entered the 12% separating gel, the voltage was increased to 120 V. Protein separation was carried out until the dye front reached the end of the gel. The molecular weight of the separated proteins is determined through the comparison with the PageRuler Prestained Protein Ladder (Figure 30).

Stacking buffer 4x

500 mM Tris/HCl

0,4% (w/v) SDS (w/v)

pH 6,8

Separating buffer 4x

1,5 M Tris/HCl

0,4% (w/v) SDS

pH 8,8

Ammonium peroxodisulfate solution (APS)

10% (w/v) APS in ddH₂O

Loading buffer 2x

100 mM Tris/HCl

100 mM DTT

20% (v/v) Glycerine

5 mM EDTA

4% (w/v) SDS

0,2% (v/v) Bromphenolblue

pH 6,8

SDS running buffer

124 mM Tris

960 mM Glycine

0,04% (w/v) SDS

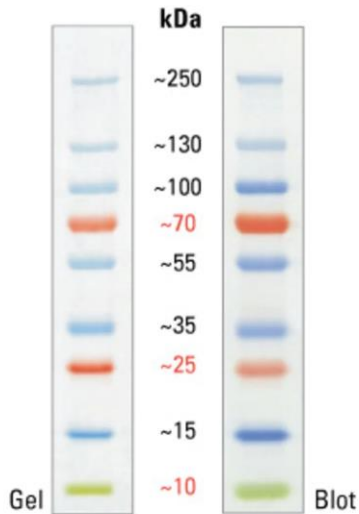


Figure 30 SDS-PAGE band profile of the PageRuler Prestained Protein Ladder. Images are from a 4 20% Tris glycine gel (SDS-PAGE) and subsequent transfer to membrane. (ThermoFisher Scientific)

Table 5: Pipetting scheme for one polyacrylamide gel.

Reagent	5% Stacking gel	12% Separating gel
4x Gel buffer	1.25 ml	2,5 ml
Acrylamide	840 μ l	3,7 ml
APS	50 μ l	80 μ l
TEMED	3,8 μ l	6 μ l
ddH ₂ O	2,8 ml	3,8 ml

4.1.1.11 Semi-dry Western Blot.

After SDS-PAGE separation, proteins were transferred from the SDS gel onto a nitrocellulose membrane for detection using specific antibodies. Three sheets of Whatman paper were cut and placed on a blotting chamber. Then, the gel was placed on the Whatman papers, followed by the nitrocellulose membrane and three Whatman paper on top. Before preparation of the sandwich, the Whatman paper and the membrane were immersed, and the membrane was blotted at 1 mA/cm² for 90 minutes. The electric field enables the proteins to move from the gel onto the membrane. Next, the membrane was stained with Ponceau red solution and rinsed with PBS until the protein band were visible. Afterwards, the membrane was blocked in blocking solution for 1

hour at RT with constant shaking to avoid unspecific binding of antibodies. The primary antibody was diluted in blocking buffer to the desired working concentration and incubated with the membrane overnight at 4°C. The next day, the membrane was washed three times for 10 minutes with PBS to remove unbound primary antibodies. The second antibody directed against the primary antibody and conjugated to Horseradish Peroxidase (HRP) was diluted 1:2000 in blocking buffer and added to the membrane for 2 hours at room temperature with constant shaking. Then, the membrane was washed three times with PBS for 10 minutes to remove unbound antibodies again. Finally, the membrane was developed through the ECL detection system. The addition of ECL solution and H₂O₂ causes the HRP to produce a light signal which can be detected using an X-ray film.

Blotting buffer 10x

48 mM Tris
39 mM Glycine
0,04% (w/v) SDS
pH 9,5

Phosphate buffered saline (PBS)

10 mM Tris
140 mM NaCl
2.7 mM KCl
1.4 mM K₂HPO₄
0.8 mM KH₂PO₄
pH 7,4

Developer

571 mM Na₂SO₄
452 mM Na₂CO₃
80 mM Hydroquinone
34 mM KBr
6,4 mM Metol

Western Blot transfer buffer

80% (v/v) 1x Blotting buffer
20% (v/v) Methanol

Ponceau red solution

0,2% Ponceau S
3% Trichloroacetic acid

Blocking buffer

5% (w/v) milk powder in PBS

ECL solution

200 mM Tris
5 mM p-Coumaric acid
0,8 mM Luminol
pH 8,5

Fixer

500 ml AGFA Rapid Fixer G354
in 2,5 l ddH₂O

4.1.2 Cell culture methods.

4.1.2.1 Cultivation of *P. falciparum* parasites.

P. falciparum parasites cultivation was done under sterile conditions. It was carried out in small or big petri dishes with complemented media and fresh human erythrocytes. Transfectants and freshly thawed parasites were cultivated with Albumax media and fresh O+ or A+ blood. All other parasites were cultured with RPS media. Parasites were incubated at 37°C in petri dishes filled with the appropriate cell culture medium under the followed conditions 95% N₂, 5% CO₂ and 5% O₂ (Haynes et al. 1976)

RPS medium

500 ml RPMI 1640
10% (v/v) Human plasma
2 μ M Hypoxanthine
100 μ g/ml Neomycin

Albumax media

500 ml RPMI 1640
5% (v/v) Human plasma
5% (v/v) Albumax
2 μ M Hypoxanthine
100 μ g/ml Neomycin

6 well plate: 5mL media and 200 μ l.

Small plate: 12mL media and 500 μ l of blood.

Big plate: 36mL media and 1.5mL blood.

4.1.2.2 Synchronisation of *P. falciparum* parasites via sorbitol.

Sorbitol allows ring stage synchronisation of parasite cultures by selective lysis of trophozoite and schizont parasite stages (Lambros and Vanderberg 1979). Since the late-stage parasites induce a higher permeability of their host cells, sorbitol enters and lyse the late-stage infected erythrocytes, causing an osmotic imbalance. Ring stage infected erythrocytes survive the sorbitol treatment. Infected erythrocytes were resuspended in 5 ml (small plate) or 10 ml (big plate) sorbitol. After incubation for 10 min at 37°C, ring-stage infected erythrocytes were harvested at 3000 rpm for 2 minutes. After washing twice with prewarmed RPS media, the red blood cells were transferred to a new prepared petri dish.

Sorbitol solution

5% (w/v) Sorbitol

4.1.2.3 Gelatin flotation selection.

Gelatine floatation was used to enrich the knob-forming, mature-stage *P. falciparum* iRBCs (Goodyer et al. 1994). Centrifugation at 3000 rpm for 2 min allowed us to harvest the parasites. Then, they were resuspended in prewarmed gelatine solution followed by incubation at 37°C for 15-20 min. The supernatant (containing the enriched parasites) was carefully removed to a new tube and washed once with 10 ml medium. Afterwards, the parasites were re-seeded, and enrichment was followed via Giemsa smears.

4.1.2.4 Giemsa staining.

This staining was used to evaluate the parasitemia. To do that, 5 μ l of erythrocytes was streaked on a microscope slide, air-dried, fixed with methanol and stained for 10min with Giemsa solution. Then the percentage of infected RBCs in relation to the uninfected RBCs was counted using light microscopy (100x magnification, oil immersion objectives).

Giemsa solution

10% (v/v) Giemsa in H₂O

4.1.2.5 Freezing of *P. falciparum* parasites.

For the long term storage, infected erythrocytes (5-15% parasitemia in ring stage) were harvested at 3000 rpm for 2 minutes. Then 500 μ l of infected erythrocytes was diluted 1:2 with the freezing solution in a cryo conservation tube. After 30 minutes of freezing in liquid nitrogen, tubes were stored at - 80°C or in the liquid nitrogen tank (Diggs et al. 1975).

Freezing solution

28% (w/v) glycerol in ddH₂O

3% (w/v) D-sorbitol in ddH₂O

0,65% (w/v) NaCl in ddH₂O

4.1.2.6 Thawing of *P. falciparum* parasites.

The frozen parasites in the cryopreservation tube were thawed in a prewarm (37°C) water bath. Then 200 μ l prewarmed 12% NaCl solution was added drop-wise with the agitation of the tube under the flow. Subsequently, 5 ml prewarmed 1.6 % NaCl solution was added drop-wise, followed in the same way by a 0.9% NaCl/Glucose solution with the agitation of the tube. Finally, the erythrocytes were harvested at 3000 rpm for 2 minutes, and parasites were re-seeded in a new plate with fresh blood and prewarmed Albumax media.

Thawing solutions

I. 12% (w/v) NaCl in ddH₂O

II. 1.6% (w/v) NaCl in ddH₂O

III. 0.9% (w/v) NaCl in ddH₂O, 0.2% (w/v) Glucose in ddH₂O

4.1.2.7 Transfection of *P. falciparum* parasites.

A synchronised ring-stage parasite culture with a parasitemia of 10-20% was aliquoted and harvested at 3000 rpm for 2 minutes for transfection. 12 ml Albumax medium and 400 μ l fresh 0+

blood was mixed and prewarmed. Transfection requires a large amount of plasmid DNA which was prepared by maxi preparation. To do so, 500 μ l DNA was precipitated, dried under the flow and resuspended in 30 μ l TE buffer. Then 370 μ l prewarmed Cytomix was added. After the addition of 200 μ l infected erythrocytes, the mix was transferred to an electroporation cuvette followed by electroporation at 350 μ F, 950 kV and high capacitance (Fidock and Wellemms, 1997). Immediately, the transfected parasites were mixed with medium and blood and transferred to a new petri dish. After 6 hours of incubation, WR99210 / Blasticidin / G418 was added for the positive selection of the transfected parasites. The media were changed daily until no more live parasites could be seen. Then media and the respective drug were changed every 4 days until the parasite was seen again via Giemsa staining. After the parasite growth reached a parasitemia of 2%, a part of the infected erythrocytes was frozen in liquid nitrogen for later experiments.

Tris-EDTA (TE) buffer

10 mM Tris/HCl
1 mM EDTA
pH 8.0

Cytomix (100 ml)

10 ml Stock solution II
6 ml 2M KCl
1 ml Stock solution III
500 μ l 1M MgCl₂
7.5 μ l 2M CaCl₂
Fill up to 100 ml with ddH₂O

pH adjusted with a stock solution I to 7.6

Cytomix stock solutions

- I. 10 M KOH
- II. 250 mM HEPES
20 mM EGTA
- III. 1 M phosphate (K₂HPO₄, KH₂PO₄) buffer pH 7.6.

WR99210: final concentration: 2,5 nM

Blasticidin: Final concentration: 12 μ g/ml

G418: Final concentration: 400 μ g/ml

4.1.2.8 Selection linked integration (SLI).

As both vectors used in this project do not contain a promoter to drive expression, only upon the integration of the plasmid into the correct gene locus (behind the endogenous promoter of the GOI) does transcription can occur. During translation, ribosome "skipping" causes the production of 2 separate proteins from only one mRNA (Straimer et al. 2012). In our case, this leads to the synthesis of the protein of interest (POI) through the *gImS* system (Figure 21) and a truncated protein in the SLI-TGD system (Figure 13). Also, the production of the selectable marker protein (in this case, the protein conferring resistance to Neomycin/G418). This eliminates the need for long-term drug cycling of parasites to select for rare integration events, as integrant parasites can

be selected from the parasite population by applying selective pressure (G418). Once transfectant parasite lines were established and frozen (back up), 400 µg/ml G418 was added to the culture media to select the correct integrant parasites. The culture media was changed daily for the first ten days and then every other day until parasites re-emerged (Birnbaum et al. 2017).

4.1.2.9 Limiting dilution parasites subcloning.

Limiting dilution was used to select and obtain single clones of *P. falciparum* transgenic cell lines. A total of ~34-35 parasites were resuspended in 23 ml of media containing appropriate drug and mixed with 240 µl of blood. 200 µl of this mixture was spread into a 96 well plate which averages ~0.3 parasites/well. Media was changed every 3-4 days for three weeks, and the growth assay was used to detect grown parasites. These likely originated from a single *P. falciparum* clone and were put into the routine culture for further experiments.

4.1.2.10 Plasmodium Cybr green growth assay.

The Sybr green growth assay in the *Plasmodium* system permits the evaluation of the growth rate of the parasite during the blood-stage growth over a period of 72 hours. Sybr green is an asymmetrical cyanine dye that intercalates unspecifically into the dsDNA, thereby allowing its staining and thus its measurement via any detection method. Parasites were synchronized at their ring-stage development. With a parasitemia of 0,2% and a hematocrit of 1,25%, parasite mutants and control were cultured in a 96-well plate (dark colour) for 72 hours. Then, the plate was frozen at -80C for a minimum period of 24 hours. The following day, parasites were allowed to thaw for 2 hours at RT. 50 µl of Syber green buffer was added to each well containing the parasites and incubated in the darkness for 1 hour at RT. Finally, parasites were measured in a Clariostar plate reader using the programme IC50.

SybrGreen Buffer pH 7,4:

0,16 g Saponin
5,0 mL 1 M Tris-HCl
1,0 mL 0,5 M EDTA
1,6 mL Triton X100
1/10000 Syber green solution
Adjust to 100 mL with ddH₂O

IC50 Programmme

Excitation: 482+/-16 Emission: 530+/-40
Gain: 840 Focal High: 10,7
Flashes/well: 10 Top optic

4.1.2.11 Chondroitin sulfate A (CSA) selection assay.

A regular selection of parasites expressing CSA binding PfEMP1 variants (Reeder et al. 1999) is required since *P. falciparum* regularly undergoes switching of PfEMP1 variants (Biggs et al. 1991) with different binding capabilities to the host cell endothelium receptors (Biggs et al. 1992). To select the iRBCs that bind to CSA (panning), 10 mL of sterile 1 mg/ml CSA in PBS was adsorbed overnight on a tissue culture flask. The following day, the flask was washed three times with 10 ml and blocked at RT for one hour with 10 ml of 1% BSA in PBS, followed by washing using 10ml cytoadhesion medium. Gelatine floatation was used to enrich late stages parasites and washed in cytoadhesion media. Then, enriched parasites resuspended in 10 ml cytoadhesion medium were applied to the flask (previously incubated with CSA) followed by one hour incubation at RT. Finally, the flask was washed five times with 10 ml of cytoadhesion media and bound iRBCs were removed from the flask and re-seeded. Giemsa-stained smears was used to follow the enrichment of the parasites before and after gelatine floatation as well as after cytoadhesion. All the procedure was performed under sterile conditions (Diehl 2019).

Cytoadhesion media: 8g of RPMI powder was dissolved in 400mL of ddH₂O. After adjustment of the pH to 7,2 with NaOH, the volume was adjusted to 500 mL, and the resulting media was sterile filtered.

4.1.2.12 Chondroitin sulphate A (CSA) binding assay.

The binding assay permits the assessment of the adhesion capability of iRBCs to the host receptor (in our case, the CSA ligand) through the PfEMP1 protein (Beeson et al. 1999). For this purpose, 20 µl of CSA solution (f.c 1mg/ml in PBS) were applied in triplicate onto circle marked spots in a petri dish. A ligand-free control (in this case PBS), as well as a control with the addition of the CSA solution (1/10 volume) to the parasites during the cytoadherence phase of the assay, were executed in parallel. The controls were used to demonstrate later that the binding of the parasites in the assay is specific to CSA. Then, the parafilm was used to seal the petri dish, and adsorption of the ligand on the petri dish was achieved overnight at 4°C. On the following day, each spot was washed three times with PBS and blocked for one hour at RT with 1% BSA in PBS. Gelatine floatation was used to enrich late stages parasites and diluted to a concentration of 5×10^7 iRBCs/ml in cytoadhesion media. Then, the blocked spots were washed once with 20 µl of cytoadhesion medium, and 20 µl of the iRBCs in cytoadhesion media

were applied onto the spots followed by an incubation of one hour at RT. The non-bound RBCs and iRBCs were removed by washing with 18 ml of cytoadhesion medium using an orbital shaker for 13 rounds at 70 rpm. The Remaining medium was removed, and the plate was washed once without shaking with 12 ml PBS. Then, the plate was fixed one hour at RT with 12 ml of 2% glutaraldehyde in PBS. Later, the fixative was removed, and the plate was washed twice with PBS and stained for 10 min at RT with filtered 10% Giemsa in ddH₂O. The plate was washed twice with PBS after the removal of the Giemsa solution. Finally, the plate was rinsed once with ddH₂O and dried overnight. To evaluate the binding efficiency of the parasites, pictures were taken with a binocular microscope. For each spot, three pictures were taken in DIC with a 10x objective. The parasites were counted using Ilastik and ImageJ software. First, Ilastik was trained with several images to distinguish background and iRBCs and later ImageJ was used to count the number of cells (Diehl 2019).

4.1.3 Microscopy based methods.

4.1.3.1 Immunofluorescence Assay.

This assay was used to investigate the subcellular localisation of exported proteins markers on an epifluorescence microscope using specific antibodies. Its principle relies on detecting the marker protein of interest using a primary antibody followed by a secondary antibody directed against the primary antibody coupled with a specific fluorophore (Wickham et al. 2001). Practically, parasites in culture were washed three times in PBS, spread on slides, dried and fixed in 90% acetone / 10% methanol solution for 10 min at -20°C. Subsequently, the slides were blocked in 3% BSA in PBS for one hour at RT and incubated with the primary antibody overnight at 4°C in a humid chamber. Following the next day, the slides were washed three times with PBS and incubated for 2 hr at RT with a secondary antibody directed against the primary antibody. After washing the slides three times in PBS, 1 ng/ml DAPI was used to stain the nucleus for 10 min in the darkness. Finally, the slides were treated with fluoromount and sealed with a coverslip and incubated overnight at 4°C. On the next day, images were taken using a Zeiss Axio-observer microscope and processed using Image J.

4.1.3.2 Scanning electron microscopy (SEM).

SEM was used to investigate the morphology of knobs on the plasma membrane of fixed infected erythrocytes. Late-stage parasites in culture were purified using MACS and fixed overnight at 4°C in 1% glutaraldehyde in PBS. On the next day, coverslips were coated with 0,1% polylysine for 20 min at RT. Following the coating, fixed parasites were washed three times in PBS, and 20 µl of cells were applied onto coverslips and incubated for 20min at RT. Next, the coverslip with coated parasites was gently washed three times with PBS and dehydrated each 10 min in a series 25%, 50%, 75% and finally in 100% acetone of ddH₂O. Following the critical point dehydration, parasites were then coated with 10 nm Au/Pd at a -10° angle and imaged with a Zeiss Lec15030 electron microscope.

4.1.3.3 Transmission electron microscopy (TEM)

TEM was used to study the subcellular structures and knobs of the infected erythrocytes. Cells were first fixed overnight at 4°C in 2% Glutaraldehyde and 2% Paraformaldehyde in CaCo solution (100mM Sodium cacodylate). The next day, the cells were washed three times with the CaCo solution for 5 min and fixed a second time with 1% Osmium in CaCo for 60 min at RT. The cells were then washed two times in ddH₂O and contrasted overnight at 4°C using 1% U- acetate in ddH₂O. Following the next day, cells were washed two times with ddH₂O for 10 min at RT and dehydrated each time for 10 min using 30%, 50%, 70%, 90% and two times in 100% acetone. Finally, cells were treated with 25%, 50% and 75% trace (original word Spurr in German) levels at RT for 45 min and kept in 100% acetone overnight until sections were prepared and imaged using a Jeol 1400 microscope operating at 80kV.

4.2 Materials

4.2.1 *Plasmodium falciparum* strains and Cell lines used in this project.

Strains	Description	Origin
CS2	Laboratory isolate from the Brazilian ItG2F6 with high binding to HA and CSA due to expression of the PfEMP1 variant VAR2CSA (Beeson et al. 2000).	Dr. Mathias Diehl (Mathias Diehl Thesis 2019)
CS2(CSA)	Obtained via re-selection of CS2 parasites (from Mathias Diehl Thesis 2019) for CSA binding.	Dr. Mathias Diehl (Mathias Diehl Thesis 2019)
CS2PF800^{gImS}	CS2(CSA) with the plasmid PF3D7_0301800 ^{gImS} integrated into the PF3D7_0301800 gene. A Clonal cell line that enables GlcN dependent downregulation of PF3D7_0301800 protein	Generated during this project. (See map in appendix)
CS2PF800^{gImS}[KAHRP::mCh]	CS2PF800 ^{gImS} cell line transfected with the plasmid KAHRP::mCh.	Generated during this project. (See map in appendix)
CS2PF800^{M9}	CS2(CSA) with the plasmid PF3D7_0301800 ^{M9} integrated into the PF3D7_0301800 gene. A Clonal cell line that PF3D7_0301800 protein cannot be downregulated via GlcN. Used as control	Generated during this project. (See map in appendix)
ΔPF3D7_0301800	CS2(CSA) with the plasmid ΔPF3D7_0301800 integrated into the PF3D7_0301800 gene, leading to the truncation of the gene.	Generated during this project. (See map in appendix)
ΔPfj23	CS2(CSA) with the plasmid ΔPfj23 integrated into the Pfj23 gene, leading to the truncation of the transmembrane domains of the Pfj23 protein.	Generated during this project. (See map in appendix)
ΔPfj23^[Pfj23::HA]	CS2ΔPfj23 cell line transfected with the plasmid Pfj23::HA.	Generated during this project. (See map in appendix)
ΔPfj23^[SBP1::HA]	CS2ΔPfj23 cell line transfected with the plasmid SBP1::HA.	Generated during this project. (See map in appendix)
ΔCBP1	CS2(CSA) with the plasmid ΔCBP1 integrated into the CBP1 gene, leading to the truncation of the gene.	Generated during this project. (See map in appendix)

ΔPF3D7_0220300	CS2(CSA) with the plasmid Δ PF3D7_0220300 integrated into the PF3D7_0220300, leading to truncation of the gene.	Generated during this project. (See map in appendix)
ΔPF3D7_0220600	CS2(CSA) with the plasmid Δ PF3D7_0220600 integrated into the PF3D7_0220600 gene, leading to the truncation of the gene.	Generated during this project. (See map in appendix)
ΔPF3D7_0220700	CS2(CSA) with the plasmid Δ PF3D7_0220700 integrated into the PF3D7_0220700 gene, leading to the truncation of the gene.	Generated during this project. (See map in appendix)
ΔPF3D7_0301600	CS2(CSA) with the plasmid Δ PF3D7_0301600 integrated into the PF3D7_0301600 gene, leading to the truncation of the gene.	Generated during this project. (See map in appendix)
ΔPIESP1	CS2(CSA) with the plasmid Δ PIESP1 integrated into the PIESP1 gene, leading to the truncation of the gene.	Generated during this project. (See map in appendix)
ΔPF3D7_0701900	CS2(CSA) with the plasmid Δ PF3D7_0701900 integrated into the PF3D7_0701900 gene, leading to the truncation of the gene.	Generated during this project. (See map in appendix)
ΔPF3D7_1038600	CS2(CSA) with the plasmid Δ PF3D7_1038600 integrated into the PF3D7_1038600 gene, leading to the truncation of the gene.	Generated during this project. (See map in appendix)
PF3D7_1102600	CS2(CSA) with the plasmid Δ PF3D7_1102600 integrated into the PF3D7_1102600 gene, leading to the truncation of the gene.	Generated during this project. (See map in appendix)
ΔRESA	CS2(CSA) with the plasmid Δ RESA integrated into the RESA gene, leading to the truncation of the gene.	Generated during this project. (See map in appendix)
ΔGBPH2	CS2(CSA) with the plasmid Δ GBPH2 integrated into the GBPH2 gene, leading to the truncation of the gene.	Generated during this project. (See map in appendix)
ΔPF3D7_1401200	CS2(CSA) with the plasmid Δ PF3D7_1401200 integrated into the PF3D7_1401200 gene, leading to the truncation of the gene.	Generated during this project. (See map in appendix)
ΔPF3D7_0113300	CS2(CSA) with the plasmid Δ PF3D7_0113300 integrated into the	Generated during this project. (See map in appendix)

	<i>PF3D7_0113300</i> gene, leading to the truncation of the gene.	
--	---	--

4.2.2 *E. coli* strains used in this project.

Strain	Description	Origin
TOP10	<i>F- mcrA Δ(mrr-hsdRMS-mcrBC) Φ80lacZΔM15 Δ lacX74 recA1 araD139</i>	Life Technologies
PMC 103	<i>Δ(araleu)7697 galU galK rpsL (StrR) endA1 nup mcrA Δ A(mcrBC-hsdRMS-mrr)102 recD sbcC</i>	(Doherty et al. 1993)

4.2.3 Plasmids.

Description	Resistance Marker		Source
	<i>E. coli</i>	<i>P. falciparum</i>	
<i>PF3D7_0301800^{gImS}</i>	Amp	hDHFR, NeoR	Cloned in this project
<i>PF3D7_0301800^{M9}</i>	Amp	hDHFR, NeoR	Cloned in this project
<i>KAHRP::mCh</i>	Amp	BSD	Dr. Cecilia Sanchez
<i>ΔPF3D7_0301800</i>	Amp	hDHFR, NeoR	Cloned in this project
<i>ΔPfj23</i>	Amp	hDHFR, NeoR	Cloned in this project
<i>SBP1::HA</i>	Amp	BSD	Cloned in this project
<i>Pfj23::HA</i>	Amp	BSD	Cloned in this project
<i>ΔPF3D7_0220300</i>	Amp	hDHFR, NeoR	Cloned in this project
<i>ΔPF3D7_0220600</i>	Amp	hDHFR, NeoR	Cloned in this project
<i>ΔPF3D7_0220700</i>	Amp	hDHFR, NeoR	Cloned in this project
<i>ΔPF3D7_0301600</i>	Amp	hDHFR, NeoR	Cloned in this project
<i>ΔPIESP1</i>	Amp	hDHFR, NeoR	Cloned in this project
<i>ΔPF3D7_0701900</i>	Amp	hDHFR, NeoR	Cloned in this project

<i>ΔPF3D7_1038600</i>	Amp	hDHFR, NeoR	Cloned in this project
<i>ΔPF3D7_1102600</i>	Amp	hDHFR, NeoR	Cloned in this project
<i>ΔRESA3</i>	Amp	hDHFR, NeoR	Cloned in this project
<i>ΔGBPH2</i>	Amp	hDHFR, NeoR	Cloned in this project
<i>ΔPF3D7_1401200</i>	Amp	hDHFR, NeoR	Cloned in this project
<i>ΔPF3D7_0113300</i>	Amp	hDHFR, NeoR	Cloned in this project
<i>ΔCBP1</i>	Amp	hDHFR, NeoR	Cloned in this project
<i>pSLI-TGD</i>	Amp	hDHFR, NeoR	Dr. Tobias Spielmann
<i>pSLI-glmS/M9</i>	Amp	hDHFR, NeoR	Dr. Markus Ganter

4.2.4 Oligonucleotides.

Description	5'- 3' Sequence
	Lower case letters depict the overhangs containing the restriction sites and additional 4 nucleotides for efficient digestion. Additionally, a stop codon (TAA) was added at the beginning of each forward primer (for the SLI_TGD) to prevent a possible expression of the insert on the vector and after its integration.
3HA_54_R	GGTACATCGTATGGATAAGAACC
pARL_fw	CGTTAATAATAAATACACGCAG
#7GD_0113300_NotI_fw	cgatgcggccgcTAATATATGAAAGTCTGCACGAG
#7GD_0113300_MluI_rv	cgatacgcgtCGTTTCTTCATATTTATTGTCCT
#8GD_0220300_NotI_fw	cgatgcggccgcTAACACTATAAACCTTAAATTA ACTAATAG
#8GD_0220300_MluI_rv	cgatacgcgtTGGTGCTGTTGAATATCTGTC
#9GD_0220600_NotI_fw	cgatgcggccgcTAAGTATTTATTCTTATAGTTACATTTACC
#9GD_0220600_MluI_rv	cgatacgcgtTACACTTTCTGAATCAACTTCTACC
#10GD_0220700_NotI_fw	cgatgcggccgcTAAGTGCTAATAATCATGAAATAGC
#10GD_0220700_MluI_rv	cgatacgcgt AACACTCGACATTC ACTATC

#12GD_GEXP21_Notl_fw	cgatgcggccgcTAAGACAGATAGGAATAGGAGTG
#12GD_GEXP21_Mlul_rv	cgatacgcggtGGATGCTTTCTCTTCATCTTGC
#13GD_0301800_Notl_fw	cgatgcggccgcTAACAAACTACCTTGATTATGCAG
#13GD_0301800_Mlul_rv	cgatacgcggtTTCTTCTGACCTTGATCTGC
#14GD_PIESP1_Notl_fw	cgatgcggccgcTAATCTTGAGCGTGTAACAATG
#14GD_PIESP1_Mlul_rv	cgatacgcggtGTCTTCATTATCACCATCTTTAG
#15GD_0701900_Notl_fw	cgatgcggccgcTAACATGTGAAAGAATAATAATAGAAAAGG
#15GD_0701900_Mlul_rv	cgatacgcggtCCTAAGTACGTCCACTTGTGT
#1GD_Pf3D7_1038600_Notl_fw	cgatgcggccgcTAATTA CTCTATAAAAGAAAACATTTCC
#1GD_Pf3D7_1038600_Mlul_rv	cgatacgcggtATATGATAGGTCTAAATAAGGTTCC
#2GD_GEXP14_Notl_fw	cgatgcggccgcTAAGAGAAGTTTAGTAATTTACATGTTGG
#2GD_GEXP14_Mlul_rv	cgatacgcggtAACTAAAGTTTCCACTTCGC
#3GD_1149200_Notl_fw	cgatgcggccgcTAATCGTTATGTTCTAAGCGTTTGG
#3GD_1149200_Mlul_rv	cgatacgcggtATTGAACTCCCTTGTATGG
#4GD_GBPH2_Notl_fw	cgatgcggccgcTAATGGATGTCCAAGAAAGAAATG
#4GD_GBPH2_Mlul_rv	cgatacgcggtCCAGGCTTTCATTATTTGTCC
#5GD_1401200_Notl_fw	cgatgcggccgcTAATTATGTATAATAGCATTATCATGC
#5GD_1401200_Mlul_rv	cgatacgcggtTGTGGGTACACCAAACC
#6GD_CBP1_Notl_fw	cgatgcggccgcTAATGCCTACTGATATTCTCCTC
#6GD_CBP1_Mlul_rv	cgatacgcggtTAAGGGCTCACCTTCATCAC
#16GD_Pfj23_Notl_fw	cgatgcggccgcTAATCCACAAGTTATTCTAGTTTCG
#16GD_Pfj23_Mlul_rv	cgatacgcggtTGTTTCTTCATCACTACAACC
#16GD_Pfj23_int_5	CGAAATGAGTATGAATTTTTTATAC
#16GD_Pfj23_int_3	GTA TTT CTT CAC CTT CTT CC
Pfj23_XhoI_F	cgatctcgagATGATAAAAGATCATAATAATAACG
Pfj23_AvrII_R	cgatcctaggTTTAAATTTTATGAAATGAAATTTATC
Pfj23_-2000_start_Notl_F	cgatgcggccgcGTGGGTTTCCTTATTTACATTC

Pfj23_-2000_start_XhoI_R	cgatctcgagAATATTCTTTTTAATAATAACATTG
FWD_PF3D7_0301800_Not	cgatgcgccgcCATTATTAGTAACATTTCTAATAAACTTATCC
Rev_PF3D7_0301800_MluI	cgatacgcgTGT AAA TAA ACT TTT AAC CCA CGT ATT AC
5'F_0301800_5'	AACTCATAAAGAACCCTTTG
3'R_0301800_5'	CAACTTCATTATGAATAAACGG

4.2.5 Antibodies and Enzymes.

Antibodies	Manufacturer
α -Rex1 (rabbit)	Dr. Matthew Dixon Australia
α -PfEMP3	PD. Dr. Jude Przyborski
α -KAHRP (rabbit)	PD. Dr. Jude Przyborski
α -GFP (Mouse)	Roche (Basel)
α -GFP (Chicken)	Abcam (Cambridge)
α -HA (Mouse)	Roche
α -SERP (rabbit)	PD. Dr. Jude Przyborski
α -Aldolase (rabbit)	PD. Dr. Jude Przyborski
α -EXP2 (rabbit)	PD. Dr. Jude Przyborski
α -SBP1 BR5 (rabbit)	Prof. Dr. Catherine Braun- Beton
α -REX2 (rabbit)	PD. Dr. Jude Przyborski
α -chicken-Cy2 (goat)	Dako (Jena)
α -mouse-Cy3 (goat)	Dako (Jena)
α -rabbit-Cy3 (goat)	Dako (Jena)
α -EXP1 (rabbit)	PD. Dr. Jude Przyborski
α -mouse-HRP (goat)	Dako (Jena)
α -rabbit-HRP (goat)	Dako (Jena)
α -PfEMP1 (rabbit)	PD. Dr. Jude Przyborski
Enzymes	Manufacturer
KOD hot start polymerase	Novagen (St. Louis)

Antarctic phosphatase	New England Biolabs (Ipswich)
Restriction enzymes: NotI, XhoI, AvrII, MluI, KpnI, XmaI	New England Biolabs (Ipswich)
T4 Ligase	Life technologies (Carlsbad)

4.2.6 Chemicals.

Chemical	Manufacturer	Chemical	Manufacturer
KCl	Roth (Karlsruhe)	Acetic acid	Merck (Darmstadt)
KH ₂ PO ₄	Roth (Karlsruhe)	Acetone	Merck (Darmstadt)
Luminol	Applichem (Chicago)	Acrylamide	Roth (Karlsruhe)
Methanol	VWR (Radnor)	AlbuMAXII	Invitrogen (Groningen)
MgCl ₂	Roth (Karlsruhe)	APAD	Sigma Aldrich (Taufkirchen)
MgSO ₄	Roth (Karlsruhe)	APS	Roth (Karlsruhe)
Milk powder	Roth (Karlsruhe)	Blasticidin	Invivo Gen (Toulouse)
NaCl	Roth (Karlsruhe)	Bromophenolblue	GE healthcare (Chicago)
NaOH	Roth (Karlsruhe)	BSA	Roth (Karlsruhe)
NBT tablets	Sigma Aldrich (Taufkirchen)	CaCl ₂	Roth (Karlsruhe)
Neomycin	Sigma Aldrich (Taufkirchen)	Cresol red	Sigma Aldrich (Taufkirchen)
(NH ₄) ₂ SO ₄	Roth (Karlsruhe)	CSA	Sigma Aldrich (Taufkirchen)
PageRuler Prestained Protein Ladder	Thermo Fisher Scientific (Waltham)	CTA	Sigma Aldrich (Taufkirchen)
Paraformaldehyde	Roth (Karlsruhe)	DAPI	Roth (Karlsruhe)

P-coumaric acid	Sigma Aldrich (Taufkirchen)	Diaphorase	Sigma Aldrich (Taufkirchen)
Peptone	Roth (Karlsruhe)	DTT	Appllichem (Chicago)
Ponceau S blubs	Roth (Karlsruhe)	Glycine	Sigma Aldrich (Taufkirchen)
RPMI 1640	Life technologies (Carlsbad)	EDTA	Roth (Karlsruhe)
RPMI- powder	Life technologies (Carlsbad)	Ethanol	VWR (Radnor)
Saponin	Roth (Karlsruhe)	G418	Thermo Fisher Scientific (Waltham)
SDS	Roth (Karlsruhe)	Gelatine	Sigma Aldrich (Taufkirchen)
Super optimal broth	Roth (Karlsruhe)	Giemsa	Merck (Darmstadt)
Sodium L-Lactate	Roth (Karlsruhe)	Glucose	Roth (Karlsruhe)
Sorbitol	Roth (Karlsruhe)	Glutaraldehyde	Roth (Karlsruhe)
TEMED	Roth (Karlsruhe)	Glycerol	Roth (Karlsruhe)
Tris	Roth (Karlsruhe)	HCl	Roth (Karlsruhe)
Triton-X-100	Roth (Karlsruhe)	Heparin	Sigma Aldrich (Taufkirchen)
Yeast extract	Roth (Karlsruhe)	HEPES	Roth (Karlsruhe)
1 kb + DNA size-standard	Thermo Fisher Scientific (Waltham)	Hypoxanthine	CC Pro (Oberdorla)
		K ₂ HPO ₄	Roth (Karlsruhe)

4.2.7 Kits.

Description	Manufacturer
Plasmid Maxi Kit	Qiagen (Hilden)
DNA Mini kit	Qiagen (Hilden)
PCR pure kit	Qiagen (Hilden)
Plasmid Miniprep Kit	Peqlab (Erlangen)

PeqGOLD Gel extraction kit	Peqlab (Erlangen)
PeqGOLD, Cycle pure kit	Peqlab (Erlangen)

4.2.8 Equipments.

Description	Model and Manufacturer
Sterile Workbench	ThermoScientific, HERAsafeKS
Pipetboy	IntegraBioscience
Freezer	ThermoScientific Herafreeze top
Fridge	Liebherr
PCR- Cyclers	Eppendorf Mastercycler gradient
Heating block	Eppendorf Thermomixer 5436
Pipettes	Gilson
Spectrometer	UVIKON 923 Double beam UV/VIS spectrometer
Shaker	Heidolph UNIMAX1010
Roller	MAGV, TRM50
Plate reader	Biotek Cytation Imaging reader / Clarios Gießen
Transmission electron microscope	Jeol 1400
Scanning electron microscope	Zeiss Leo15030
Magnetic cell sorter	Milyenti Biotech Magnetic cell sorter
Incubator	Labotech Inkubator C200
Water bath	ThermoScientific Precision GP10
Centrifuges	Hettich Mikro 220R, Heraeus Labofuge 400e, SORVALL RC 5B Plus, Beckman J2-MC
Light microscope	KernOptics
Fluorescent microscope	Zeiss Axio-observer
Clariostart plate reader	BMG Labtech

4.2.9 Plastic Ware.

Description	Manufacturer
Pipette tips 1000, 200, 10 μ l	Sarstedt (Nümbrecht)
Petri dishes: CSA binding	Corning (New York)
<i>E. coli</i> petri dishes	Sarstedt (Nümbrecht)
50, 15 ml Falcons	Corning (New York)
Cell culture petri dishes	Sarstedt (Nümbrecht)
6 well plates	Sarstedt (Nümbrecht)
96 well plates flat/ U- bottom	Sarstedt (Nümbrecht)
Plastic pipettes 25, 10, 5, 2 ml	Sarstedt (Nümbrecht)

References

- Adderley, J., T. Williamson, and C. Doerig. 2021. 'Parasite and host erythrocyte kinomics of Plasmodium infection', *Trends Parasitol.*
- An, X., and N. Mohandas. 2008. 'Disorders of red cell membrane', *Br J Haematol*, 141: 367-75.
- Ashley, E. A., A. Pyae Phyo, and C. J. Woodrow. 2018. 'Malaria', *Lancet*, 391: 1608-21.
- Band, Gavin, Ellen M. Leffler, Muminatou Jallow, Fatoumatta Sisay-Joof, Carolyn M. Ndila, Alexander W. Macharia, Christina Hubbard, Anna E. Jeffreys, Kate Rowlands, Thuy Nguyen, Sonia M. Goncalves, Cristina V. Ariani, Jim Stalker, Richard D. Pearson, Roberto Amato, Eleanor Drury, Giorgio Sirugo, Umberto D'Alessandro, Kalifa A. Bojang, Kevin Marsh, Norbert Peshu, David J. Conway, Thomas N. Williams, Kirk A. Rockett, and Dominic P. Kwiatkowski. 2021. 'The protective effect of sickle cell haemoglobin against severe malaria depends on parasite genotype', *bioRxiv*: 2021.03.30.437659.
- Bannister, L., and G. Mitchell. 2003. 'The ins, outs and roundabouts of malaria', *Trends Parasitol*, 19: 209-13.
- Banumathy, G., V. Singh, S. R. Pavithra, and U. Tatu. 2003. 'Heat shock protein 90 function is essential for Plasmodium falciparum growth in human erythrocytes', *J Biol Chem*, 278: 18336-45.
- Batinovic, S., E. McHugh, S. A. Chisholm, K. Matthews, B. Liu, L. Dumont, S. C. Charnaud, M. P. Schneider, P. R. Gilson, T. F. de Koning-Ward, M. W. A. Dixon, and L. Tilley. 2017. 'An exported protein-complex involved in the trafficking of virulence determinants in Plasmodium-infected erythrocytes', *Nat Commun*, 8: 16044.
- Battle, K. E., T. C. D. Lucas, M. Nguyen, R. E. Howes, A. K. Nandi, K. A. Twohig, D. A. Pfeffer, E. Cameron, P. C. Rao, D. Casey, H. S. Gibson, J. A. Rozier, U. Dalrymple, S. H. Keddie, E. L. Collins, J. R. Harris, C. A. Guerra, M. P. Thorn, D. Bisanzio, N. Fullman, C. K. Huynh, X. Kulikoff, M. J. Kutz, A. D. Lopez, A. H. Mokdad, M. Naghavi, G. Nguyen, K. A. Shackelford, T. Vos, H. Wang, S. S. Lim, C. J. L. Murray, R. N. Price, J. K. Baird, D. L. Smith, S. Bhatt, D. J. Weiss, S. I. Hay, and P. W. Gething. 2019. 'Mapping the global endemicity and clinical burden of Plasmodium vivax, 2000-17: a spatial and temporal modelling study', *Lancet*, 394: 332-43.
- Baumeister, S., M. Winterberg, C. Duranton, S. M. Huber, F. Lang, K. Kirk, and K. Lingelbach. 2006. 'Evidence for the involvement of Plasmodium falciparum proteins in the formation of new permeability pathways in the erythrocyte membrane', *Mol Microbiol*, 60: 493-504.
- Baumeister, S., M. Winterberg, J. M. Przyborski, and K. Lingelbach. 2010. 'The malaria parasite Plasmodium falciparum: cell biological peculiarities and nutritional consequences', *Protoplasma*, 240: 3-12.
- Beck, J. R., V. Muralidharan, A. Oksman, and D. E. Goldberg. 2014. 'PTEX component HSP101 mediates export of diverse malaria effectors into host erythrocytes', *Nature*, 511: 592-5.
- Beeson, J. G., G. V. Brown, M. E. Molyneux, C. Mhango, F. Dzinjalama, and S. J. Rogerson. 1999. 'Plasmodium falciparum isolates from infected pregnant women and children are associated with distinct adhesive and antigenic properties', *J Infect Dis*, 180: 464-72.
- Behari, R., and K. Haldar. 1994. 'Plasmodium falciparum: protein localization along a novel, lipid-rich tubovesicular membrane network in infected erythrocytes', *Exp Parasitol*, 79: 250-9.
- Biggs, B. A., R. F. Anders, H. E. Dillon, K. M. Davern, M. Martin, C. Petersen, and G. V. Brown. 1992. 'Adherence of infected erythrocytes to venular endothelium selects for antigenic variants of Plasmodium falciparum', *J Immunol*, 149: 2047-54.
- Biggs, B. A., L. Gooze, K. Wycherley, W. Wollish, B. Southwell, J. H. Leech, and G. V. Brown. 1991. 'Antigenic variation in Plasmodium falciparum', *Proc Natl Acad Sci U S A*, 88: 9171-4.
- Birnbaum, J., S. Flemming, N. Reichard, A. B. Soares, P. Mesen-Ramirez, E. Jonscher, B. Bergmann, and T. Spielmann. 2017. 'A genetic system to study Plasmodium falciparum protein function', *Nat Methods*, 14: 450-56.
- Birnbaum, J., S. Scharf, S. Schmidt, E. Jonscher, W. A. M. Hoeijmakers, S. Flemming, C. G. Toenhake, M. Schmitt, R. Sabitzki, B. Bergmann, U. Frohlike, P. Mesen-Ramirez, A. Blancke Soares, H. Herrmann, R. Bartfai, and T. Spielmann. 2020. 'A Kelch13-defined endocytosis pathway mediates artemisinin resistance in malaria parasites', *Science (New York, N.Y.)*, 367: 51-59.
- Blobel, G., and B. Dobberstein. 1975a. 'Transfer of proteins across membranes. I. Presence of proteolytically processed and unprocessed nascent immunoglobulin light chains on membrane-bound ribosomes of murine myeloma', *J Cell Biol*, 67: 835-51.

- . 1975b. 'Transfer of proteins across membranes. II. Reconstitution of functional rough microsomes from heterologous components', *J Cell Biol*, 67: 852-62.
- Boddey, J. A., T. G. Carvalho, A. N. Hodder, T. J. Sargeant, B. E. Sleeb, D. Marapana, S. Lopaticki, T. Nebl, and A. F. Cowman. 2013. 'Role of plasmepsin V in export of diverse protein families from the Plasmodium falciparum exportome', *Traffic*, 14: 532-50.
- Boddey, J. A., and A. F. Cowman. 2013. 'Plasmodium nesting: remaking the erythrocyte from the inside out', *Annu Rev Microbiol*, 67: 243-69.
- Boddey, J. A., R. L. Moritz, R. J. Simpson, and A. F. Cowman. 2009. 'Role of the Plasmodium export element in trafficking parasite proteins to the infected erythrocyte', *Traffic*, 10: 285-99.
- Botha, M., E. R. Pesce, and G. L. Blatch. 2007. 'The Hsp40 proteins of Plasmodium falciparum and other apicomplexa: regulating chaperone power in the parasite and the host', *Int J Biochem Cell Biol*, 39: 1781-803.
- Bozdech, Z., M. Llinas, B. L. Pulliam, E. D. Wong, J. Zhu, and J. L. DeRisi. 2003. 'The transcriptome of the intraerythrocytic developmental cycle of Plasmodium falciparum', *PLoS Biol*, 1: E5.
- Brandt, G. S., and S. Bailey. 2013. 'Dematin, a human erythrocyte cytoskeletal protein, is a substrate for a recombinant FIKK kinase from Plasmodium falciparum', *Mol Biochem Parasitol*, 191: 20-3.
- Breman, J. G. 2009. 'Eradicating malaria', *Sci Prog*, 92: 1-38.
- Burda, P. C., T. Crosskey, K. Lauk, A. Zurborg, C. Sohnchen, B. Liffner, L. Wilcke, E. Pietsch, J. Strauss, C. M. Jeffries, D. I. Svergun, D. W. Wilson, M. Wilmanns, and T. W. Gilberger. 2020. 'Structure-Based Identification and Functional Characterization of a Lipocalin in the Malaria Parasite Plasmodium falciparum', *Cell Rep*, 31: 107817.
- CDC. 2015. 'Malaria: Laveran and the Discovery of the Malaria Parasite', CDC Global Health – Division of Parasitic Diseases and Malaria
- Accessed September 23, 2015. <https://www.cdc.gov/malaria/about/history/laveran.html>.
- Chang, H. H., A. M. Falick, P. M. Carlton, J. W. Sedat, J. L. DeRisi, and M. A. Marletta. 2008. 'N-terminal processing of proteins exported by malaria parasites', *Mol Biochem Parasitol*, 160: 107-15.
- Charnaud, S. C., M. W. A. Dixon, C. Q. Nie, L. Chappell, P. R. Sanders, T. Nebl, E. Hanssen, M. Berriman, J. A. Chan, A. J. Blanch, J. G. Beeson, J. C. Rayner, J. M. Przyborski, L. Tilley, B. S. Crabb, and P. R. Gilson. 2017. 'The exported chaperone Hsp70-x supports virulence functions for Plasmodium falciparum blood stage parasites', *PLoS One*, 12: e0181656.
- Charnaud, S. C., T. K. Jonsdottir, P. R. Sanders, H. E. Bullen, B. K. Dickerman, B. Kouskousis, C. S. Palmer, H. M. Pietrzak, A. E. Laumaea, A. B. Erazo, E. McHugh, L. Tilley, B. S. Crabb, and P. R. Gilson. 2018. 'Spatial organization of protein export in malaria parasite blood stages', *Traffic*, 19: 605-23.
- Chisholm, S. A., M. Kalanon, T. Nebl, P. R. Sanders, K. M. Matthews, B. K. Dickerman, P. R. Gilson, and T. F. de Koning-Ward. 2018. 'The malaria PTEX component PTEX88 interacts most closely with HSP101 at the host-parasite interface', *FEBS J*, 285: 2037-55.
- Cobb, D. W., A. Florentin, M. A. Fierro, M. Krakowiak, J. M. Moore, and V. Muralidharan. 2017. 'The Exported Chaperone PfHsp70x Is Dispensable for the Plasmodium falciparum Intraerythrocytic Life Cycle', *mSphere*, 2.
- Collins, C. R., S. Das, E. H. Wong, N. Andenmatten, R. Stallmach, F. Hackett, J. P. Herman, S. Muller, M. Meissner, and M. J. Blackman. 2013. 'Robust inducible Cre recombinase activity in the human malaria parasite Plasmodium falciparum enables efficient gene deletion within a single asexual erythrocytic growth cycle', *Mol Microbiol*, 88: 687-701.
- Cooke, B. M., D. W. Buckingham, F. K. Glenister, K. M. Fernandez, L. H. Bannister, M. Marti, N. Mohandas, and R. L. Coppel. 2006. 'A Maurer's cleft-associated protein is essential for expression of the major malaria virulence antigen on the surface of infected red blood cells', *J Cell Biol*, 172: 899-908.
- Counihan, N. A., S. A. Chisholm, H. E. Bullen, A. Srivastava, P. R. Sanders, T. K. Jonsdottir, G. E. Weiss, S. Ghosh, B. S. Crabb, D. J. Creek, P. R. Gilson, and T. F. de Koning-Ward. 2017. 'Plasmodium falciparum parasites deploy RhopH2 into the host erythrocyte to obtain nutrients, grow and replicate', *Elife*, 6.
- Cowman, A. F., and B. S. Crabb. 2006. 'Invasion of red blood cells by malaria parasites', *Cell*, 124: 755-66.
- Cowman, A. F., J. Healer, D. Marapana, and K. Marsh. 2016. 'Malaria: Biology and Disease', *Cell*, 167: 610-24.

- Cowman, A. F., C. J. Tonkin, W. H. Tham, and M. T. Duraisingh. 2017. 'The Molecular Basis of Erythrocyte Invasion by Malaria Parasites', *Cell Host Microbe*, 22: 232-45.
- Cox, Francis Eg. 2010. 'History of the discovery of the malaria parasites and their vectors', *Parasites & Vectors*, 3: 5.
- Crabb, B. S., B. M. Cooke, J. C. Reeder, R. F. Waller, S. R. Caruana, K. M. Davern, M. E. Wickham, G. V. Brown, R. L. Coppel, and A. F. Cowman. 1997. 'Targeted gene disruption shows that knobs enable malaria-infected red cells to cytoadhere under physiological shear stress', *Cell*, 89: 287-96.
- Cutts, E. E., N. Laasch, D. M. Reiter, R. Trenker, L. M. Slater, P. J. Stansfeld, and I. Vakonakis. 2017. 'Structural analysis of P. falciparum KAHRP and PfEMP1 complexes with host erythrocyte spectrin suggests a model for cytoadherent knob protrusions', *PLoS Pathog*, 13: e1006552.
- Daniyan, M. O., A. Boshoff, E. Prinsloo, E. R. Pesce, and G. L. Blatch. 2016. 'The Malarial Exported PFA0660w Is an Hsp40 Co-Chaperone of PfHsp70-x', *PLoS One*, 11: e0148517.
- Das, A., C. Syin, H. Fujioka, H. Zheng, N. Goldman, M. Aikawa, and N. Kumar. 1997. 'Molecular characterization and ultrastructural localization of Plasmodium falciparum Hsp 60', *Mol Biochem Parasitol*, 88: 95-104.
- Das, Dibyajyoti, Sowmya Ramaswamy Krishnan, Arijit Roy, and Gopalakrishnan Bulusu. 2019. 'A network-based approach reveals novel invasion and Maurer's clefts-related proteins in Plasmodium falciparum', *Molecular Omics*, 15: 431-41.
- Dasanna, A. K., C. Lansche, M. Lanzer, and U. S. Schwarz. 2017. 'Rolling Adhesion of Schizont Stage Malaria-Infected Red Blood Cells in Shear Flow', *Biophys J*, 112: 1908-19.
- Dasgupta, S., T. Auth, N. S. Gov, T. J. Satchwell, E. Hanssen, E. S. Zuccala, D. T. Riglar, A. M. Toye, T. Betz, J. Baum, and G. Gompfer. 2014. 'Membrane-wrapping contributions to malaria parasite invasion of the human erythrocyte', *Biophys J*, 107: 43-54.
- Davies, H., H. Belda, M. Broncel, X. Ye, C. Bisson, V. Introini, D. Dorin-Semlat, J. P. Semlat, M. Tiburcio, B. Gamain, M. Kaforou, and M. Treeck. 2020. 'An exported kinase family mediates species-specific erythrocyte remodelling and virulence in human malaria', *Nat Microbiol*, 5: 848-63.
- Day, J., A. Passecker, H. P. Beck, and I. Vakonakis. 2019. 'The Plasmodium falciparum Hsp70-x chaperone assists the heat stress response of the malaria parasite', *FASEB J*, 33: 14611-24.
- de Koning-Ward, T. F., M. W. Dixon, L. Tilley, and P. R. Gilson. 2016. 'Plasmodium species: master renovators of their host cells', *Nat Rev Microbiol*, 14: 494-507.
- de Koning-Ward, T. F., P. R. Gilson, J. A. Boddey, M. Rug, B. J. Smith, A. T. Papenfuss, P. R. Sanders, R. J. Lundie, A. G. Maier, A. F. Cowman, and B. S. Crabb. 2009. 'A newly discovered protein export machine in malaria parasites', *Nature*, 459: 945-9.
- de Koning-Ward, T. F., P. R. Gilson, and B. S. Crabb. 2015. 'Advances in molecular genetic systems in malaria', *Nat Rev Microbiol*, 13: 373-87.
- Desai, S. A., D. J. Krogstad, and E. W. McCleskey. 1993. 'A nutrient-permeable channel on the intraerythrocytic malaria parasite', *Nature*, 362: 643-6.
- Desai, S. A., and R. L. Rosenberg. 1997. 'Pore size of the malaria parasite's nutrient channel', *Proc Natl Acad Sci U S A*, 94: 2045-9.
- Diehl, Mathias. 2019. 'Using new genetic tools to elucidate the importance of exported proteins in intra-erythrocytic survival of the malaria parasite Plasmodium falciparum', Heidelberg University.
- Diehl, Mathias, Sebastian Weber, Marek Cyrklaff, Cecilia P. Sanchez, Carlo A. Beretta, Lena Roling, Caroline S. Simon, Julien Guizetti, Matthias P. Mayer, and Jude M. Przyborski. 2021. 'Co-chaperone involvement in knob biogenesis implicates host-derived chaperones in malaria virulence', *bioRxiv*: 2021.03.11.434953.
- Diggs, C., K. Joseph, B. Flemmings, R. Snodgrass, and F. Hines. 1975. 'Protein synthesis in vitro by cryopreserved Plasmodium falciparum', *Am J Trop Med Hyg*, 24: 760-3.
- Doherty, J. P., R. Lindeman, R. J. Trent, M. W. Graham, and D. M. Woodcock. 1993. 'Escherichia coli host strains SURE and SRB fail to preserve a palindrome cloned in lambda phage: improved alternate host strains', *Gene*, 124: 29-35.
- Dondorp, A. M., P. A. Kager, J. Vreeken, and N. J. White. 2000. 'Abnormal blood flow and red blood cell deformability in severe malaria', *Parasitol Today*, 16: 228-32.
- Elsworth, B., K. Matthews, C. Q. Nie, M. Kalanon, S. C. Charnaud, P. R. Sanders, S. A. Chisholm, N. A. Counihan, P. J. Shaw, P. Pino, J. A. Chan, M. F. Azevedo, S. J. Rogerson, J. G. Beeson, B. S. Crabb, P. R. Gilson, and T. F. de Koning-Ward. 2014. 'PTEX is an essential nexus for protein export in malaria parasites', *Nature*, 511: 587-91.

- Fernandez, V., Q. Chen, A. Sundstrom, A. Scherf, P. Hagblom, and M. Wahlgren. 2002. 'Mosaic-like transcription of var genes in single Plasmodium falciparum parasites', *Mol Biochem Parasitol*, 121: 195-203.
- Florens, L., X. Liu, Y. Wang, S. Yang, O. Schwartz, M. Peglar, D. J. Carucci, J. R. Yates, 3rd, and Y. Wu. 2004. 'Proteomics approach reveals novel proteins on the surface of malaria-infected erythrocytes', *Mol Biochem Parasitol*, 135: 1-11.
- Fried, M., and P. E. Duffy. 1996. 'Adherence of Plasmodium falciparum to Chondroitin Sulfate A in the Human Placenta', *Science (New York, N.Y.)*, 272: 1502-04.
- Ganter, M., J. M. Goldberg, J. D. Dvorin, J. A. Paulo, J. G. King, A. K. Tripathi, A. S. Paul, J. Yang, I. Coppens, R. H. Jiang, B. Elsworth, D. A. Baker, R. R. Dinglasan, S. P. Gygi, and M. T. Duraisingh. 2017. 'Plasmodium falciparum CRK4 directs continuous rounds of DNA replication during schizogony', *Nat Microbiol*, 2: 17017.
- Garten, M., A. S. Nasamu, J. C. Niles, J. Zimmerberg, D. E. Goldberg, and J. R. Beck. 2018. 'EXP2 is a nutrient-permeable channel in the vacuolar membrane of Plasmodium and is essential for protein export via PTEX', *Nat Microbiol*, 3: 1090-98.
- Ghorbal, M., M. Gorman, C. R. Macpherson, R. M. Martins, A. Scherf, and J. J. Lopez-Rubio. 2014. 'Genome editing in the human malaria parasite Plasmodium falciparum using the CRISPR-Cas9 system', *Nat Biotechnol*, 32: 819-21.
- Gilson, P. R., S. A. Chisholm, B. S. Crabb, and T. F. de Koning-Ward. 2017. 'Host cell remodelling in malaria parasites: a new pool of potential drug targets', *Int J Parasitol*, 47: 119-27.
- Gilson, P. R., R. Kumarasingha, J. Thompson, X. Zhang, J. S. Penington, R. Kalhor, H. E. Bullen, A. M. Lehane, M. G. Dans, T. F. de Koning-Ward, J. K. Holien, T. P. Soares da Costa, M. D. Hulett, M. J. Buskes, B. S. Crabb, K. Kirk, A. T. Papenfuss, A. F. Cowman, and B. M. Abbott. 2019. 'A 4-cyano-3-methylisoquinoline inhibitor of Plasmodium falciparum growth targets the sodium efflux pump PfATP4', *Sci Rep*, 9: 10292.
- Glenister, F. K., K. M. Fernandez, L. M. Kats, E. Hanssen, N. Mohandas, R. L. Coppel, and B. M. Cooke. 2009. 'Functional alteration of red blood cells by a megadalton protein of Plasmodium falciparum', *Blood*, 113: 919-28.
- Goel, S., M. Palmkvist, K. Moll, N. Joannin, P. Lara, R. R. Akhouri, N. Moradi, K. Ojemalm, M. Westman, D. Angeletti, H. Kjellin, J. Lehtio, O. Blixt, L. Idestrom, C. G. Gahmberg, J. R. Storry, A. K. Hult, M. L. Olsson, G. von Heijne, I. Nilsson, and M. Wahlgren. 2015. 'RIFINs are adhesins implicated in severe Plasmodium falciparum malaria', *Nat Med*, 21: 314-7.
- Goodyer, I. D., J. Johnson, R. Eisenthal, and D. J. Hayes. 1994. 'Purification of mature-stage Plasmodium falciparum by gelatine flotation', *Ann Trop Med Parasitol*, 88: 209-11.
- Gruring, C., A. Heiber, F. Kruse, S. Flemming, G. Franci, S. F. Colombo, E. Fasana, H. Schoeler, N. Borgese, H. G. Stunnenberg, J. M. Przyborski, T. W. Gilberger, and T. Spielmann. 2012. 'Uncovering common principles in protein export of malaria parasites', *Cell Host Microbe*, 12: 717-29.
- Hanssen, E., P. Carlton, S. Deed, N. Klonis, J. Sedat, J. DeRisi, and L. Tilley. 2010. 'Whole cell imaging reveals novel modular features of the exomembrane system of the malaria parasite, Plasmodium falciparum', *Int J Parasitol*, 40: 123-34.
- Hanssen, E., P. Hawthorne, M. W. Dixon, K. R. Trenholme, P. J. McMillan, T. Spielmann, D. L. Gardiner, and L. Tilley. 2008. 'Targeted mutagenesis of the ring-exported protein-1 of Plasmodium falciparum disrupts the architecture of Maurer's cleft organelles', *Mol Microbiol*, 69: 938-53.
- Haynes, J. D., C. L. Diggs, F. A. Hines, and R. E. Desjardins. 1976. 'Culture of human malaria parasites Plasmodium falciparum', *Nature*, 263: 767-9.
- Heiber, A., F. Kruse, C. Pick, C. Gruring, S. Flemming, A. Oberli, H. Schoeler, S. Retzlaff, P. Mesen-Ramirez, J. A. Hiss, M. Kadekoppala, L. Hecht, A. A. Holder, T. W. Gilberger, and T. Spielmann. 2013. 'Identification of new PNEPs indicates a substantial non-PEXEL exportome and underpins common features in Plasmodium falciparum protein export', *PLoS Pathog*, 9: e1003546.
- Hennessy, F., W. S. Nicoll, R. Zimmermann, M. E. Cheetham, and G. L. Blatch. 2005. 'Not all J domains are created equal: implications for the specificity of Hsp40-Hsp70 interactions', *Protein Sci*, 14: 1697-709.
- Herrera, R., C. Anderson, K. Kumar, A. Molina-Cruz, V. Nguyen, M. Burkhardt, K. Reiter, R. Shimp, Jr., R. F. Howard, P. Srinivasan, M. J. Nold, D. Ragheb, L. Shi, M. DeCotiis, J. Aebig, L. Lambert, K. M. Rausch, O. Muratova, A. Jin, S. G. Reed, P. Sinnis, C. Barillas-Mury, P. E. Duffy, N. J. MacDonald,

- and D. L. Narum. 2015. 'Reversible Conformational Change in the Plasmodium falciparum Circumsporozoite Protein Masks Its Adhesion Domains', *Infect Immun*, 83: 3771-80.
- Hiller, N. L., S. Bhattacharjee, C. van Ooij, K. Liolios, T. Harrison, C. Lopez-Estrano, and K. Haldar. 2004. 'A host-targeting signal in virulence proteins reveals a secretome in malarial infection', *Science (New York, N.Y.)*, 306: 1934-7.
- Ho, C. M., J. R. Beck, M. Lai, Y. Cui, D. E. Goldberg, P. F. Egea, and Z. H. Zhou. 2018. 'Malaria parasite translocon structure and mechanism of effector export', *Nature*, 561: 70-75.
- Joannin, N., Y. Kallberg, M. Wahlgren, and B. Persson. 2011. 'RSpred, a set of Hidden Markov Models to detect and classify the RIFIN and STEVOR proteins of Plasmodium falciparum', *BMC Genomics*, 12: 119.
- Joice, R., S. K. Nilsson, J. Montgomery, S. Dankwa, E. Egan, B. Morahan, K. B. Seydel, L. Bertuccini, P. Alano, K. C. Williamson, M. T. Duraisingh, T. E. Taylor, D. A. Milner, and M. Marti. 2014. 'Plasmodium falciparum transmission stages accumulate in the human bone marrow', *Sci Transl Med*, 6: 244re5.
- Jones, M. L., S. Das, H. Belda, C. R. Collins, M. J. Blackman, and M. Treeck. 2016. 'A versatile strategy for rapid conditional genome engineering using loxP sites in a small synthetic intron in Plasmodium falciparum', *Sci Rep*, 6: 21800.
- Jonsdottir, T. K., N. A. Counihan, J. K. Modak, B. Kouskousis, P. R. Sanders, M. Gabriela, H. E. Bullen, B. S. Crabb, T. F. de Koning-Ward, and P. R. Gilson. 2021. 'Characterisation of complexes formed by parasite proteins exported into the host cell compartment of Plasmodium falciparum infected red blood cells', *Cell Microbiol*: e13332.
- Kats, L. M., K. M. Fernandez, F. K. Glenister, S. Herrmann, D. W. Buckingham, G. Siddiqui, L. Sharma, R. Bamert, I. Lucet, M. Guillotte, O. Mercereau-Puijalon, and B. M. Cooke. 2014. 'An exported kinase (FIKK4.2) that mediates virulence-associated changes in Plasmodium falciparum-infected red blood cells', *Int J Parasitol*, 44: 319-28.
- Kaur, Jasweer, Vikash Kumar, Amrit Pal Singh, Vineeta Singh, Anjali Bisht, Taru Dube, Jiban Jyoti Panda, Ankita Behl, Prakash Chandra Mishra, and Rachna Hora. 2018. 'Plasmodium falciparum protein 'PfJ23' hosts distinct binding sites for major virulence factor 'PfEMP1' and Maurer's cleft marker 'PfSBP1'', *Pathogens and Disease*, 76.
- Kilili, G. K., and D. J. LaCount. 2011. 'An erythrocyte cytoskeleton-binding motif in exported Plasmodium falciparum proteins', *Eukaryot Cell*, 10: 1439-47.
- Knuepfer, E., M. Rug, N. Klonis, L. Tilley, and A. F. Cowman. 2005. 'Trafficking of the major virulence factor to the surface of transfected P. falciparum-infected erythrocytes', *Blood*, 105: 4078-87.
- Koch, M., and J. Baum. 2016. 'The mechanics of malaria parasite invasion of the human erythrocyte - towards a reassessment of the host cell contribution', *Cell Microbiol*, 18: 319-29.
- Kraemer, S. M., and J. D. Smith. 2006. 'A family affair: var genes, PfEMP1 binding, and malaria disease', *Curr Opin Microbiol*, 9: 374-80.
- Kulzer, S., S. Charnaud, T. Dagan, J. Riedel, P. Mandal, E. R. Pesce, G. L. Blatch, B. S. Crabb, P. R. Gilson, and J. M. Przyborski. 2012. 'Plasmodium falciparum-encoded exported hsp70/hsp40 chaperone/co-chaperone complexes within the host erythrocyte', *Cell Microbiol*, 14: 1784-95.
- Kulzer, S., M. Rug, K. Brinkmann, P. Cannon, A. Cowman, K. Lingelbach, G. L. Blatch, A. G. Maier, and J. M. Przyborski. 2010. 'Parasite-encoded Hsp40 proteins define novel mobile structures in the cytosol of the P. falciparum-infected erythrocyte', *Cell Microbiol*, 12: 1398-420.
- Kumar, N., G. Koski, M. Harada, M. Aikawa, and H. Zheng. 1991. 'Induction and localization of Plasmodium falciparum stress proteins related to the heat shock protein 70 family', *Mol Biochem Parasitol*, 48: 47-58.
- Laloo, D. G., D. Shingadia, D. J. Bell, N. J. Beeching, C. J. M. Whitty, P. L. Chiodini, and P. H. E. Advisory Committee on Malaria Prevention in UK Travellers. 2016. 'UK malaria treatment guidelines 2016', *J Infect*, 72: 635-49.
- Lambros, C., and J. P. Vanderberg. 1979. 'Synchronization of Plasmodium falciparum erythrocytic stages in culture', *J Parasitol*, 65: 418-20.
- Lanzer, M., H. Wickert, G. Krohne, L. Vincensini, and C. Braun Breton. 2006. 'Maurer's clefts: a novel multi-functional organelle in the cytoplasm of Plasmodium falciparum-infected erythrocytes', *Int J Parasitol*, 36: 23-36.

- Lebepe, C. M., P. R. Matambanadzo, X. H. Makhoba, I. Achilonu, T. Zininga, and A. Shonhai. 2020. 'Comparative Characterization of Plasmodium falciparum Hsp70-1 Relative to E. coli DnaK Reveals the Functional Specificity of the Parasite Chaperone', *Biomolecules*, 10.
- Lee, M. C. S., S. E. Lindner, J. J. Lopez-Rubio, and M. Llinas. 2019. 'Cutting back malaria: CRISPR/Cas9 genome editing of Plasmodium', *Brief Funct Genomics*, 18: 281-89.
- Lisewski, A. M., J. P. Quiros, C. L. Ng, A. K. Adikesavan, K. Miura, N. Putluri, R. T. Eastman, D. Scafield, S. J. Regenbogen, L. Altenhofen, M. Llinas, A. Sreekumar, C. Long, D. A. Fidock, and O. Lichtarge. 2014. 'Supergenomic network compression and the discovery of EXP1 as a glutathione transferase inhibited by artesunate', *Cell*, 158: 916-28.
- Liu, J., E. S. Istvan, I. Y. Gluzman, J. Gross, and D. E. Goldberg. 2006. 'Plasmodium falciparum ensures its amino acid supply with multiple acquisition pathways and redundant proteolytic enzyme systems', *Proc Natl Acad Sci U S A*, 103: 8840-5.
- Looker, O., A. J. Blanch, B. Liu, J. Nunez-Iglesias, P. J. McMillan, L. Tilley, and M. W. A. Dixon. 2019. 'The knob protein KAHRP assembles into a ring-shaped structure that underpins virulence complex assembly', *PLoS Pathog*, 15: e1007761.
- Low, L. M., Y. Azasi, E. S. Sherling, M. Garten, J. Zimmerberg, T. Tsuboi, J. Brzostowski, J. Mu, M. J. Blackman, and L. H. Miller. 2019. 'Deletion of Plasmodium falciparum Protein RON3 Affects the Functional Translocation of Exported Proteins and Glucose Uptake', *mBio*, 10.
- Lustigman, S., R. F. Anders, G. V. Brown, and R. L. Coppel. 1990. 'The mature-parasite-infected erythrocyte surface antigen (MESA) of Plasmodium falciparum associates with the erythrocyte membrane skeletal protein, band 4.1', *Mol Biochem Parasitol*, 38: 261-70.
- Maier, A. G., M. Rug, M. T. O'Neill, J. G. Beeson, M. Marti, J. Reeder, and A. F. Cowman. 2007. 'Skeleton-binding protein 1 functions at the parasitophorous vacuole membrane to traffic PfEMP1 to the Plasmodium falciparum-infected erythrocyte surface', *Blood*, 109: 1289-97.
- Maier, A. G., M. Rug, M. T. O'Neill, M. Brown, S. Chakravorty, T. Szeszak, J. Chesson, Y. Wu, K. Hughes, R. L. Coppel, C. Newbold, J. G. Beeson, A. Craig, B. S. Crabb, and A. F. Cowman. 2008. 'Exported proteins required for virulence and rigidity of Plasmodium falciparum-infected human erythrocytes', *Cell*, 134: 48-61.
- Maier, Alexander G., Brian M. Cooke, Alan F. Cowman, and Leann Tilley. 2009. 'Malaria parasite proteins that remodel the host erythrocyte', *Nature Reviews Microbiology*, 7: 341-54.
- Mancio-Silva, L., and M. M. Mota. 2015. 'A mediator for malaria stickiness in A versus O blood', *Nat Med*, 21: 307-8.
- Marapana, D. S., L. F. Dagley, J. J. Sandow, T. Nebl, T. Triglia, M. Pasternak, B. K. Dickerman, B. S. Crabb, P. R. Gilson, A. I. Webb, J. A. Boddey, and A. F. Cowman. 2018. 'Plasmepsin V cleaves malaria effector proteins in a distinct endoplasmic reticulum translocation interactome for export to the erythrocyte', *Nat Microbiol*, 3: 1010-22.
- Marti, M., R. T. Good, M. Rug, E. Knuepfer, and A. F. Cowman. 2004. 'Targeting malaria virulence and remodeling proteins to the host erythrocyte', *Science (New York, N.Y.)*, 306: 1930-3.
- Matthews, K., M. Kalanon, S. A. Chisholm, A. Sturm, C. D. Goodman, M. W. Dixon, P. R. Sanders, T. Nebl, F. Fraser, S. Haase, G. I. McFadden, P. R. Gilson, B. S. Crabb, and T. F. de Koning-Ward. 2013. 'The Plasmodium translocon of exported proteins (PTEX) component thioredoxin-2 is important for maintaining normal blood-stage growth', *Mol Microbiol*, 89: 1167-86.
- Matthews, K. M., M. Kalanon, and T. F. de Koning-Ward. 2019. 'Uncoupling the Threading and Unfoldase Actions of Plasmodium HSP101 Reveals Differences in Export between Soluble and Insoluble Proteins', *mBio*, 10.
- Matthews, K. M., E. L. Pitman, and T. F. de Koning-Ward. 2019. 'Illuminating how malaria parasites export proteins into host erythrocytes', *Cell Microbiol*, 21: e13009.
- Matz, J. M., J. R. Beck, and M. J. Blackman. 2020. 'The parasitophorous vacuole of the blood-stage malaria parasite', *Nat Rev Microbiol*, 18: 379-91.
- Matz, J. M., K. Matuschewski, and T. W. Kooij. 2013. 'Two putative protein export regulators promote Plasmodium blood stage development in vivo', *Mol Biochem Parasitol*, 191: 44-52.
- McHugh, E., S. Batinovic, E. Hanssen, P. J. McMillan, S. Kenny, M. D. Griffin, S. Crawford, K. R. Trenholme, D. L. Gardiner, M. W. Dixon, and L. Tilley. 2015. 'A repeat sequence domain of the ring-exported protein-1 of Plasmodium falciparum controls export machinery architecture and virulence protein trafficking', *Mol Microbiol*, 98: 1101-14.

- McHugh, Emma, Olivia M. S. Carmo, Adam Blanch, Oliver Looker, Boyin Liu, Snigdha Tiash, Dean Andrew, Steven Batinovic, Andy J. Y. Low, Hyun-Jung Cho, Paul McMillan, Leann Tilley, and Matthew W. A. Dixon. 2020. 'Role of Plasmodium falciparum Protein GEXP07 in Maurer's Cleft Morphology, Knob Architecture, and P. falciparum EMP1 Trafficking', *mBio*, 11.
- Mesen-Ramirez, P., B. Bergmann, T. T. Tran, M. Garten, J. Stacker, I. Naranjo-Prado, K. Hohn, J. Zimmerberg, and T. Spielmann. 2019. 'EXP1 is critical for nutrient uptake across the parasitophorous vacuole membrane of malaria parasites', *PLoS Biol*, 17: e3000473.
- Mesen-Ramirez, P., F. Reinsch, A. Blancke Soares, B. Bergmann, A. K. Ullrich, S. Tenzer, and T. Spielmann. 2016. 'Stable Translocation Intermediates Jam Global Protein Export in Plasmodium falciparum Parasites and Link the PTEX Component EXP2 with Translocation Activity', *PLoS Pathog*, 12: e1005618.
- Mikkelsen, R. B., M. Kamber, K. S. Wadwa, P. S. Lin, and R. Schmidt-Ullrich. 1988. 'The role of lipids in Plasmodium falciparum invasion of erythrocytes: a coordinated biochemical and microscopic analysis', *Proc Natl Acad Sci U S A*, 85: 5956-60.
- Mills, J. P., M. Diez-Silva, D. J. Quinn, M. Dao, M. J. Lang, K. S. Tan, C. T. Lim, G. Milon, P. H. David, O. Mercereau-Puijalon, S. Bonnefoy, and S. Suresh. 2007. 'Effect of plasmodial RESA protein on deformability of human red blood cells harboring Plasmodium falciparum', *Proc Natl Acad Sci U S A*, 104: 9213-7.
- Milner, D. A., Jr. 2018. 'Malaria Pathogenesis', *Cold Spring Harb Perspect Med*, 8.
- Mota, M. M., G. Pradel, J. P. Vanderberg, J. C. Hafalla, U. Frevert, R. S. Nussenzweig, V. Nussenzweig, and A. Rodriguez. 2001. 'Migration of Plasmodium sporozoites through cells before infection', *Science (New York, N.Y.)*, 291: 141-4.
- Mueller, I., P. A. Zimmerman, and J. C. Reeder. 2007. 'Plasmodium malariae and Plasmodium ovale--the "bashful" malaria parasites', *Trends Parasitol*, 23: 278-83.
- Mundwiler-Pachlatko, E., and H. P. Beck. 2013. 'Maurer's clefts, the enigma of Plasmodium falciparum', *Proc Natl Acad Sci U S A*, 110: 19987-94.
- Nash, G. B., E. O'Brien, E. C. Gordon-Smith, and J. A. Dormandy. 1989. 'Abnormalities in the mechanical properties of red blood cells caused by Plasmodium falciparum', *Blood*, 74: 855-61.
- Nessel, T., J. M. Beck, S. Rayatpisheh, Y. Jami-Alahmadi, J. A. Wohlschlegel, D. E. Goldberg, and J. R. Beck. 2020. 'EXP1 is required for organisation of EXP2 in the intraerythrocytic malaria parasite vacuole', *Cell Microbiol*, 22: e13168.
- NIH. 2020. 'NIH researchers discover new set of channels connecting malaria parasite and blood cells', NIH, Accessed Thursday, July 30, 2020. <https://www.nih.gov/news-events/news-releases/nih-researchers-discover-new-set-channels-connecting-malaria-parasite-blood-cells>.
- Nilsson, S., D. Angeletti, M. Wahlgren, Q. Chen, and K. Moll. 2012. 'Plasmodium falciparum antigen 332 is a resident peripheral membrane protein of Maurer's clefts', *PLoS One*, 7: e46980.
- Nunes, M. C., J. P. Goldring, C. Doerig, and A. Scherf. 2007. 'A novel protein kinase family in Plasmodium falciparum is differentially transcribed and secreted to various cellular compartments of the host cell', *Mol Microbiol*, 63: 391-403.
- Oberli, A., L. Zurbrugg, S. Rusch, F. Brand, M. E. Butler, J. L. Day, E. E. Cutts, T. Lavstsen, I. Vakonakis, and H. P. Beck. 2016. 'Plasmodium falciparum Plasmodium helical interspersed subtelomeric proteins contribute to cytoadherence and anchor P. falciparum erythrocyte membrane protein 1 to the host cell cytoskeleton', *Cell Microbiol*, 18: 1415-28.
- Oberstaller, J., T. D. Otto, J. C. Rayner, and J. H. Adams. 2021. 'Essential Genes of the Parasitic Apicomplexa', *Trends Parasitol*, 37: 304-16.
- Okombo, J., M. Kanai, I. Deni, and D. A. Fidock. 2021. 'Genomic and Genetic Approaches to Studying Antimalarial Drug Resistance and Plasmodium Biology', *Trends Parasitol*.
- Pachlatko, E., S. Rusch, A. Muller, A. Hemphill, L. Tilley, E. Hanssen, and H. P. Beck. 2010. 'MAHRP2, an exported protein of Plasmodium falciparum, is an essential component of Maurer's cleft tethers', *Mol Microbiol*, 77: 1136-52.
- Pasloske, B. L., D. I. Baruch, M. R. van Schravendijk, S. M. Handunnetti, M. Aikawa, H. Fujioka, T. F. Taraschi, J. A. Gormley, and R. J. Howard. 1993. 'Cloning and characterization of a Plasmodium falciparum gene encoding a novel high-molecular weight host membrane-associated protein, PfEMP3', *Mol Biochem Parasitol*, 59: 59-72.

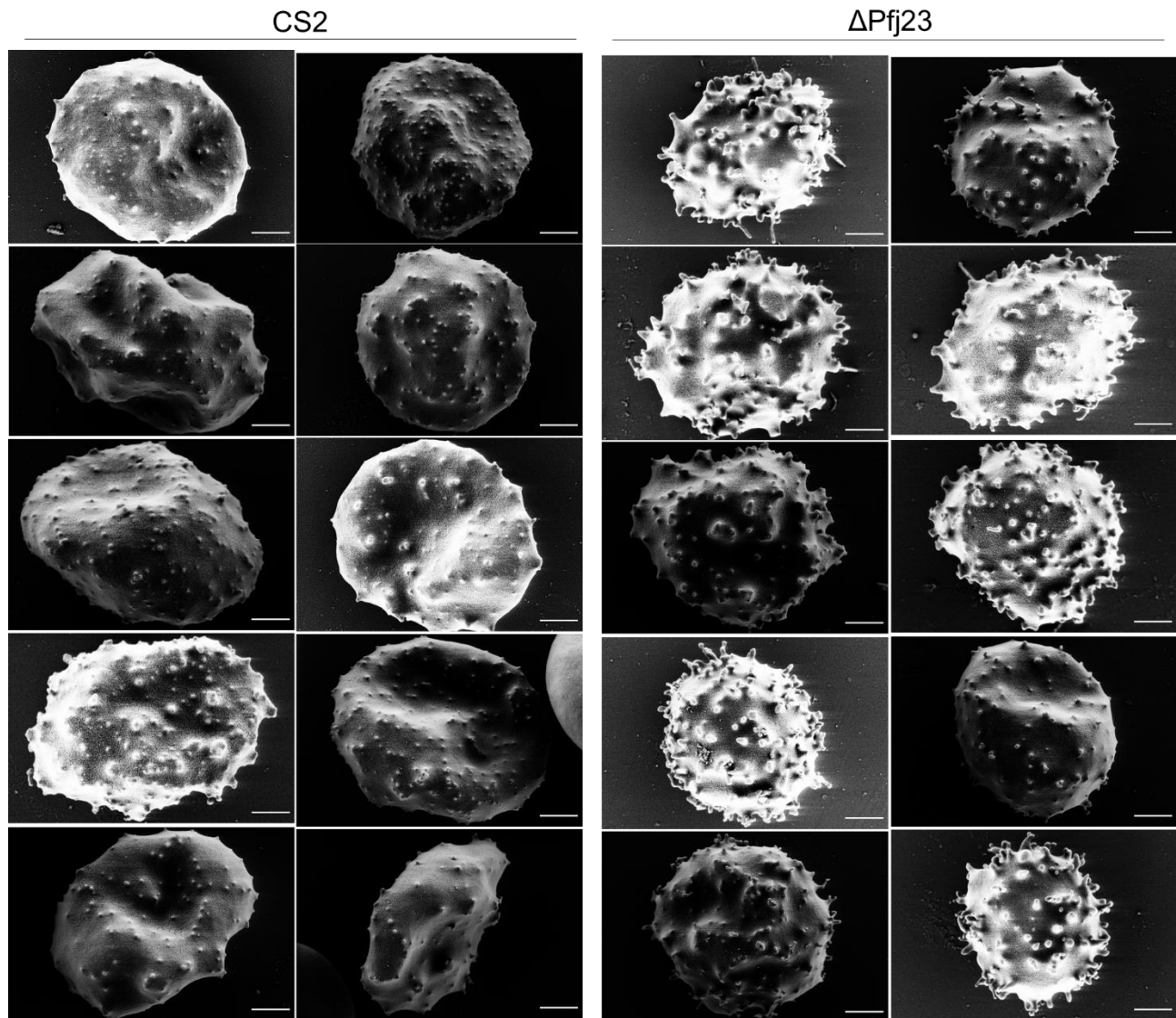
- Pei, X., X. Guo, R. Coppel, S. Bhattacharjee, K. Haldar, W. Gratzer, N. Mohandas, and X. An. 2007. 'The ring-infected erythrocyte surface antigen (RESA) of Plasmodium falciparum stabilizes spectrin tetramers and suppresses further invasion', *Blood*, 110: 1036-42.
- Pei, X., X. Guo, R. Coppel, N. Mohandas, and X. An. 2007. 'Plasmodium falciparum erythrocyte membrane protein 3 (PfEMP3) destabilizes erythrocyte membrane skeleton', *J Biol Chem*, 282: 26754-58.
- Plewes, K., S. J. Leopold, H. W. F. Kingston, and A. M. Dondorp. 2019. 'Malaria: What's New in the Management of Malaria?', *Infect Dis Clin North Am*, 33: 39-60.
- Pologe, L. G., and J. V. Ravetch. 1986. 'A chromosomal rearrangement in a P. falciparum histidine-rich protein gene is associated with the knobless phenotype', *Nature*, 322: 474-7.
- Prommana, P., C. Uthapibull, C. Wongsombat, S. Kamchonwongpaisan, Y. Yuthavong, E. Knuepfer, A. A. Holder, and P. J. Shaw. 2013. 'Inducible knockdown of Plasmodium gene expression using the glmS ribozyme', *PLoS One*, 8: e73783.
- Przyborski, J. M., and M. Lanzer. 2005. 'Protein transport and trafficking in Plasmodium falciparum-infected erythrocytes', *Parasitology*, 130: 373-88.
- Przyborski, J. M., B. Nyboer, and M. Lanzer. 2016. 'Ticket to ride: export of proteins to the Plasmodium falciparum-infected erythrocyte', *Mol Microbiol*, 101: 1-11.
- Reeder, J. C., A. F. Cowman, K. M. Davern, J. G. Beeson, J. K. Thompson, S. J. Rogerson, and G. V. Brown. 1999. 'The adhesion of Plasmodium falciparum-infected erythrocytes to chondroitin sulfate A is mediated by P. falciparum erythrocyte membrane protein 1', *Proc Natl Acad Sci U S A*, 96: 5198-202.
- Rug, M., M. Cyrklaff, A. Mikkonen, L. Lemgruber, S. Kuelzer, C. P. Sanchez, J. Thompson, E. Hanssen, M. O'Neill, C. Langer, M. Lanzer, F. Frischknecht, A. G. Maier, and A. F. Cowman. 2014. 'Export of virulence proteins by malaria-infected erythrocytes involves remodeling of host actin cytoskeleton', *Blood*, 124: 3459-68.
- Rug, M., S. W. Prescott, K. M. Fernandez, B. M. Cooke, and A. F. Cowman. 2006. 'The role of KAHRP domains in knob formation and cytoadherence of P falciparum-infected human erythrocytes', *Blood*, 108: 370-8.
- Sanchez, C. P., C. Karathanasis, R. Sanchez, M. Cyrklaff, J. Jager, B. Buchholz, U. S. Schwarz, M. Heilemann, and M. Lanzer. 2019. 'Single-molecule imaging and quantification of the immune-variant adhesin VAR2CSA on knobs of Plasmodium falciparum-infected erythrocytes', *Commun Biol*, 2: 172.
- Sanyal, S., S. Egee, G. Bouyer, S. Perrot, I. Safeukui, E. Bischoff, P. Buffet, K. W. Deitsch, O. Mercereau-Puijalon, P. H. David, T. J. Templeton, and C. Lavazec. 2012. 'Plasmodium falciparum STEVOR proteins impact erythrocyte mechanical properties', *Blood*, 119: e1-8.
- Schulze, J., M. Kwiatkowski, J. Borner, H. Schluter, I. Bruchhaus, T. Burmester, T. Spielmann, and C. Pick. 2015. 'The Plasmodium falciparum exportome contains non-canonical PEXEL/HT proteins', *Mol Microbiol*, 97: 301-14.
- Sherling, E. S., E. Knuepfer, J. A. Brzostowski, L. H. Miller, M. J. Blackman, and C. van Ooij. 2017. 'The Plasmodium falciparum rhoptry protein RhopH3 plays essential roles in host cell invasion and nutrient uptake', *Elife*, 6.
- Silva, M. D., B. M. Cooke, M. Guillotte, D. W. Buckingham, J. P. Sauzet, C. Le Scanf, H. Contamin, P. David, O. Mercereau-Puijalon, and S. Bonnefoy. 2005. 'A role for the Plasmodium falciparum RESA protein in resistance against heat shock demonstrated using gene disruption', *Mol Microbiol*, 56: 990-1003.
- Sinden, R. E. 2015. 'The cell biology of malaria infection of mosquito: advances and opportunities', *Cell Microbiol*, 17: 451-66.
- Smith, J. D. 2014. 'The role of PfEMP1 adhesion domain classification in Plasmodium falciparum pathogenesis research', *Mol Biochem Parasitol*, 195: 82-7.
- Smith, J. D., C. E. Chitnis, A. G. Craig, D. J. Roberts, D. E. Hudson-Taylor, D. S. Peterson, R. Pinches, C. I. Newbold, and L. H. Miller. 1995. 'Switches in expression of Plasmodium falciparum var genes correlate with changes in antigenic and cytoadherent phenotypes of infected erythrocytes', *Cell*, 82: 101-10.
- Snow, R. W., B. Sartorius, D. Kyalo, J. Maina, P. Amratia, C. W. Mundia, P. Bejon, and A. M. Noor. 2017. 'The prevalence of Plasmodium falciparum in sub-Saharan Africa since 1900', *Nature*, 550: 515-18.

- Sologub, L., A. Kuehn, S. Kern, J. Przyborski, R. Schillig, and G. Pradel. 2011. 'Malaria proteases mediate inside-out egress of gametocytes from red blood cells following parasite transmission to the mosquito', *Cell Microbiol*, 13: 897-912.
- Spielmann, T., and T. W. Gilberger. 2010. 'Protein export in malaria parasites: do multiple export motifs add up to multiple export pathways?', *Trends Parasitol*, 26: 6-10.
- Spielmann, T., P. L. Hawthorne, M. W. Dixon, M. Hannemann, K. Klotz, D. J. Kemp, N. Klonis, L. Tilley, K. R. Trenholme, and D. L. Gardiner. 2006. 'A cluster of ring stage-specific genes linked to a locus implicated in cytoadherence in *Plasmodium falciparum* codes for PEXEL-negative and PEXEL-positive proteins exported into the host cell', *Mol Biol Cell*, 17: 3613-24.
- Spillman, N. J., R. J. Allen, C. W. McNamara, B. K. Yeung, E. A. Winzeler, T. T. Diagona, and K. Kirk. 2013. 'Na(+) regulation in the malaria parasite *Plasmodium falciparum* involves the cation ATPase PfATP4 and is a target of the spiroindolone antimalarials', *Cell Host Microbe*, 13: 227-37.
- Spillman, N. J., and K. Kirk. 2015. 'The malaria parasite cation ATPase PfATP4 and its role in the mechanism of action of a new arsenal of antimalarial drugs', *Int J Parasitol Drugs Drug Resist*, 5: 149-62.
- Spycher, C., M. Rug, E. Pachlatko, E. Hanssen, D. Ferguson, A. F. Cowman, L. Tilley, and H. P. Beck. 2008. 'The Maurer's cleft protein MAHRP1 is essential for trafficking of PfEMP1 to the surface of *Plasmodium falciparum*-infected erythrocytes', *Mol Microbiol*, 68: 1300-14.
- Straimer, J., M. C. Lee, A. H. Lee, B. Zeitler, A. E. Williams, J. R. Pearl, L. Zhang, E. J. Rebar, P. D. Gregory, M. Llinas, F. D. Urnov, and D. A. Fidock. 2012. 'Site-specific genome editing in *Plasmodium falciparum* using engineered zinc-finger nucleases', *Nat Methods*, 9: 993-8.
- Sturm, A., R. Amino, C. van de Sand, T. Regen, S. Retzlaff, A. Rennenberg, A. Krueger, J. M. Pollok, R. Menard, and V. T. Heussler. 2006. 'Manipulation of host hepatocytes by the malaria parasite for delivery into liver sinusoids', *Science (New York, N.Y.)*, 313: 1287-90.
- Sutherland, C. J. 2016. 'Persistent Parasitism: The Adaptive Biology of Malariae and Ovale Malaria', *Trends Parasitol*, 32: 808-19.
- Sutherland, C. J., N. Tanomsing, D. Nolder, M. Oguike, C. Jennison, S. Pukrittayakamee, C. Dolecek, T. T. Hien, V. E. do Rosario, A. P. Arez, J. Pinto, P. Michon, A. A. Escalante, F. Nosten, M. Burke, R. Lee, M. Blaze, T. D. Otto, J. W. Barnwell, A. Pain, J. Williams, N. J. White, N. P. Day, G. Snounou, P. J. Lockhart, P. L. Chiodini, M. Imwong, and S. D. Polley. 2010. 'Two nonrecombining sympatric forms of the human malaria parasite *Plasmodium ovale* occur globally', *J Infect Dis*, 201: 1544-50.
- Takano, R., H. Kozuka-Hata, D. Kondoh, H. Bochimoto, M. Oyama, and K. Kato. 2019. 'A High-Resolution Map of SBP1 Interactomes in *Plasmodium falciparum*-infected Erythrocytes', *iScience*, 19: 703-14.
- Tavares, J., P. Formaglio, S. Thiberge, E. Mordelet, N. Van Rooijen, A. Medvinsky, R. Menard, and R. Amino. 2013. 'Role of host cell traversal by the malaria sporozoite during liver infection', *J Exp Med*, 210: 905-15.
- Tiburcio, M., F. Silvestrini, L. Bertuccini, A. F. Sander, L. Turner, T. Lavstsen, and P. Alano. 2013. 'Early gametocytes of the malaria parasite *Plasmodium falciparum* specifically remodel the adhesive properties of infected erythrocyte surface', *Cell Microbiol*, 15: 647-59.
- Tilley, L., R. Sougrat, T. Lithgow, and E. Hanssen. 2008. 'The twists and turns of Maurer's cleft trafficking in *P. falciparum*-infected erythrocytes', *Traffic*, 9: 187-97.
- Twohig, K. A., D. A. Pfeffer, J. K. Baird, R. N. Price, P. A. Zimmerman, S. I. Hay, P. W. Gething, K. E. Battle, and R. E. Howes. 2019. 'Growing evidence of *Plasmodium vivax* across malaria-endemic Africa', *PLoS Negl Trop Dis*, 13: e0007140.
- Venugopal, K., F. Hentzschel, G. Valkiunas, and M. Marti. 2020. '*Plasmodium* asexual growth and sexual development in the haematopoietic niche of the host', *Nat Rev Microbiol*, 18: 177-89.
- Vincensini, L., G. Fall, L. Berry, T. Blisnick, and C. Braun Breton. 2008. 'The RhopH complex is transferred to the host cell cytoplasm following red blood cell invasion by *Plasmodium falciparum*', *Mol Biochem Parasitol*, 160: 81-9.
- Vincensini, Laetitia, Sophie Richert, Thierry Blisnick, Alain Van Dorsselaer, Emmanuelle Leize-Wagner, Thierry Rabilloud, and Catherine Braun Breton. 2005. 'Proteomic Analysis Identifies Novel Proteins of the Maurer's Clefts, a Secretory Compartment Delivering *Plasmodium falciparum* Proteins to the Surface of Its Host Cell', *Molecular & Cellular Proteomics*, 4: 582-93.
- Voigt, S., M. Hanspal, P. J. LeRoy, P. S. Zhao, S. S. Oh, A. H. Chishti, and S. C. Liu. 2000. 'The cytoadherence ligand *Plasmodium falciparum* erythrocyte membrane protein 1 (PfEMP1) binds to

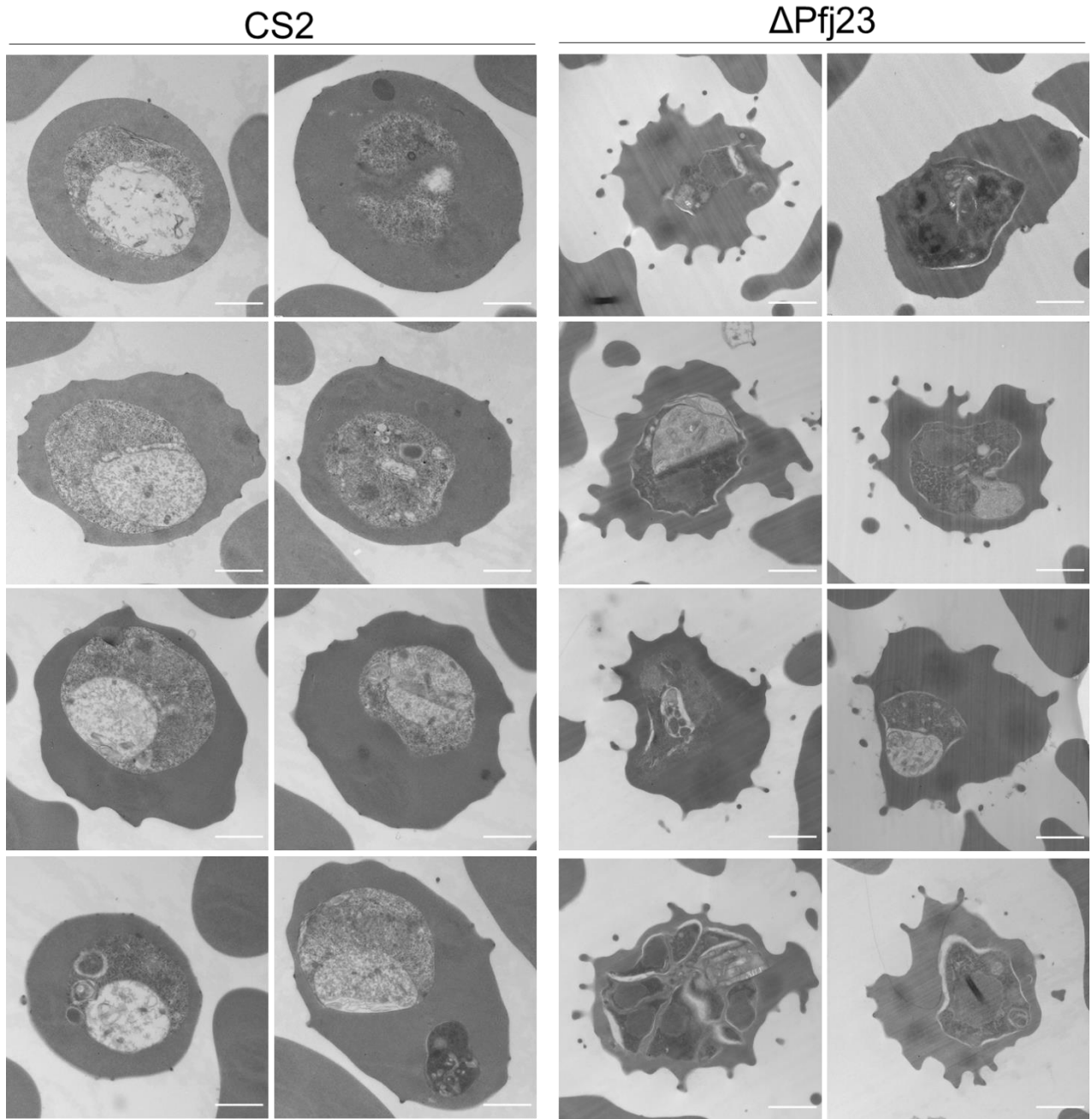
- the P. falciparum knob-associated histidine-rich protein (KAHRP) by electrostatic interactions', *Mol Biochem Parasitol*, 110: 423-8.
- Wahlgren, M., S. Goel, and R. R. Akhouri. 2017a. 'Variant surface antigens of Plasmodium falciparum and their roles in severe malaria', *Nat Rev Microbiol*, 15: 479-91.
- Wahlgren, Mats, Suchi Goel, and Reetesh R. Akhouri. 2017b. 'Variant surface antigens of Plasmodium falciparum and their roles in severe malaria', *Nature Reviews Microbiology*, 15: 479-91.
- Waller, K. L., B. M. Cooke, W. Nunomura, N. Mohandas, and R. L. Coppel. 1999. 'Mapping the binding domains involved in the interaction between the Plasmodium falciparum knob-associated histidine-rich protein (KAHRP) and the cytoadherence ligand P. falciparum erythrocyte membrane protein 1 (PfEMP1)', *J Biol Chem*, 274: 23808-13.
- Waller, R. F., M. B. Reed, A. F. Cowman, and G. I. McFadden. 2000. 'Protein trafficking to the plastid of Plasmodium falciparum is via the secretory pathway', *EMBO J*, 19: 1794-802.
- Ward, G. E., L. H. Miller, and J. A. Dvorak. 1993. 'The origin of parasitophorous vacuole membrane lipids in malaria-infected erythrocytes', *J Cell Sci*, 106 (Pt 1): 237-48.
- Warncke, J. D., and H. P. Beck. 2019. 'Host Cytoskeleton Remodeling throughout the Blood Stages of Plasmodium falciparum', *Microbiol Mol Biol Rev*, 83.
- Warncke, J. D., I. Vakonakis, and H. P. Beck. 2016. 'Plasmodium Helical Interspersed Subtelomeric (PHIST) Proteins, at the Center of Host Cell Remodeling', *Microbiol Mol Biol Rev*, 80: 905-27.
- Wassmer, S. C., T. E. Taylor, P. K. Rathod, S. K. Mishra, S. Mohanty, M. Arevalo-Herrera, M. T. Duraisingh, and J. D. Smith. 2015. 'Investigating the Pathogenesis of Severe Malaria: A Multidisciplinary and Cross-Geographical Approach', *Am J Trop Med Hyg*, 93: 42-56.
- Watanabe, J. 1997. 'Cloning and characterization of heat shock protein DnaJ homologues from Plasmodium falciparum and comparison with ring infected erythrocyte surface antigen', *Mol Biochem Parasitol*, 88: 253-8.
- Waterkeyn, J. G., M. E. Wickham, K. M. Davern, B. M. Cooke, R. L. Coppel, J. C. Reeder, J. G. Culvenor, R. F. Waller, and A. F. Cowman. 2000. 'Targeted mutagenesis of Plasmodium falciparum erythrocyte membrane protein 3 (PfEMP3) disrupts cytoadherence of malaria-infected red blood cells', *EMBO J*, 19: 2813-23.
- Watermeyer, J. M., V. L. Hale, F. Hackett, D. K. Clare, E. E. Cutts, I. Vakonakis, R. A. Fleck, M. J. Blackman, and H. R. Saibil. 2016. 'A spiral scaffold underlies cytoadherent knobs in Plasmodium falciparum-infected erythrocytes', *Blood*, 127: 343-51.
- White, N. J. 2008. 'Plasmodium knowlesi: the fifth human malaria parasite', *Clin Infect Dis*, 46: 172-3.
- WHO. 2020. "Malaria world report
- " In.
- Wickham, M. E., M. Rug, S. A. Ralph, N. Klonis, G. I. McFadden, L. Tilley, and A. F. Cowman. 2001. 'Trafficking and assembly of the cytoadherence complex in Plasmodium falciparum-infected human erythrocytes', *EMBO J*, 20: 5636-49.
- Winkler, W. C., A. Nahvi, A. Roth, J. A. Collins, and R. R. Breaker. 2004. 'Control of gene expression by a natural metabolite-responsive ribozyme', *Nature*, 428: 281-6.
- Wu, Y., L. A. Kirkman, and T. E. Wellems. 1996. 'Transformation of Plasmodium falciparum malaria parasites by homologous integration of plasmids that confer resistance to pyrimethamine', *Proc Natl Acad Sci U S A*, 93: 1130-4.
- Wu, Y., C. D. Sifri, H. H. Lei, X. Z. Su, and T. E. Wellems. 1995. 'Transfection of Plasmodium falciparum within human red blood cells', *Proc Natl Acad Sci U S A*, 92: 973-7.
- Zaw, M. T., and Z. Lin. 2019. 'Human Plasmodium knowlesi infections in South-East Asian countries', *J Microbiol Immunol Infect*, 52: 679-84.
- Zekar, L., and T. Sharman. 2021. 'Plasmodium Falciparum Malaria.' in, *StatPearls* (Treasure Island (FL)).
- Zhang, M., P. Faou, A. G. Maier, and M. Rug. 2018. 'Plasmodium falciparum exported protein PFE60 influences Maurer's clefts architecture and virulence complex composition', *Int J Parasitol*, 48: 83-95.
- Zhang, Min, Chengqi Wang, Thomas D. Otto, Jenna Oberstaller, Xiangyun Liao, Swamy R. Adapa, Kenneth Udenze, Iraad F. Bronner, Deborah Casandra, Matthew Mayho, Jacqueline Brown, Suzanne Li, Justin Swanson, Julian C. Rayner, Rays H. Y. Jiang, and John H. Adams. 2018. 'Uncovering the essential genes of the human malaria parasite Plasmodium falciparum by saturation mutagenesis', *Science (New York, N.Y.)*, 360: eaap7847.

Zhang, Q., C. Ma, A. Oberli, A. Zinz, S. Engels, and J. M. Przyborski. 2017. 'Proteomic analysis of exported chaperone/co-chaperone complexes of *P. falciparum* reveals an array of complex protein-protein interactions', *Sci Rep*, 7: 42188.

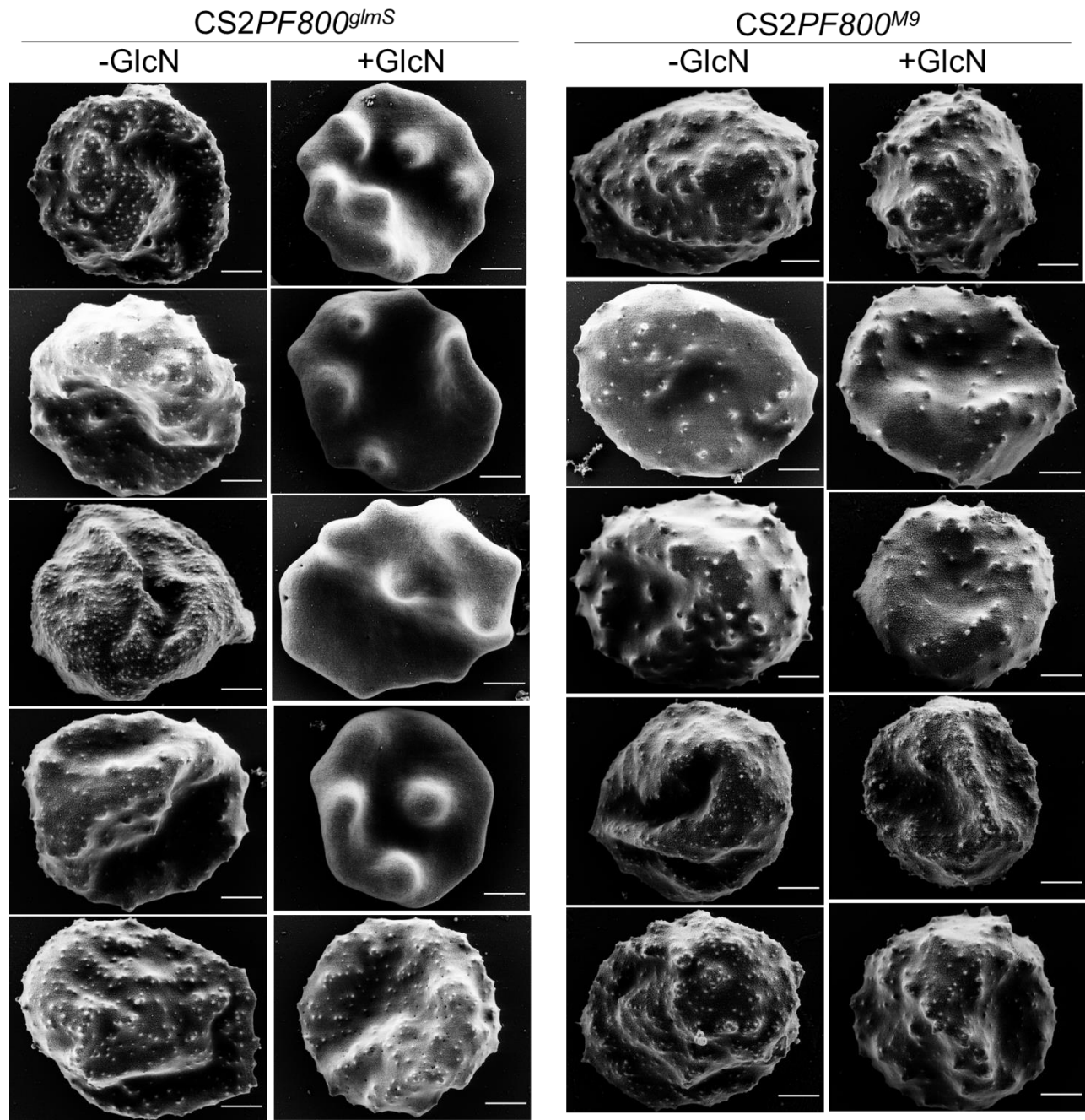
Appendices



Appendix 1: Scanning electron microscopy (SEM) of CS2 and Δ Pfj23-parasites infected red blood cells. Scale bar 1 μ m. Two independent experiments.



Appendix 2: Transmission electron microscopy (TEM) of CS2 and Δ Pfj23-parasites infected red blood cells. Scale bar 1 μ m.



Appendix 3: Scanning electron microscopy (SEM) of the *CS2PF800^{glmS}* and *CS2PF800^{M9}* parasite-infected red blood cells. GlcN: Glucosamine. Scale bar 1 μ m.

CS2PF800^{glmS}

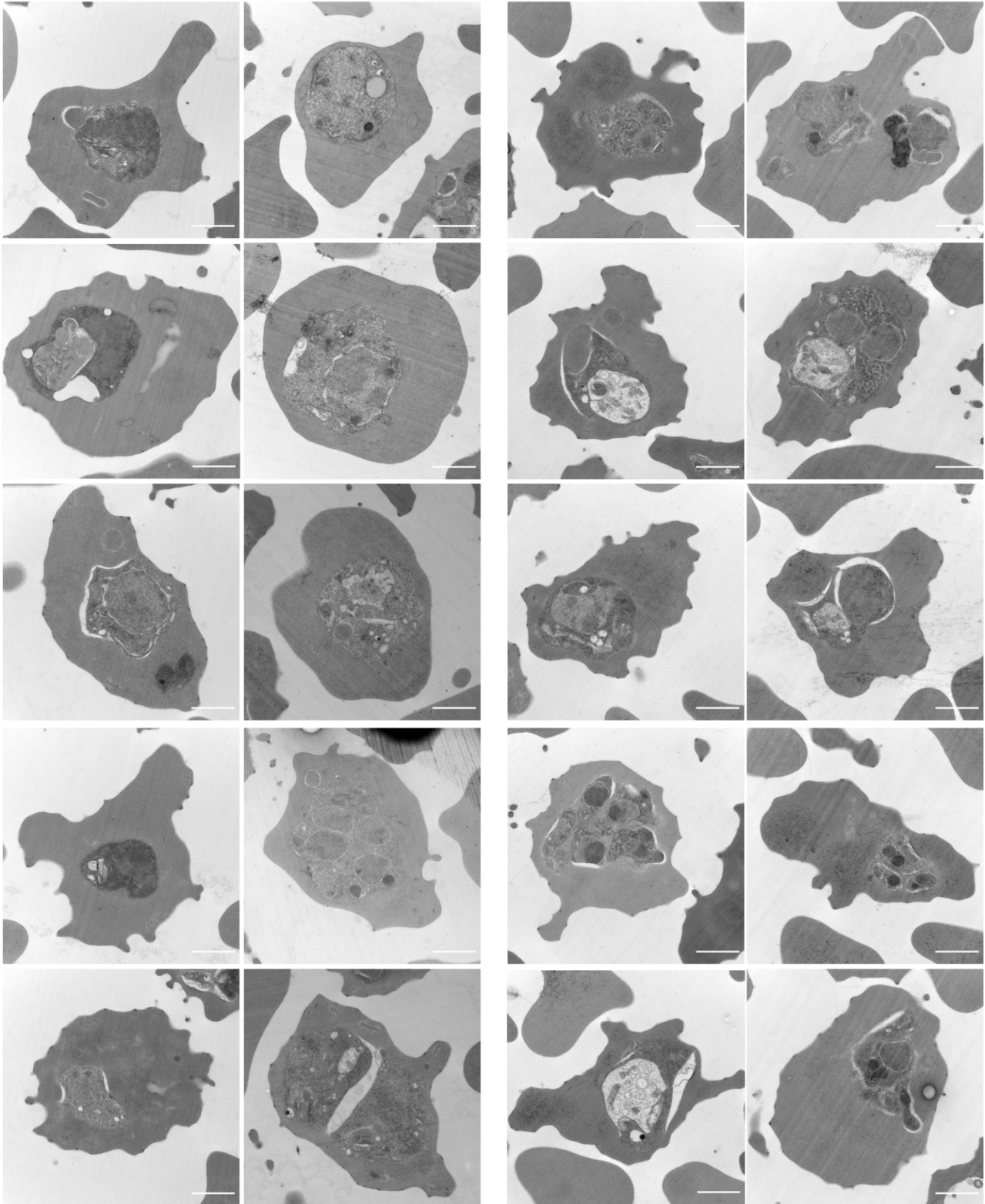
CS2PF800^{M9}

-GlcN

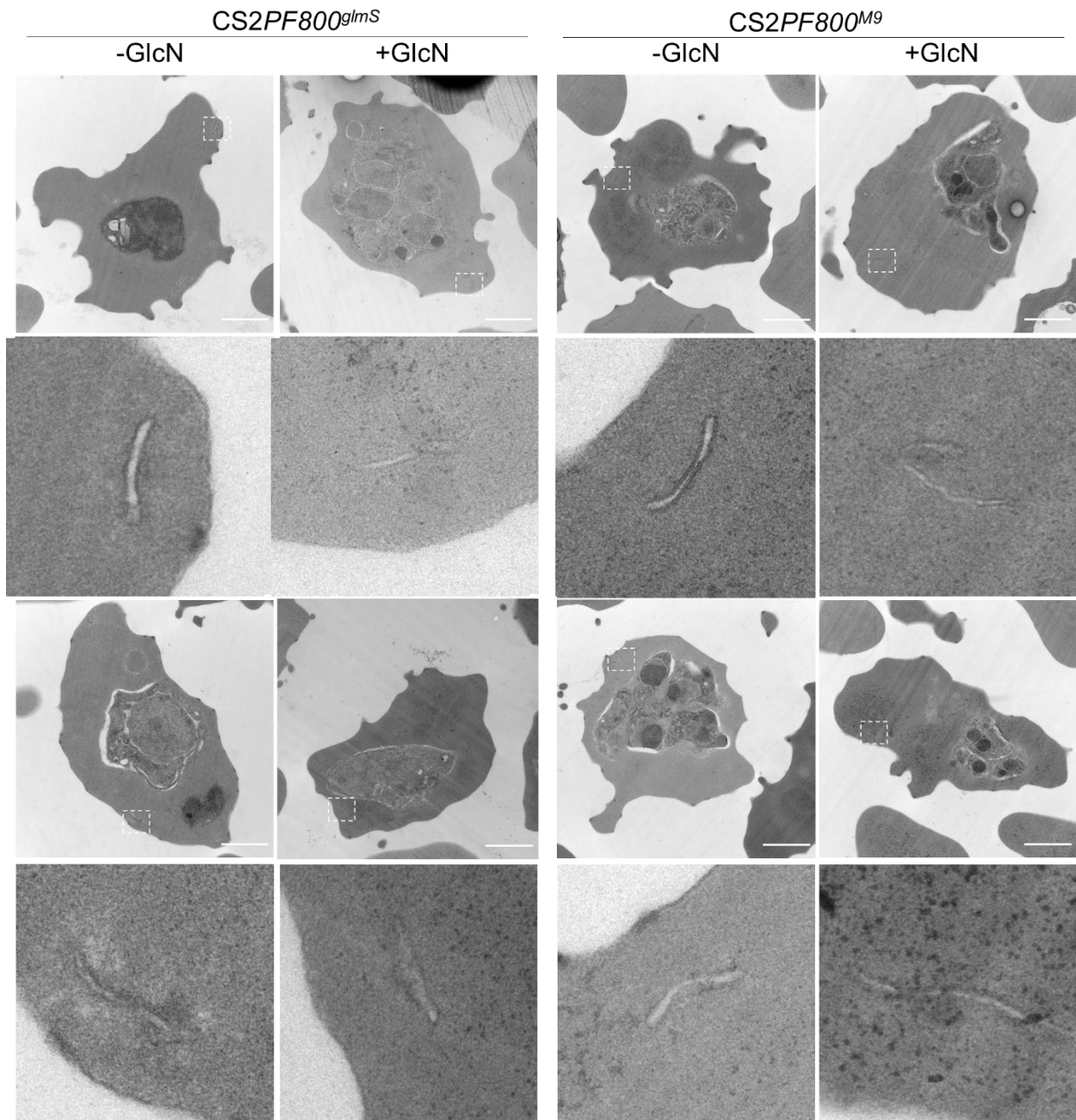
+GlcN

-GlcN

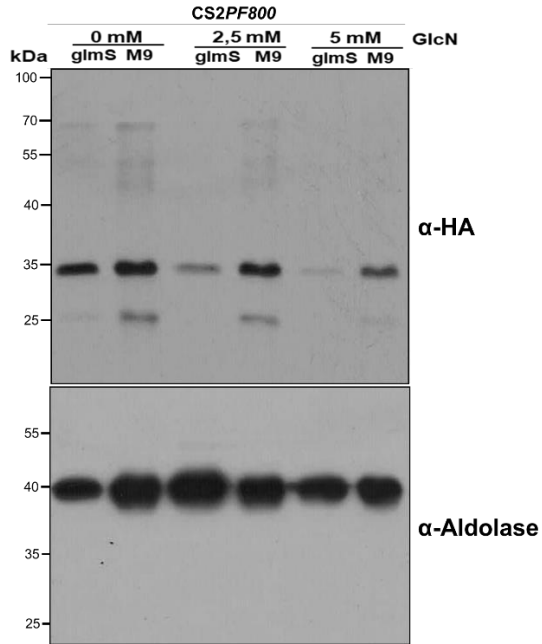
+GlcN



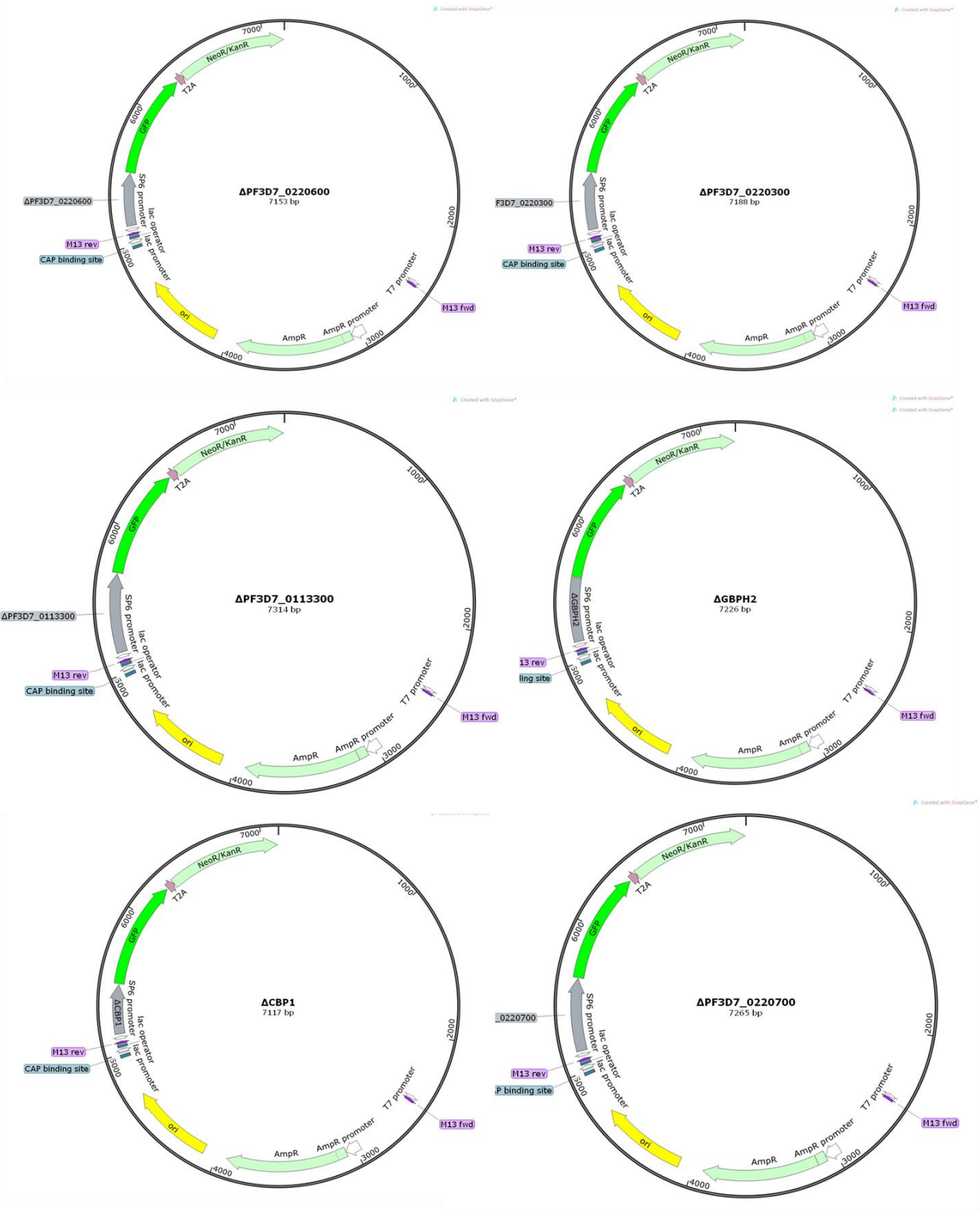
Appendix 4: Transmission electron microscopy (TEM) of the CS2PF800^{gImS} and CS2PF800^{M9} parasite-infected red blood cells. GlcN: Glucosamine. Scale bar 1 μ m.

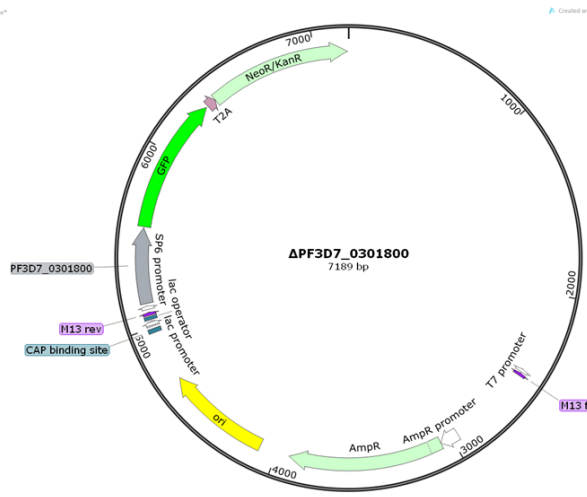
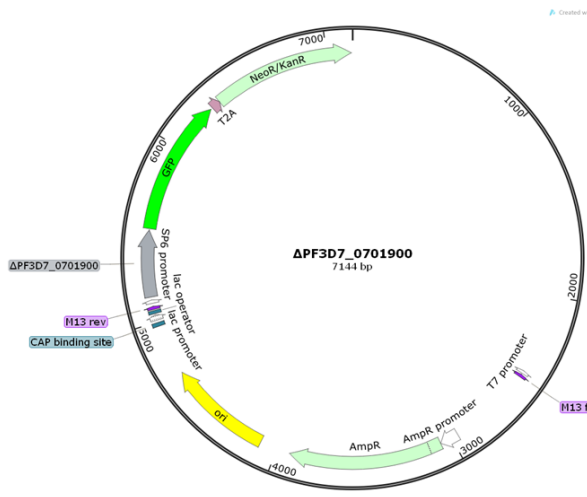
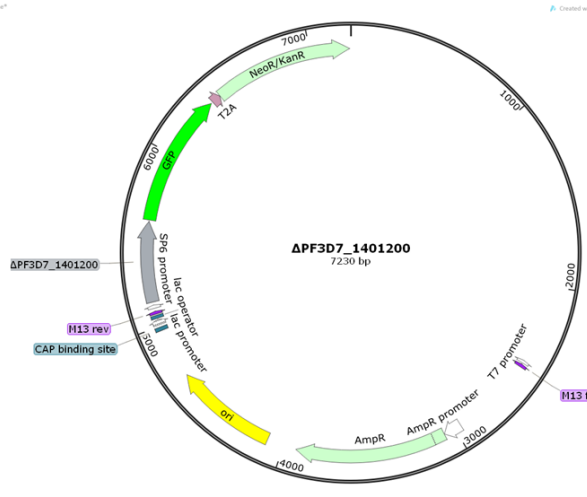
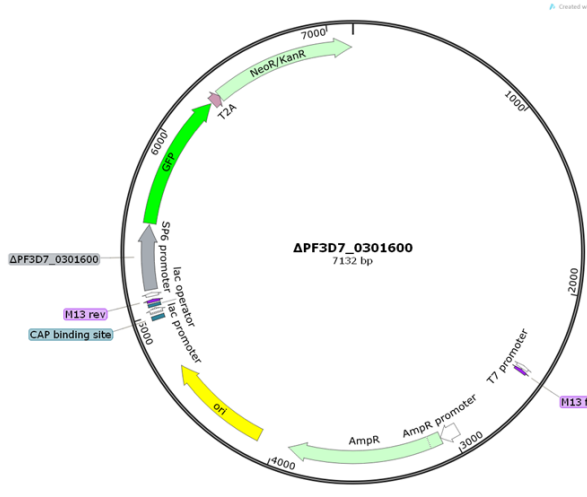
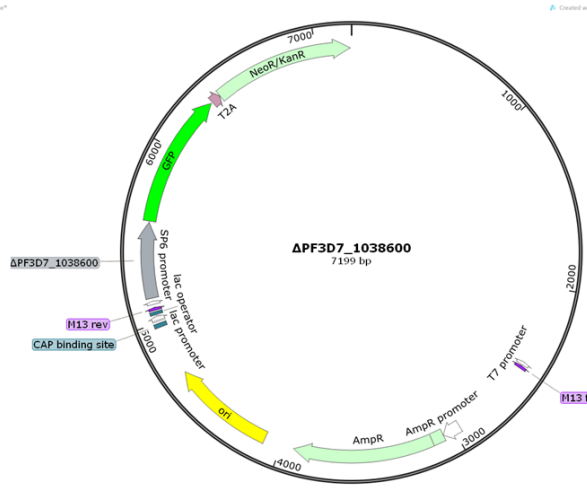
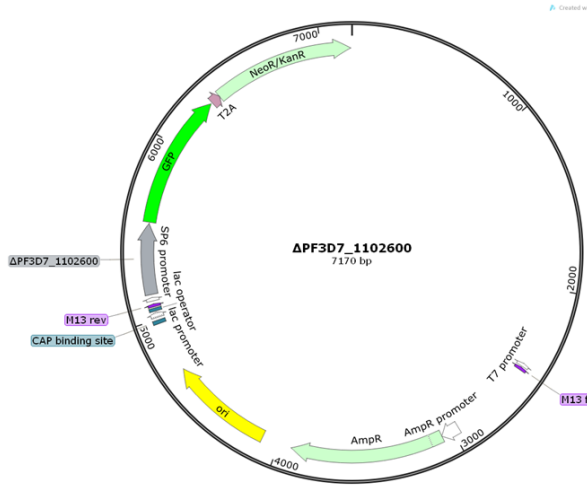


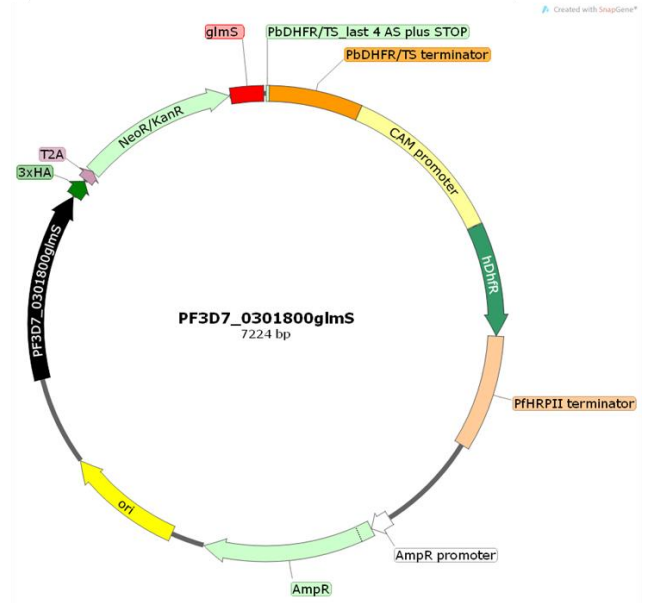
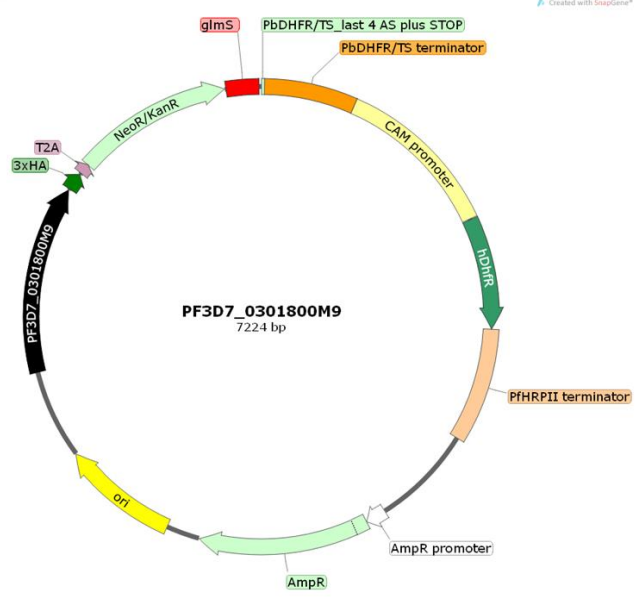
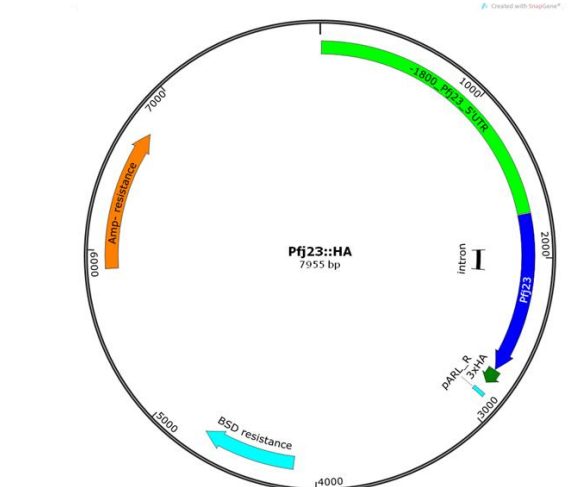
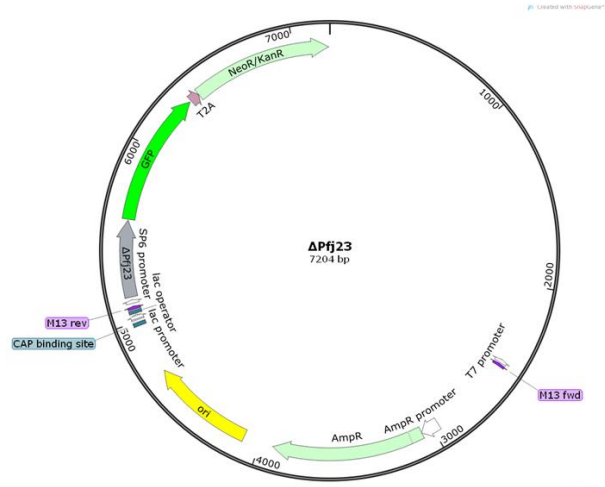
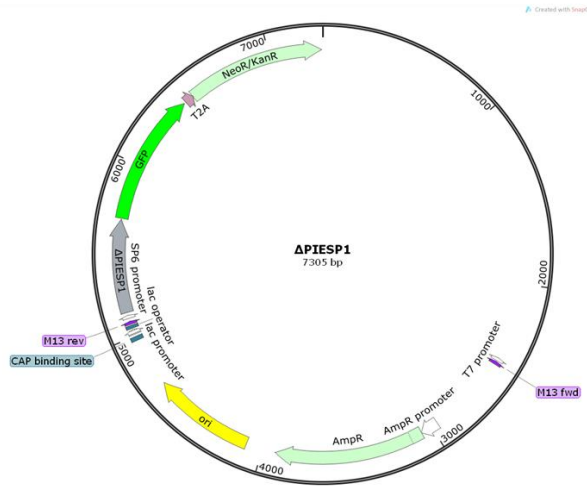
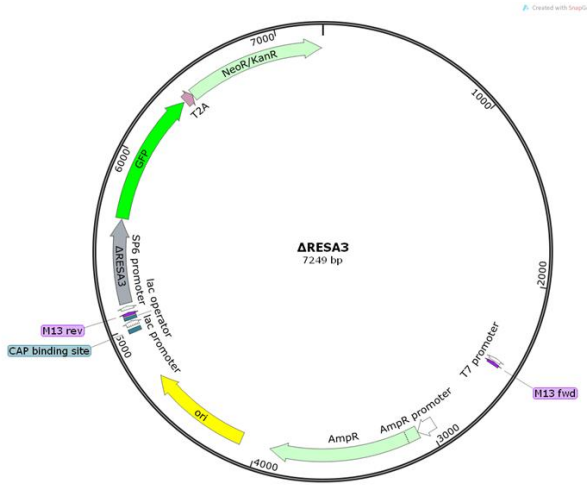
Appendix 5: Transmission electron microscopy (TEM) showing the Maurer's Clefts of the CS2PF800^{gImS} and CS2PF800^{M9} parasite-infected red blood cells. GlcN: Glucosamine. Scale bar 1 μ m.

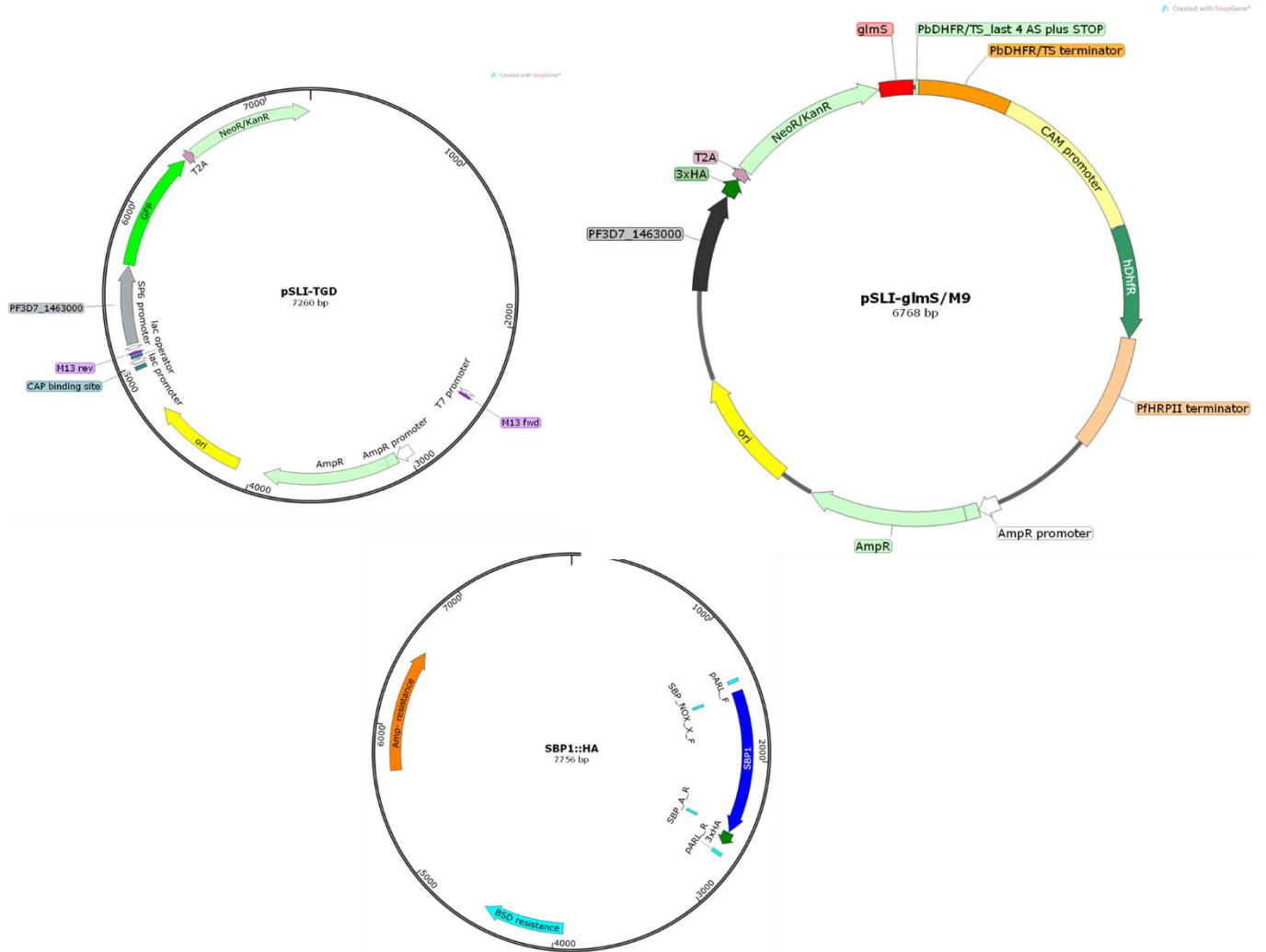


Appendix 6: Full Western blot data showing the expression of PF3D7_0301800 in the *glmS* and *M9* cell line. Downregulation of PF3D7_0301800 using different concentrations of glucosamine (GlcN). Anti-HA antibody (expected size ~35kDa) to detect the POI and Aldolase as a loading control.









Appendix 7: Vector maps